Final Report

PERFORMANCE-RELATED SPECIFICATIONS FOR CONCRETE BRIDGE SUPERSTRUCTURES

FHWA/IN/JTRP-2001/8

Volume 3
Nonmetallic Reinforcement

Robert J. Frosch
Professor of Civil Engineering
Principal Investigator

and

Christopher P. Mosley, Graduate Research Assistant
A. Koray Tureyen, Graduate Research Assistant

Joint Transportation Research Program
Project Number: C-36-56WW
File Number: 7-4-48
SPR-2325

Conducted in Cooperation with the
Indiana Department of Transportation
and the
Federal Highway Administration
U.S. Department of Transportation

Purdue University
West Lafayette, IN 47907
October 2002

ACKNOWLEDGMENTS

The work described in this report was funded by the Joint Transportation Research Program at Purdue University through SPR contract 2325. The support of the Indiana Department of Transportation (INDOT) and the Federal Highway Administration (FHWA) are gratefully acknowledged. The fiber reinforced plastic (FRP) bars used in the experimental program were donated by Technora, Marshall Industries Composites, and Hughes Bros., Inc. Their participation in this research program is also gratefully acknowledged.

The authors would like to extend thanks to Dr. Tommy Nantung from the Division of Research of INDOT for his support throughout this project. In addition, thanks are extended to the members of the Study Advisory Committee for their participation and thoughtful comments. This research is a testament to their commitment to build improved bridge superstructures with a longer service life.

TECHNICAL REPORT STANDARD TITLE PAGE

1. Report No.	2. Government Accession No.	3. Recipient's Catalog No.
FHWA/IN/JTRP-2001/8		

4. Title and Subtitle	5. Report Date
Performance Related Specifications for Concrete Bridge Superstructures- Volume 3: Nonmetallic Reinforcement	October 31, 2002
	6. Performing Organization Code

7. Author(s)	8. Performing Organization Report No.
Robert Frosch, Christopher Mosley, A. Koray Tureyen	FHWA/IN/JTRP-2001/8

9. Performing Organization Name and Address	10. Work Unit No.
Joint Transportation Research Program 1284 Civil Engineering Building Purdue University West Lafayette, Indiana 47907-1284	
	11. Contract or Grant No. SPR-2325

12. Sponsoring Agency Name and Address	13. Type of Report and Period Covered
Indiana Department of Transportation State Office Building 100 North Senate Avenue Indianapolis, IN 46204	Final Report
	14. Sponsoring Agency Code

15. Supplementary Notes

Prepared in cooperation with the Indiana Department of Transportation and Federal Highway Administration.

16. Abstract

In Volume 3 of the final report, research work conducted to investigate the behavior of fiber reinforced polymer (FRP) reinforcement is summarized. This study focused on the behavior of FRP reinforced concrete structures with an emphasis on bond and shear. For the bond investigation, three series of beam splice tests were performed on specimens reinforced with steel, glass FRP, and aramid FRP to determine the effect of the different types of reinforcement on bond, cracking, and deflections. The test results indicate that the use of FRP reinforcement leads to lower bond strengths and, therefore, require longer development lengths. The specimen crack widths and deflections were substantially larger for FRP specimens than steel specimens due to the significantly lower modulus of elasticity. Analysis of the test results resulted in recommendations for modifying the empirical development length equation of ACI 318-99 design code for use with FRP reinforcement. For the shear investigation, two series of beam tests were conducted on specimens reinforced with steel, glass FRP, and aramid FRP to determine the effect of the different types of reinforcement on the concrete shear strength. All specimens did not contain transverse reinforcement. The test results indicate that the use of FRP reinforcement leads to lower concrete shear strengths than steel reinforcement for equal reinforcement cross-sectional areas (longitudinal reinforcement percentages). Analysis of the test results resulted in recommendations for the calculation of concrete shear strength. Based on the findings of this research, design and construction recommendations are provided that can be used for the design and construction of FRP reinforced bridge decks.

17. Key Words	18. Distribution Statement
Corrosion, durability, fiber reinforced polymer (FRP) reinforcement, concrete bridge decks, concrete bond strength, concrete shear strength.	No restrictions. This document is available to the public through the National Technical Information Service, Springfield, VA 22161

19. Security Classif. (of this report)	20. Security Classif. (of this page)	21. No. of Pages	22. Price
Unclassified	Unclassified	73	

Form DOT F 1700.7 (8-69)

TABLE OF CONTENTS

LIST OF TABLES

LIST OF FIGURES

1. INTRODUCTION

1.1 Reinforcement Corrosion

Corrosion of steel reinforcement is a serious problem in reinforced concrete structures. As steel corrodes, it undergoes large volume expansion that causes excessive tensile stresses in the concrete that can eventually cause spalling. Not only does reinforcement corrosion lead to aesthetic problems in structures, but it can also affect structural performance and ultimately reduce service life. Corrosion of steel reinforcement can lead to a loss of flexural tensile strength due to a loss of steel cross-section. At the same time, corrosion of steel can weaken the surrounding concrete, destroy bond, and lead to a loss of flexural compressive strength.

Reinforced concrete exposed to water is highly susceptible to corrosion, and the problem worsens when it is exposed to salts, which is the case in marine environments, parking garages, and bridge decks. There are many methods for reducing the risk of reinforcement corrosion in reinforced concrete such as decreasing the permeability of the concrete, increasing the concrete cover, waterproofing the concrete, and coating the reinforcement. In many instances, more than one of the methods mentioned above are employed. Providing a barrier to electrically isolate the reinforcement, such as applying an epoxy coating on steel reinforcement, is a common application. The use of epoxy-coated reinforcement does have its drawbacks such as affecting bond performance, which is addressed in many design codes. In addition, this barrier is not foolproof and can often be compromised by construction practices (Samples, 1998).

The use of non-metallic reinforcement is gaining a significant amount of attention by the engineering and construction communities. Fiber reinforced plastic or polymer (FRP) reinforcement is by nature electrically isolated, which is of tremendous benefit both economically and structurally. FRP reinforcing bars have a much higher strength to weight ratio than steel bars. FRP is generally one-fourth the weight of steel and has ultimate tensile strength much higher than the yield of conventional ASTM Grade 60 steel reinforcement.

It should be noted that the behavior of FRP bars is very different than that of steel bars and the behavior is highly dependent on fiber type. FRP reinforcement is linear elastic up to failure, which poses a problem as far as structural ductility is concerned. Another concern is that the modulus of elasticity of FRP bars is significantly lower than that of steel. Bars reinforced with glass fibers (GFRP) typically have a modulus of elasticity of 20-25% of steel, whereas carbon fiber reinforced bars (CFRP) have a modulus much closer to steel (75%). Aramid FRP (AFRP) bars have a modulus of elasticity anywhere from that of GFRP to slightly above that of steel, depending on the matrix. At present there are no manufacturing standards for FRP reinforcement; therefore, their characteristics are highly variable from producer to producer. It is due to these differences that the design of FRP reinforced concrete must be approached with a great deal of caution. Most design equations used for reinforced concrete are based on laboratory tests using steel reinforcement. Naturally, design of FRP reinforced concrete should utilize equations that reflect test data for FRP reinforced specimens. For that reason there has been a considerable amount of research involving FRP reinforcement.

1.2 Fiber Reinforced Plastic (FRP) Reinforcement

There are many benefits to the use of FRP reinforcement in structural applications. Corrosion resistance and high ultimate tensile strength are two of the most important characteristics encouraging its use. The low density of the material is of importance as well. FRP bars do not fatigue when stressed to less than half their ultimate capacity. Finally, FRP bars have a coefficient of thermal expansion that is close to that of concrete, which is important in situations where a large thermal gradient is expected (Ehsani, 1992).

There are several obstacles, however, to overcome in using FRP reinforcement in concrete. The most critical of these is the fact that the material is linear elastic up to failure. Properly designed steel reinforced concrete is under-reinforced so the reinforcement will yield (ductile behavior) before the concrete is crushed in compression. In effect, under-reinforcing a structure with FRP will result in a brittle failure of the reinforcement. The resulting lack of ductility in the FRP reinforced structure provides no warning signs of distress and compromises the safety of the public. Over-reinforcing a structure with FRP will result in concrete failure in compression, which is a brittle failure mode as well.

As stated earlier, the modulus of elasticity (Young's Modulus, E) of most FRP reinforcement is lower than that of steel. The result is larger deflections and crack widths for a given stress. While neither result jeopardizes the safety of the public, they are serviceability issues that must be considered. These serviceability concerns ultimately limit the stress that can be developed in the reinforcement; therefore, in many cases the ultimate strength of the bar will not affect design. Due to these differences, there is adequate evidence that the reduced modulus of elasticity could also affect the bond and shear performance of FRP reinforced concrete.

The cost of reinforcement is another issue that may restrict wide spread use. Based on stiffness, CFRP reinforcement is 10 to 25 times the cost of steel reinforcement (Jerrett, 1995). The same is true of GFRP and AFRP bars. Though there is certainly life-cycle cost benefits associated with FRP reinforcement, many projects may not be able to afford the capital expenditure required to incorporate this type of reinforcement.

Fiber reinforced plastic reinforcement is not subject to standards governing its production. This has led to a plethora of different fiber types, resin matrices, and deformations or coatings. Although there are a multitude of different FRP bars on the market, most commercially available bars are produced by a pultrusion process. An example of this process is shown in Figure 1.1 for the production of a GFRP bar.

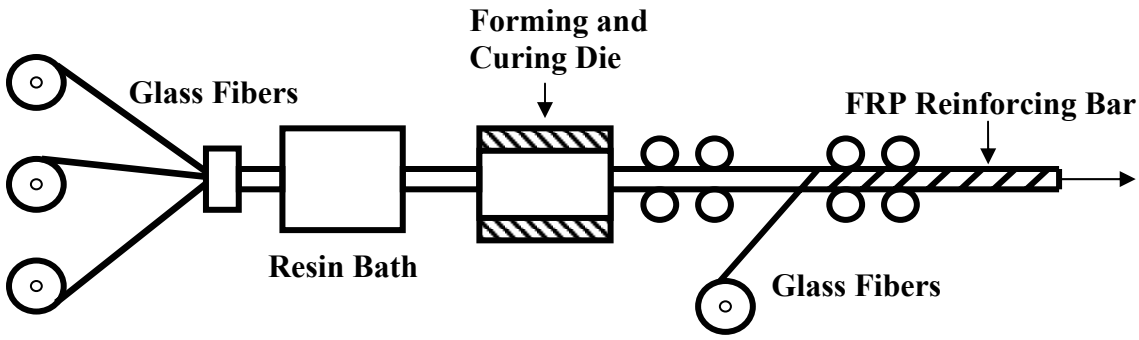

Figure 1.1: Production of a GFRP Bar

The production of most FRP bars involves pulling a multitude of fibers through a resin bath as shown on the left side of the figure. The fiber-resin matrix continues through a series of forms, giving it a circular cross-section, while a curing compound is applied. The FRP bar then passes through rollers that produce the desired diameter and help prevent die wicking (formation of voids in the bar). Finally, surface indentations can be applied to the bars before the matrix hardens. The process in Figure 1.1 shows a helical wrapping of glass fibers around the exterior of the bar. This is one of many methods that FRP reinforcing bar producers have developed to help improve bond characteristics. There are three main methods for improving the bond characteristics: forming deformations or indentations onto the bars, wrapping fibers around the exterior of the bar, and coating the surface of the bar with sand. The first two methods aim to improve bond by increasing bearing, whereas the latter improves bond by increasing friction.

1.3 Bond Background

As Ersoy (Ersoy, 1994) states, "reinforced concrete is the happy marriage of reinforcing bar and concrete." A reinforced concrete member generally relies on concrete to resist flexural compressive stress. When the concrete can no longer do so, reinforcement resists flexural tensile stress. Any structural system that is based on reinforced concrete, whether the concrete is reinforced with steel or fiber reinforced polymers (FRP), relies on the bond between the concrete and the reinforcing material for the successful transferal of stress from concrete to reinforcement. A system devoid of adequate bond will fail, likely in a very brittle manner. In order to design satisfactory reinforced concrete structures and make for a "happy marriage," appropriate development lengths must be provided.

Bond stresses are present in reinforcement whenever there is a change in stress along the length of the reinforcement. There are several mechanisms that contribute to bonding action and allow the reinforcement to resist the forces or stresses imparted on it. First, there is adhesion between the concrete and the reinforcing material. The amount of adhesion is highly dependent on the characteristics of the concrete and the reinforcing material in question. The second mechanism is friction between the concrete and reinforcement. This mechanism is dependent on the concrete quality, surface texture of the reinforcement, and the presence of confining (radial) pressure. If a smooth, cylindrical length of reinforcement embedded in concrete was pulled to a stress that exceeded the bond stress contributed by those two mechanisms alone, the system would experience slip and would fail immediately. Adhesion and friction generally do not generate a significant amount of bond stress. Therefore, deformations are manufactured on reinforcement, thus generating a third bond mechanism, which is referred to as bearing or mechanical interlock (MacGregor, 1997). The forces due to bearing on reinforcement deformations are shown in Figure 1.2. From statics it can be concluded that equal and opposite forces bear on the concrete.

The bearing of concrete on reinforcement deformations causes two force components, a longitudinal and radial component. If the longitudinal component is large enough, the concrete between successive deformations shear, resulting in a pullout failure. Alternatively, when reinforcement with low shear strength is used, the deformations may shear off the reinforcing bar. If the radial component of bearing is large enough, the concrete surrounding the reinforcement can split along the length of the bar. The cracks caused by this phenomenon are called splitting cracks, which can propagate to the surface of the concrete and are potential failure planes. The resultant of the longitudinal and radial components is inclined at an angle, β, which is dependent on the materials involved.

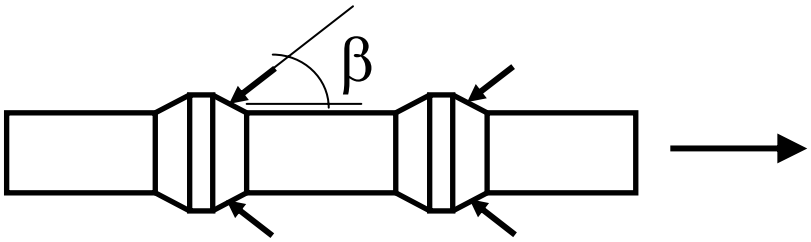

Figure 1.2: Bearing Forces Applied to Reinforcement

1.3.1 Failure Modes

There are generally two modes of bond failure. The first is often termed a pullout failure, which is caused by high longitudinal stress. The second is termed a splitting failure, which is caused by high radial stress. A splitting failure is considered a lower bound failure mode as it can occur at a lower reinforcement stress than a pullout failure. The failure planes associated with a splitting failure are shown in the cross-sections illustrated in Figure 1.3. The reinforcement stress at which splitting failure occurs is primarily a function of the minimum distance between reinforcing bars in a plane or the concrete cover provided, the tensile strength of the concrete, and the average bond stress (MacGregor, 1997).

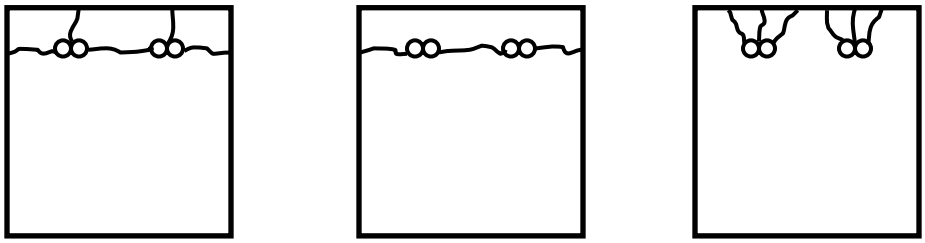

(a.) Side and top splitting **(b.) Side splitting** **(c.) Top splitting**

Figure 1.3: Splitting Cracks

It is important to note that the amount of cover affects the stress that a reinforcing bar can develop. For a given development length, providing smaller covers results in lower stress levels being developed by the reinforcement at failure. In under-reinforced members, additional concrete cover does not provide additional flexural strength because the steel yields before the concrete fails in compression. Consequently, designers typically provide the minimum amount of cover allowed by the governing design code. Therefore, the minimum cover requirement often controls the maximum bond stress that can be developed.

The minimum cover is generally specified by building codes and is based on exposure conditions. Since the concrete often serves as the only source of corrosion protection, concrete exposed to weather requires more cover than concrete that is not. However, since FRP reinforcement does not need a corrosion barrier, it is likely that the amount of cover required would be similar to that required of steel reinforced concrete that is not exposed to weather.

1.3.2 ACI 318-71 Design Provisions

The development length design provisions used presently in ACI 318-99 (ACI 318, 1999) are remarkably different from those used 25 years previously. The contemporary design equation at that time was the equation in ACI 318-71 (ACI 318, 1971), which was in the following form:

$$l_d = 0.04 \frac{a_b \ f_y}{\sqrt{f'_c}} \qquad \text{(Eq. 1-1)}$$

where:

$l_d = development\ length\ of\ reinforcement, (in.)$

$A_b = cross\text{-}sectional\ area\ of\ reinforcing\ bar, (in.^2)$

$f_y = specified\ yield\ stress\ of\ reinforcement, (psi)$

$f'_c = specified\ compressive\ strength\ of\ concrete, (psi)$

The equation was designed so that the calculated development length develops 5/4 of the yield stress of the reinforcement, thus helping insure ductility in the design. In addition, the derivation was based on a maximum bond stress of 800 psi. The 5/4 term is "hidden" in the 0.04 factor on the right side of the equation. No ϕ factor is included in the equation because a ϕ factor of 0.9 is already included in the flexural design (ACI 318, 1971). It is important to note that Equation 1-1 does not consider the effect of concrete cover or presence of transverse reinforcement, which both play an important role in splitting behavior.

1.3.3 Orangun Equation

In a paper published in the March 1977 ACI (American Concrete Institute) Journal, Orangun, Jirsa, and Breen (Orangun, 1977) proposed a development length design equation based on a non-linear regression analysis of available test data. All test data included specimens that were reinforced with steel.

The design equation suggested by Orangun et. al. accounts for the effect of concrete cover and the presence of transverse reinforcement and is shown below:

$$l_d = \frac{10{,}200\ d_b}{\sqrt{f'_c}\ (1 + 2.5 \frac{C}{d_b} + K_{tr})\ \phi} \geq 12\ in. \qquad \text{(Eq. 1-2)}$$

where:

$l_d = development\ length\ of\ reinforcment, (in.)$

$d_b = diameter\ of\ reinforcing\ bar, (in.)$

$f'_c = specified\ compressive\ strength\ of\ concrete, (psi)$

$C = lesser\ of\ clear\ cover\ or\ 1/2\ clear\ spacing\ between\ bars, (in.) \leq 2.5$

$K_{tr} = \frac{A_{tr}\ f_{yt}}{600\ s\ d_b} \leq 2.5$

$\phi = capacity\ reduction\ factor = 0.8$

$A_{tr} = area\ of\ transverse\ reinforcement\ normal\ to\ C, (in^2)$

$f_{yt} = specified\ yield\ stress\ of\ transverse\ reinforcement, (psi)$

$s = spacing\ of\ transverse\ reinforcement, (in.)$

Equation 1-2 was developed for Grade 60 reinforcement (f_y = 60 ksi), therefore, f_y does not appear in the equation. The authors recommend the development length calculated in Equation 1-2 be multiplied by the applicable factors given below:

Grade 40 Reinforcement 0.6
Grade 75 Reinforcement 1.3
Top Reinforcement (12 in. of concrete below bar)..... 0.9
Wide Spacing, $C_s/(C_b d_b) > 3$ 0.9
Wide Spacing, $C_s/(C_b d_b) > 6$ 0.7
Reinforcement in a flexural member in excess of that required ..... $(A_{s,req}/A_{s,pro})$

where:

C_s = half clear spacing between bars or splices or half available concrete width per bar or splice resisting splitting in the failure plane, in.
C_b = clear bottom cover to main reinforcement, in.
d_b = diameter of main reinforcement, in.
$A_{s,req}$ = area of steel required, in^2
$A_{s,pro}$ = area of steel provided, in^2

While the equation accounts for cover and transverse reinforcement, it becomes an abstract and cumbersome design provision. Comparison of Equation 1-1 and Equation 1-2 indicates an increase in development length of 10-25% for minimum cover and spacing over that required by Equation 1-2, whereas development lengths of large diameter bars in the presence of increased cover and transverse reinforcement decrease by as much as 60% (Orangun, 1977).

1.3.4 ACI 318-99 Design Provisions

Significant changes to the development length equation in the ACI 318 Building Requirements have been made recently, specifically in 1989 and 1995. While a historical background of the current equation is not necessary, it should be said that the current equation is based on the recommendations proposed by Orangun et. al. (Orangun, 1977), but is not quite as abstract or cumbersome to the designer as the original equation. The development length equation for ACI 318-99 (ACI 318, 1999) is the following:

$$\frac{l_d}{d_b} = \frac{3}{40}\frac{f_y}{\sqrt{f'_c}}\frac{\alpha\beta\gamma\lambda}{\left(\frac{c + K_{tr}}{d_b}\right)} \qquad \text{(Eq. 1-3)}$$

where:

l_d = development length of reinforcment, (in.)
d_b = diameter of reinforcing bar, (in.)
f'_c = specified compressive strength of concrete, (psi)
f_y = specified yield strength of reinforcement, (psi)
c = lesser of clear cover or 1/2 clear spacing between bars, (in.) ≤ 2.5
α = reinforcement location factor
β = coating factor
γ = reinforcement size factor
λ = lightweight aggregate factor
K_{tr} = transverse reinforcement index $= \dfrac{A_{tr} f_{yt}}{1500\, s\, n}$
A_{tr} = area of transverse reinforcement within s crossing the failure plane, (in^2)
f_{yt} = specified yield stress of transverse reinforcement, (psi)
s = spacing of transverse reinforcement, (in.)
n = number of bars being developed along the plane of splitting

The values of the modification factors (Greek letters) are the following:

α = Bar Location Factor
- Horizontal reinforcement with more than 12 in. of fresh concrete cast below the development length 1.3
- Other reinforcement 1.0

β = Coating Factor
- Epoxy-coated bars with cover less than $3d_b$, or clear spacing less than $6d_b$ 1.5
- All other epoxy-coated bars 1.2
- Uncoated reinforcement 1.0

γ = Bar Size Factor
- No. 6 and smaller bars 0.8
- No. 7 and larger bars 1.0

λ = Lightweight Aggregate Concrete Factor
- When lightweight aggregate is used 1.3
- However, when f_{ct} is specified, λ shall be permitted to be taken as $6.7\sqrt{f'_c}\,/\,f_{ct}$ but not less than 1.0
- When normal-weight concrete is used 1.0

The value of f_{ct} is specified as the average splitting tensile strength of lightweight aggregate concrete in psi. The product of $\alpha\beta$ need not be greater than 1.7.

The minimum development length of a straight bar is specified as 12 in. The code limits the value of $(c + K_{tr}) / d_b$ to a maximum of 2.5, which as the commentary indicates, guards against a pullout failure. Since the code acknowledges the effect of cover on splitting behavior, it is important to report the minimum cover and spacing requirements specified in the code.

For any concrete exposed to earth or weather, the minimum cover shall be:

No. 6 through No. 18 bars	2 in.
No. 5 bar or smaller	1 ½ in.

For concrete not exposed to weather:

Beams and Columns	1 ½ in.

The minimum spacing between parallel bars in a layer is specified as d_b, but not less than 1 in.

1.3.5 AASHTO Design Specifications

The American Association of State Highway and Transportation Officials (AASHTO) produces *Standard Specifications For Highway Bridges* and *AASHTO LRFD Bridge Design Specifications*, both of which include pertinent information required for the design of highway bridges. Since FRP reinforcement clearly has applications beneficial to the service life of highway superstructures, the specifications of AASHTO should be taken into consideration. The development length provisions set forth in the *AASHTO Standard Specifications, Sixteenth Edition (AASHTO, 1996)* (*AASHTO LRFD Bridge Design Specifications (AASHTO, 1998)* development length provisions are the same) are found in Chapter 8 as follows:

No. 11 bars and smaller:

$$l_d = 0.04 \frac{A_b \; f_y}{\sqrt{f'_c}} \qquad \text{(Eq. 1-4)}$$

but not less than:

$$0.0004 \, d_b \; f_y$$

where:

l_d = *development length of reinforcement, (in.)*

A_b = *cross-sectional area of reinforcing bar, (in^2)*

f_y = *specified yield stress of reinforcement, (psi)*

f'_c = *specified compressive strength of concrete, (psi)*

Clearly, Equation 1-4 is the same as Equation 1-1. However, the code includes multiplication factors for a number of different conditions. The following factors shown are to be multiplied by the development length calculated in Equation 1-4:

Top reinforcement
with more than 12 in. of fresh concrete cast below the reinforcement.....1.4

Lightweight aggregate concrete
when f_{ct} is specified..... $\frac{6.7\sqrt{f'_c}}{f_{ct}}$
but not less than 1.0
When f_{ct} is not specified
"all lightweight" concrete..... 1.33
"sand lightweight" concrete.....1.18
Linear interpolation may be used when partial sand replacement is used.

Bars coated with epoxy
with cover less than $3d_b$ or clear spacing between bars less than $6d_b$..... 1.5
All other cases.....1.15
The product obtained when combining the factor for top reinforcement with the applicable factor for epoxy coated reinforcement need not be taken greater than 1.7.

Reinforcement being developed in the length under consideration is spaced laterally at least 6 in. on center with at least 3 in. of clear cover measured in the direction of spacing.....0.8

Anchorage or development for reinforcement strength is not specifically required or reinforcement in flexural member is in excess of that required by analysis ... . (A_s required)/(A_s provided)

Reinforcement is enclosed within a spiral of not less than ¼ in. in diameter and not more than 4 in. pitch 0.75

The development length calculated including multiplication factors shall not be less than 12 in.

The provisions state that the minimum distance between bars shall be no less than 1.5 bar diameters, 1.5 times the maximum aggregate size, or 1 ½ in. The cover requirements are summarized below:

Concrete exposed to earth or weather:	
Primary reinforcement	2 in.
Stirrups, ties, and spirals	1 ½ in.
Top reinforcement exposed to deicing salts	2 ½ in.
Concrete not exposed to earth or weather:	
Primary reinforcement	1 ½ in.
Stirrups, ties, and spirals	1 in.

1.3.6 Research on Bond of FRP Reinforcement

A literature review of research performed on bond in reinforced concrete identified two widely used bond test methods, pullout and beam tests. The majority of research performed on the bond of FRP reinforcement to concrete has been in the form of pullout tests. Pullout tests, while relatively inexpensive and easy to perform, subject concrete around the bonded rebar to confining pressure, which can provide an overestimate of bond strength. Beam tests are considered to provide a more realistic representation of bond behavior; and therefore, bond strengths that are more accurate. Examples of each type of test setup can be seen in Figure 1.4.

Pullout tests (Figure 1.4(a.)) do not generate forces that are an accurate reflection of the conditions that a reinforcing bar in reinforced concrete is subjected to in normal service conditions. In reinforced concrete, bending is generally the mechanism that introduces tension into the reinforcement, not an axial load. Between cracks in the concrete, the tensile stress is shared between the reinforcement and the concrete, and the stress is transferred by what is called in-and-out bond stresses. Due to the fact that pullout tests generate confining pressure on the concrete surrounding the reinforcement, the concrete is not free to crack; and consequently, no in-and-out bond stresses can develop (MacGregor, 1997).

Tests of 48 beam and 18 pullout specimens by Ehsani et al. (Ehsani, 1992) indicate lower bond strengths for beam specimens than pull-out specimens. Zenon et al. (Zenon, 1998) observed the same phenomenon. Therefore, test results from pullout tests represent upper-bound bond strength. Despite this drawback, pullout tests are valuable in investigating the possible bond benefits of particular aspects of different FRP reinforcement. Comparing different deformation heights and spacing as well as different surface coatings are appropriate uses of pullout tests. The conclusions of several of the testing programs involving pullout tests are described below, and although not specifically addressed, other literature (Boothby, Cosenz, Jerrett) has indicated similar findings.

Nanni et al. (Nanni, 1998, Nanni and Al-Zahrani, 1995, Nanni and Bakis, 1995, Nanni and Boothby, 1995) and Larralde et al. (Larralde and Silva-Rodriguez, 1993, Larralde and Mueller-Rockholz, 1998, Larralde and Silva-Rodriguez, 1994) have conducted pullout tests on a variety of FRP bars. Both have reported that the failure was governed by shearing of the bar deformations. In pullout tests with steel reinforced specimens, the failure is generally governed by crushing of the concrete in front of the deformations. Nanni concluded that the failure mode in FRP reinforced specimens indicated that the resin was the controlling parameter and found that epoxy based resins performed better than vinyl-ester resins. Failure of the deformations before reaching the ultimate bar capacity is a serious concern in utilizing FRP reinforcement.

Karlsson (Karlsson, 1997) and Tepfers et al. (Tepfers, 1998) reported three modes of failure in pull-out tests performed with FRP bars. Crushing of the concrete, shearing of the reinforcement deformations, and a combination of the two modes was observed for concrete strengths of approximately 4,200 psi, 8,500 psi, and 6,200 psi, respectively. Apparently, the benefit of high concrete strengths on bond strength can be undermined by the lack of reinforcement deformation shear strength. Tests by Malvar (Malvar, 1994, Malvar, 1995) indicate that deformations formed simultaneously with the bar performed better than those that were applied afterward.

A beam test in which the reinforcement is spliced in a region of constant moment is shown in Figure 1.4(b.). It should be noted that this is only an example of a beam test setup, as many different setups have been reported in the literature. The major findings of beam tests by Zenon et al. (Zenon, 1998), Ehsani et al. (Ehsani, 1992), Kanakubo et al. (Kanakubo, 1992, Kanakubo, 1993), Makitani et al. (Makitani, 1992), and Tighiouart et al. (Tighuart, 1998) are summarized below:

- Bar stresses increase as development length increases, but the relationship between development length and bar stress developed is not linear.
- When the mode of failure is splitting, an increase in concrete strength results in a pronounced increase in bond strength.
- Development lengths between 1.3 and 1.9 times the development length required of a comparable steel specimen are required for FRP bars.
- Bond strengths are higher for smaller diameter bars.
- A top bar effect was observed indicating a reduction in bond strength ranging from 1.1 to 1.3 for bars cast above more than 12 in. of concrete.
- There is no consensus regarding the effect of the modulus of elasticity of the fibers in the reinforcement on bond performance.

Limited investigations have been conducted regarding the deterioration of bond in aggressive environments. Al-Dulaijan et al. (Al-Dulaijan, 1996) found significant bond degradation after subjecting specimens

to high pH and temperature. This effect should be investigated further since concrete is an alkali environment (high pH), and in many instances is subjected to high temperatures. Mashima and Iwanmoto (Mashima, 1992) conducted pullout tests on specimens made with several types of FRP after performing up to 600 cycles of freezing and thawing. Their findings indicate that Aramid fiber bars do not perform well after repeated freeze-thaw cycles, a condition that can be experienced in bridge decks. Bond strength reduction was as much as 50% in 500 cycles.

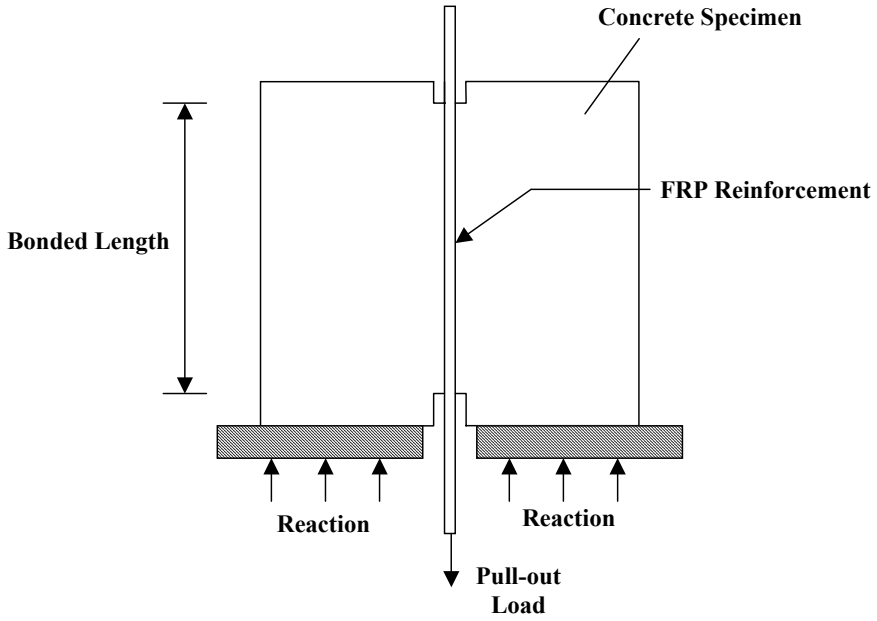

(a.) Pullout Test Setup (Adapted from Reference 15)

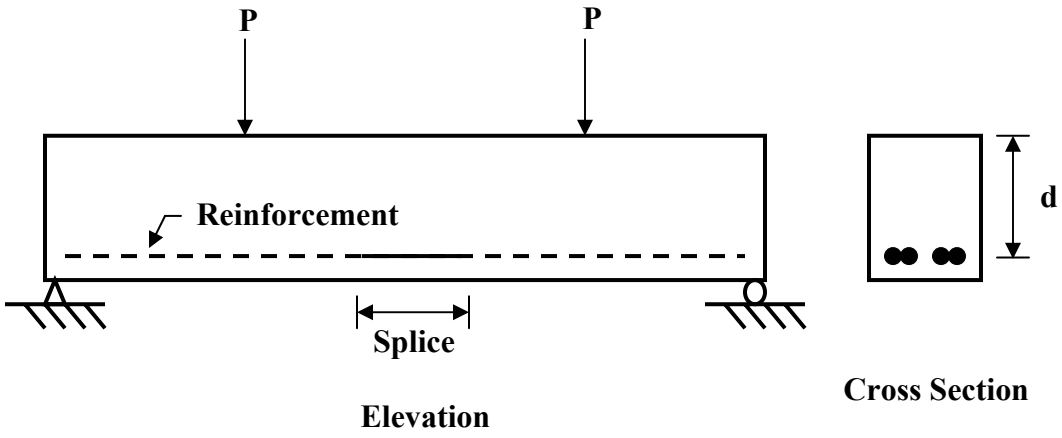

(b.) Beam Test Setup

Figure 1.4: Types of Bond Tests

1.3.7 ACI Committee 440 Proposed Recommendations

ACI Committee 440 has proposed the *Guide for the Design and Construction of Concrete Reinforced with FRP Bars (ACI 440, 2000)* based on research and experience generated to this point. While the guide has not been

endorsed outside of the committee or distributed by ACI for public use, it is likely that many of the recommendations will be eventually published and incorporated into a design document. Chapter 11 of the proposed guide involves the development of FRP reinforcement in concrete.

For splitting controlled failure, the committee has suggested the following equation:

$$l_{bf} = K_2 \frac{d_b^{\,2} f_{fu}}{\sqrt{f'_c}} \qquad \text{(Eq. 1-5)}$$

where:

l_{bf} = development length required, (in.)

K_2 = constant determined experimentally

d_b = reinforcing bar diameter, (in.)

f_{fu} = design tensile strength of reinforcement considering environmental factors, (psi) = $C_E\ f_{fu}$*

C_E = environmental reduction factor, dependent on fiber type and exposure conditions

f_{fu}* = guaranteed tensile strength, (psi)

f'_c = specified concrete strength, (psi)

The value of f_{fu} is defined as the mean tensile strength of a sample of test coupons minus three standard deviations. The committee proposes values of C_E based on fiber type and exposure conditions, which are shown in Table 1.1.

Table 1.1: Proposed Values of C_E

Exposure Condition	Fiber Type	Environmental Reduction Factor, C_E
Concrete not exposed to earth and weather	Carbon	1.0
	Glass	0.8
	Aramid	0.9
Concrete exposed to earth and weather	Carbon	0.9
	Glass	0.7
	Aramid	0.8

The proposed document does not recommend a specific value for K_2, but the K_2 factors suggested by several investigators are shown in Table 1.2. The equation is in the same form as the development length equation in the AASHTO specification and ACI 318-77. The $\pi/4$ term that is included in the bar area of Equation 1-1 is absorbed by the K_2 term in Equation 1-5.

Table 1.2: Proposed K_2

Investigator	K_2
Pleimann (Pleimann)	1/19.4 (GFRP) 1/18.0 (AFRP)
Gao (Gao, 1998)	1/16.7
Ehsani (Ehsani, 1996)	1/21.3
Tighiouart (Tighiouart, 1998)	1/15.6

For pullout controlled failure, the committee has suggested the following equation:

$$l_{bf} = \frac{d_b \ f_{fu}}{2700} \qquad \text{(Eq. 1-6)}$$

The form of this development length equation (Equation 1-6) is unique in comparison to the others discussed thus far. According to this recommendation, the development length is not dependent on $\sqrt{f'_c}$.

The design recommendations state, "if the concrete cover exceeds two bar diameters, a pull-out failure is more likely…" (ACI 440, 2000). The committee does not specify which equation should be used in design, but does recommend a modification factor be used with Equation 1-6. This modification factor, called a concrete cover modification factor, is recommended in instances in which the cover is between d_b and $2d_b$, and varies linearly from 1.5 to 1.2. For cover greater than $2d_b$ the modification factor becomes 1.0. The committee recommends that concrete cover should be no less than d_b.

The development length calculated in either Equation 1-5 or 1-6 should be multiplied by a bar location modification factor of 1.3 if the reinforcement layer is above more than 12 in. of concrete.

1.4 Shear Background

1.4.1 Mechanisms of Shear Transfer

A century of research has been conducted on shear in reinforced concrete beams without transverse reinforcement. However, an understanding of shear behavior is still limited. Therefore design methods are based on empirical formulations based on laboratory tests and observations. A 1973 ACI-ASCE Committee 426 (Shear Strength of Reinforced Concrete Members) report (ACI 426, 1973) identified four mechanisms of shear transfer; namely, shear stresses in the uncracked concrete, interface shear transfer, dowel action of the longitudinal reinforcing bars, and arch action. Since that report was published, the 1998 ACI-ASCE Committee 445 (Shear And Torsion) report (ACI 445, 1998) has identified a fifth mechanism of shear transfer, residual tensile stresses transmitted directly across cracks. These five mechanisms are illustrated in Figure 1.5 and will be discussed in more detail in the following. The labels in the figures coincide with the headings in the discussion that follows.

a) *Shear Stresses in Uncracked Concrete:* This shear transfer mechanism is the simplest and occurs in uncracked members and uncracked portions of cracked reinforced concrete members (Figure 1.5). The interaction of shear stresses with compressive and/or tensile stresses on the uncracked concrete produces a complex state of stresses. Depending on whether the principal tensile or compressive stresses produced from this stress field reach the corresponding strength of concrete, failure may occur either by inclined cracking (tensile strength reached) or crushing of the concrete (ACI 426, 1973) (compressive strength reached). MacGregor (MacGregor, 1997) states that this component may be capable of carrying approximately 30% of the total shear force.

b) *Interface Shear Transfer:* This shear transfer mechanism, labeled as (b) in Figure 1.5, relies on friction along the inclined crack interface which develops as the two crack surfaces slide relative to each other. Physically the aggregates protruding from the crack surface provide resistance against this slip. The mechanism was widely accepted as a shear transfer mechanism after it was described and recognized in the 1973 ACI-ASCE Committee 426 report (ACI 426, 1973), based on research by Fenwick and Paulay (Fenwick, 1968), Mattock and Hawkins (Mattock, 1972), and Taylor (Taylor, 1970). The ability of this mechanism to transfer shear depends on three factors: crack normal stresses, crack widths, and the amount of crack slip (ACI 426, 1973). As the crack width and slip increase the ability of the crack interface to transfer shear decreases. In addition, compressive stresses normal to the crack increase the shear transfer along the crack while tensile stresses decrease the shear transfer. Ersoy (Ersoy, 1994) reports that measurements on test beams without web reinforcement by indicated that 50 to 70% of the total shear might be resisted by interface shear transfer.

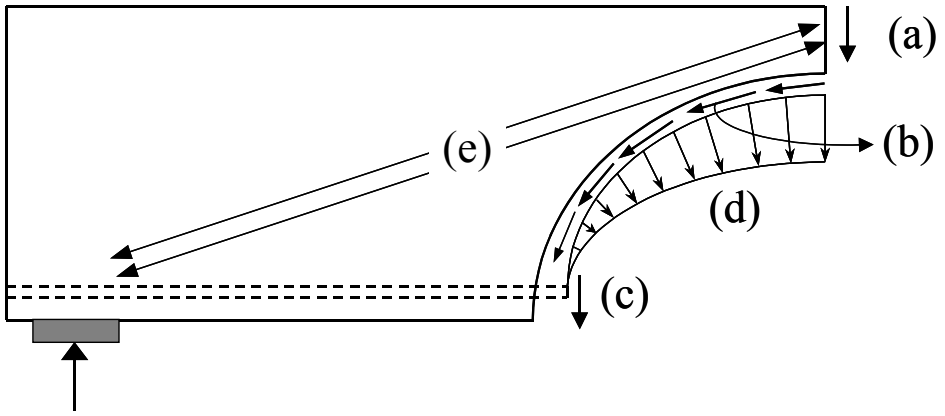

Figure 1.5: Shear Transfer Mechanisms in A Beam without Transverse Reinforcement

c) *Dowel Action:* Where longitudinal reinforcement crosses an inclined crack, it serves as a dowel transmitting shear forces across the crack (mechanism (c) in Figure 1.5). When these shear forces, combined with radial forces developed by bond forces exceeds the tensile strength of the area of concrete supporting the bars, splitting along the longitudinal reinforcement occurs. In a beam without transverse reinforcement, the strength of this action depends on the area and tensile strength of the concrete supporting the dowel bars and the crack width at the level of the dowel (Vintzeleou, 1986). As the crack width increases and/or the strength of concrete support under the bars decreases the amount of dowel shear that can be transferred decreases. It is very difficult to quantify the amount of dowel force that can be activated in any given situation; therefore, there are only semi-empirical methods treating very simple cases involving one bar are available (Vintzeleou, 1986). Due to the difficulty of quantifying dowel action separately, in general, design codes treat the dowel contribution to shear strength implicitly.

d) *Residual Tensile Stresses across Cracks:* When concrete is loaded in direct tension with a displacement controlled actuator, a significant softening branch is obtained after the peak tensile stress is reached (Gopalaratnam, 1985, Reinhardt, 1986). This softening branch is attributed to residual tensile stresses across the crack after concrete cracks. Residual tensile stresses can be explained as follows. When concrete cracks, a "clean break" does not occur. Small pieces of concrete bridge the crack and continue to transmit tensile force up to crack widths in the range of 0.002-0.006 in. (ACI 445, 1998). Reineck (Reineck, 1991) has found that residual tensile stresses across inclined cracks can provide a significant percentage of shear resistance for very shallow members (for depths less than about 4-in.), where the width of flexural and diagonal tension cracks is small.

e) *Arch Action:* Saint Venant's principle suggests that a local disturbance such as a concentrated load or reaction will dissipate in approximately one beam depth from the point at which it is applied. Schlaigh et al (Schlaigh, 1987) called these regions in a beam as D-regions, where the D stands for discontinuity or disturbed. Therefore, shear transfer by arch action (labeled (e) in Figure 1.5) is most pronounced in reinforced concrete beams with shear span to effective depth (a/d) ratios less than 2.5, where there is overlapping of the D-regions. In Figure 1.6, nominal shear strength of reinforced concrete beams without transverse reinforcement vs. a/d ratio was plotted to illustrate the effect of arch action. Figure 1.6 indicates that there is a significant increase in the nominal shear strength for a/d ratios less than approximately 2.5 to 3. This increase is attributed to increased arch action due to overlapping of D-regions in the beams.

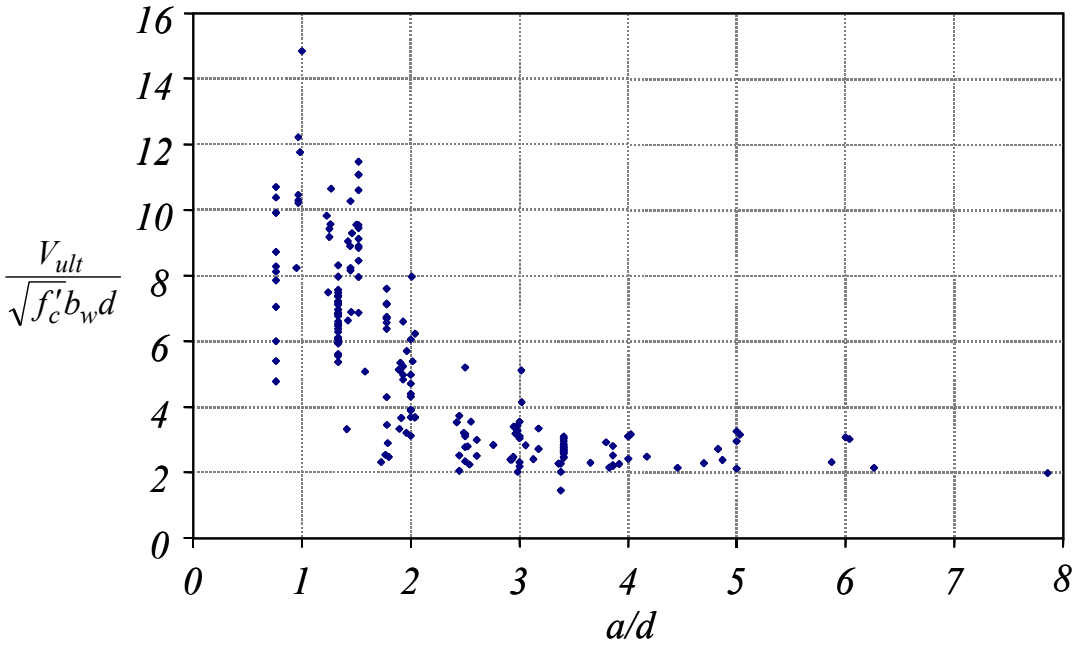

Figure 1.6: The Influence of Arch Action on Shear Strength

Any region, which is not a D-region, is called a B-region, where the B stands for beam or Bernoulli. A very simple illustration of these regions is provided in Figure 1.7. Arch action is different from the other transfer mechanisms because it does not transfer shear along the crack interface. As illustrated in Figure 1.5, arch action transfers the shear to the supports through a compression strut extending between the concentrated load and the supports.

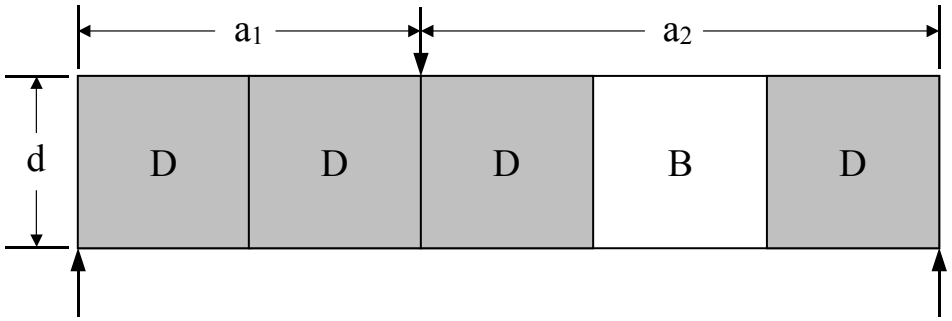

Figure 1.7: D and B-Regions in a Beam

For arch action to occur, it is necessary for load to be applied at the top of the beam while it is supported at the bottom by non-yielding supports, Figure 1.7. Arch action cannot be mobilized with support or loading arrangements shown in Figure 1.8. In addition, a horizontal tensile force to balance the compression strut must be developed at the base of the arch. This horizontal force can be developed by well-anchored longitudinal reinforcement located at the tension side of the beam.

Shear transfer in B-regions is primarily attributed to the other four mechanisms discussed previously. Therefore, the shear strength and behavior of longer beams (a/d > 2.5), where B-regions exist, is determined by beam action mechanisms and their strengths as previously discussed.

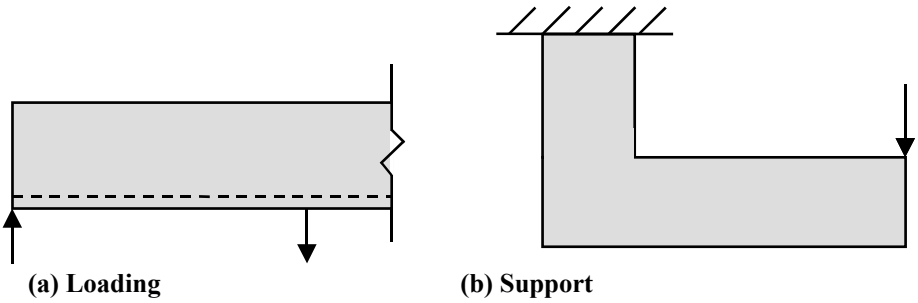

Figure 1.8: Examples of No Arch Action

1.4.2 Types of Shear Failure

Modes of shear failures for reinforced concrete beams of rectangular cross sections without transverse reinforcement, with a/d ratios greater than 1, and with properly anchored longitudinal reinforcement will be discussed in this section. A beam with these qualities will fail either by crushing or cracking of concrete in the compression zone (ACI 445, 1998). Cracking in the compression zone occurs on a horizontal plane due to the combined effect of transverse tensile stresses and compressive stresses exceeding the tensile strength of concrete in this region. Concrete cover splitting along the longitudinal bars in tension may or may not accompany failure in the compression zone. Shear failures, which involve cracking of concrete in the compression zone, are termed diagonal tension failures (DT), and those, which involve crushing in the compression zone, are termed shear compression failures (SC). Experiments reveal that the controlling mode of failure depends primarily on the a/d ratio and longitudinal reinforcement ratio, ρ. Kani (Kani, 1979) found that the concrete strength did not significantly influence the mode of failure (f_c' ranged from 2500 to 5000-psi.). These failure modes are described in detail as follows:

a) *Shear Compression Failure (SC):* Shear compression failures occur in reinforced concrete beams containing typical amounts of reinforcement (ρ = 1%-2%) for a/d ratios ranging from 1.0 to 2.5. The inclined crack is a continuation of a flexural crack for the upper end (a/d = 2.5) of the given a/d ratios. For a/d ratios closer to 1.0, the inclined crack may form by itself independent of the flexural cracks. As the applied load is increased, the inclined crack propagates deeper into the beam and may penetrate the compression zone. A reinforced concrete beam without transverse reinforcement, which is loaded with a concentrated load in the center of a simple span, with fully developed inclined cracks, is illustrated in Figure 1.9(a). Once the inclined cracks are fully developed as illustrated, the bond transfer cannot occur between the reinforcement and concrete between these cracks. Therefore the concrete between these two inclined cracks can be assumed to be non-existent. The beam essentially transforms into an equivalent tied-arch, which can be visualized as shown in Figure 1.9(b). The formation of inclined cracks, however, does not result in failure. Considerably additional loads can be carried through redistribution of internal stresses in the beam. However, since the inclined crack generally extends higher into the beam than a flexural crack, failure occurs at a capacity less than that of the development of the flexural moment capacity. The rotations in such a beam are concentrated in the vicinity of the concrete compression zone under the load point. With further loading these rotations result in compressive stresses higher than the concrete can resist, resulting in failure through crushing of concrete in the vicinity of the concentrated load.

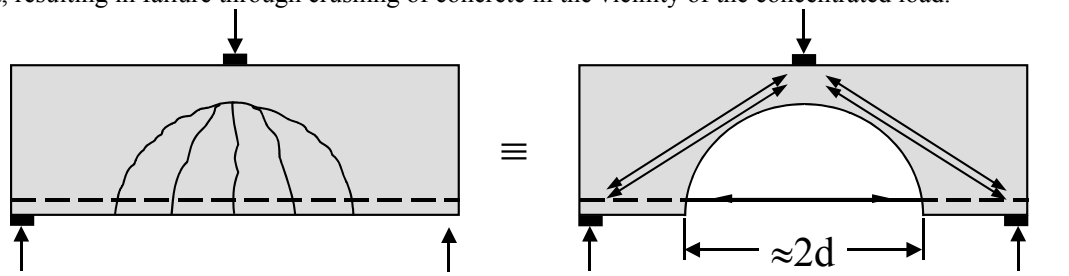

Figure 1.9: Examples of Arch Action

b) *Diagonal Tension Failure (DT):* Diagonal tension failures typically occur in relatively slender beams, where a/d is approximately in the range between 2.5 and 7, with common amounts of longitudinal reinforcement (ρ = 1%-2%). Since there is no overlapping of D-regions in this range of a/d ratios, shear is carried through beam action mechanisms previously discussed. Once an inclined crack forms in a reinforced concrete beam without transverse reinforcement for a/d ratios greater than 2.5, redistribution of stresses does not occur. Therefore, there is little reserve capacity after the onset of inclined cracks. Diagonal tension failure follows shortly afterwards. A typical crack pattern on a beam, which fails in diagonal tension, is shown in Figure 1.10.

The "bolded" crack creates the diagonal tension failure. The inclined portion of the crack penetrating into the compression zone is usually a continuation of a flexural crack. With a small increase of load, the crack penetrates into the compression zone and propagates towards the concentrated load. At the same time, a splitting crack initiates from the tension side of the inclined crack and travels toward the support. It is common for a vertical tension crack to form in the compression zone above the diagonal tension crack. It develops from the top of the beam down to the inclined crack. The sequence of events, however, is disputed among researchers. In particular, there is disagreement as to which of the two cracks form first; the splitting crack on the reinforcement that propagates towards the support or the diagonal crack that penetrates into the compression zone towards the load point.

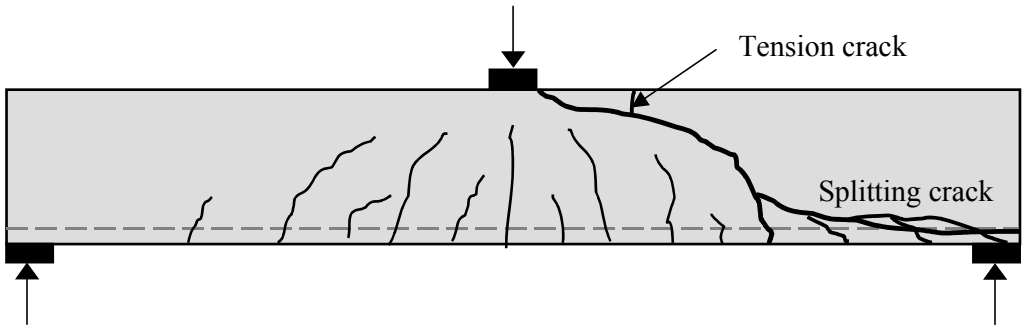

Figure 1.10: Diagonal Tension Failure

The ranges of a/d ratios provided to separate diagonal tension and shear compression failures are only approximate values as observed in tests. In a typical reinforced concrete beam (1% < ρ < 2%), the reinforcement yields prior to shear failure beyond an a/d ratio of 7.0. The longitudinal reinforcement ratio is known to change these ranges, and for heavily reinforced specimens (ρ > 3.0) the upper end of a/d ratios for shear compression failures may shift to 3.0 (Kani, 1979). The same is true for the upper end of a/d ratios for diagonal tension failures; the value can shift up to a value of 9.0. The modes of failures and the range of a/d ratios provided are only valid for simply supported, rectangular beams. Both the mode of failure and the a/d ratio may change for continuous beams and/or T-beams (Kani, 1979).

1.4.3 Factors Influencing Shear Strength

The shear strength attributed to concrete, which is named V_c by the ACI-318 99 Building Code, is affected by 5 primary variables (MacGregor, 1997). These variables will be discussed in more detail.

a) *Tensile Strength of Concrete:* The stress at which inclined cracking occurs is directly related to the tensile strength of concrete. In a beam without external axial forces, tensile stresses arise from the interaction of flexural and shear stresses. When the resulting principle tensile stress from this interaction exceeds the tensile strength of concrete, an inclined crack forms. Since the formation of inclined crack is related to tensile strength of concrete, the inclined cracking load can be related to the tensile strength from split cylinder tests. Since split cylinder tests are not routinely performed in practice, design codes generally use a relationship for the concrete tensile strength that is related to the

specified compressive strength. Tensile strength is often related to $\sqrt{f_c'}$ or $\sqrt[3]{f_c'}$. Therefore, the inclined cracking load of a member is commonly a function of this quantity.

b) *Longitudinal Reinforcement Ratio:* Figure 1.11 shows the relationship between the longitudinal reinforcement ratio, ρ, and V_c for beams without transverse reinforcement.

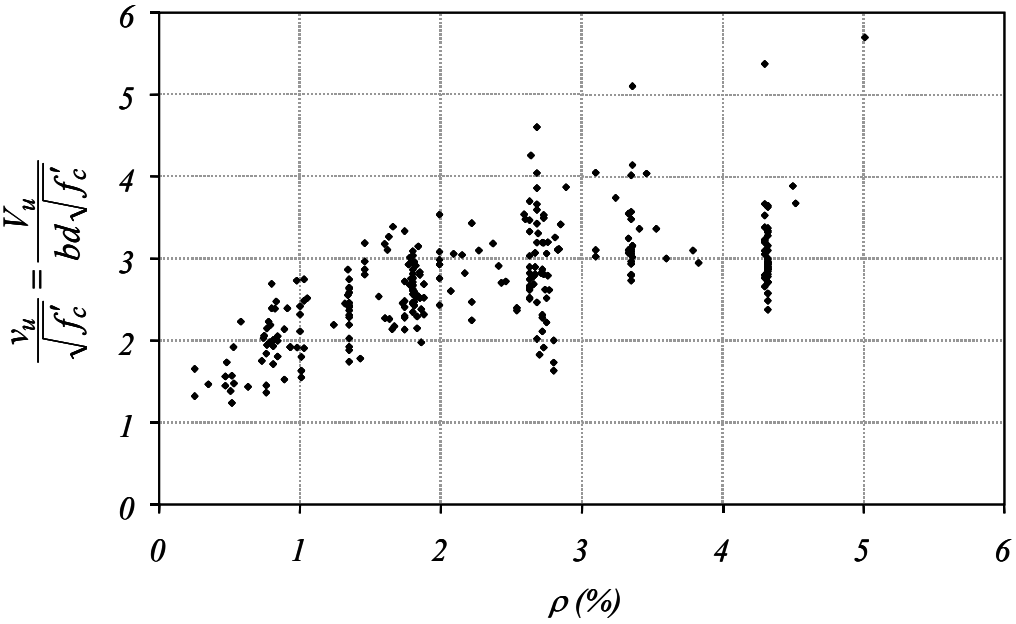

Figure 1.11: Influence of ρ on v_u

The data is taken from Tompos (Tompos, 2000) and filtered to only include beams with a/d ratios greater than 2.75 and concrete strengths less than 8500-psi. The vertical axis indicates the nominal shear stress in the section at failure ($v_u = \frac{V_u}{bd}$) normalized with $\sqrt{f_c'}$. Historically, the nominal shear stress has been used as a measure of shear strength for reinforced concrete beams without transverse reinforcement. Figure 1.11 reveals that the shear strength of beams increase as ρ increases.

The ACI building code uses $2\sqrt{f_c'}$ as the shear stress that produces shear failure. However, as illustrated, for reinforcement ratios less than 1%, the shear stress at failure may be lower than $2\sqrt{f_c'}$. In a beam reinforced with low ρ, flexural cracks penetrate higher into the section and wider cracks are experienced as compared to a beam reinforced with higher amounts of longitudinal reinforcement. Deeper flexural cracks decrease the depth of compression zone thereby reducing the contribution of uncracked concrete to shear strength. Wider cracks, on the other hand, result in a reduction in the shear strength contributions of interface shear transfer as well as residual tensile stresses. Furthermore, the decrease in the amount of longitudinal reinforcement coupled with the increase in crack widths reduces dowel action. Therefore, the longitudinal reinforcement ratio is a very important factor that influences all beam action shear transfer mechanisms. Special attention should be given to the range of ρ less than 1%, where the shear strength is not linearly related to ρ and significant reductions in shear strength can be noted.

c) *Shear Span-to-Depth Ratio (a/d):* The shear span-to-depth ratio, a/d, has a significant effect on the shear strength of a beam without transverse reinforcement. The a/d ratio provides a measure of the arch action contribution to shear strength. Deep beams with a/d ratios less than 2.5 can develop arch action and, therefore, experience an increase in shear strength. In fact, beams with a/d ratios less than

2.5 can carry shear stresses significantly in excess of the ACI 318-99 shear stress value of $2\sqrt{f_c'}$ at failure. For a/d ratios beyond 2.5 to 3, the effect of a/d ratio on inclined cracking shear and shear strength can be neglected (ACI 445, 1998).

d) *Size of beam:* As the overall depth of a beam increases the shear stress at inclined cracking tends to decrease for a given f_c', ρ, and a/d (ACI 445, 1998). The crack width along the depth of a beam without skin reinforcement is a function of the distance from the main reinforcement to the crack location. The crack widths at points above the main reinforcement tend to be wider for deeper beams. Wider crack widths decrease the contribution of residual tensile stress and the interface shear transfer mechanisms to shear strength; thereby reducing v_u. Taylor (Taylor, 1972) showed that when the aggregate and the specimen are scaled appropriately, the decreasing trend of shear strength with increasing beam depth was not observed in tests of such specimens.

e) *Axial Force:* In general, externally applied axial tensile forces tend to reduce the shear strength, while axial compressive forces increase it (ACI 445, 1998). Axial compressive stress delays the onset of flexural cracking and limits the depth of crack penetration into the beam. Axial tensile stresses, on the other hand, produce the opposite effect. However, approximately the same additional increment of shear load is required between flexural cracking in the shear span and inclined cracking regardless of whether there is axial forces (tension or compression) on the specimen or not (ACI 445, 1998). Since slender beams with a/d ratios greater than approximately 2.5 fail shortly after the onset of inclined cracking, the shear strength of such members under axial forces may change significantly due to the change in the onset of flexural cracking. Axial tension or compression, therefore, results in a decrease or increase in the shear strength (V_c) of beams with a/d ratios greater than 2.5. However, The inclination of inclined cracks on beams tested with the existence of axial forces is not significantly affected according to ACI-ASCE Committee 445 (Mattock, 1969).

1.4.4 Shear Strength of FRP Reinforced Concrete Beams Without Stirrups

The Modulus of elasticity (E) of some FRP bars may be lower than that of steel bars. As previously discussed, due to lower modulus of elasticity, there may be a drop in the shear strength of concrete members reinforced with FRP bars (ACI 440, 2000). The shear carrying mechanism for beam action was illustrated in Figure 1.5. This model considers four shear transfer mechanisms: (1) uncracked concrete contribution, (2) aggregate interlock, (3) dowel action, and (4) residual tensile stresses across inclined cracks. Using bars with a lower modulus of elasticity, while keeping the amount of longitudinal reinforcement constant will result in deeper and wider cracks. Deeper cracks translate into a smaller depth of concrete compression zone, which results in a reduction in the shear strength contribution from uncracked concrete mechanism. Naturally, larger crack widths result in a reduction in the shear strength contributions of aggregate interlock, residual tensile stresses, and doweling action. Doweling action is also reduced due to the lower modulus of elasticity. Therefore, there is a reduction in every shear mechanism, which should result in a reduction in the overall shear strength of concrete members reinforced with the FRP bars relative to that of members reinforced with steel.

Experimental research on the concrete contribution to shear strength of FRP bar reinforced concrete members is limited. Most test data on the concrete contribution has been derived from tests that were not designed to study the shear strength of these members. Only three studies describing shear failures of FRP bar reinforced concrete beams without stirrups are available in the literature. These investigations and their conclusions will be briefly summarized.

Nawy et al (Nawy, 1971) studied the flexural behavior of glass FRP reinforced concrete beams. In the experiments, 20 simply supported rectangular beams, 10 containing FRP bars as tensile reinforcement were loaded with concentrated loads at the third spans. All beams were 7 in. deep by 3-1/2 in. wide with effective depths varying from 6.25 in. to 6.5 in. The total specimen length was 78 in. and the distance between supports was 72 in. These dimensions correspond to a/d ratios varying from 3.7 to 3.84. The reinforcement ratio, ρ, was varied from 0.19 % to 0.41 % to obtain flexural failures. The FRP bars were 0.12 in. diameter, smooth bars. The tensile strength was 155-ksi while the modulus of elasticity was 7,300-ksi. The concrete strength from 6x12 in. test cylinders registered strength values ranging from 4000-psi to 5000-psi. All specimens were reported to fail in diagonal tension. Since the investigation was conducted on the flexural behavior of FRP reinforced concrete beams, no attention was given to the shear strength.

Deitz (Deitz, 1998) tested 5 full scale, two-way bridge decks reinforced with #5 glass FRP bars in tension, loaded at the third points with two concentrated loads to study the flexural behavior of FRP reinforced concrete bridge decks. The cross section of the deck panels was 7.5 in. deep by 12 in. wide and the total length of the specimens was 9 ft-9 in. A clear cover of 1 in. was used in both the top and bottom mats. Concrete strengths ranging from 4000 psi to 4500 psi were registered. 3 specimens contained glass FRP bars as reinforcement in both the top and bottom mats (FRP specimens). 2 specimens were reinforced with #5 epoxy coated steel bars in the compression zone and #5 glass FRP bars in the tension zone (hybrid specimens). The a/d ratio was 5.8 for 2 of the FRP specimens and both of the hybrid specimens. Since shear failures were observed in the first two FRP specimens, the a/d ratio of the third FRP specimen was lowered to 4.5 to study the effect of a/d ratio on the behavior. The nominal shear strength v_u of the specimens registered values ranging from $1.25\sqrt{f_c'}$ to $1.41\sqrt{f_c'}$.

Michailuck et al (Michaluck, 1998) tested 8 simply supported one-way concrete slabs reinforced with glass FRP, carbon FRP, and steel. The slabs were loaded with two concentrated loads. No data was provided on the location of these loads. The slabs were 39.4-in. (1-m) wide by 11.5-ft (3.5-m) long with a clear span of 9.84-ft (3-m). Two depths were investigated, 5.9-in. (150-mm) and 7.8-in. (200-mm). The bars were placed in the tension side of the specimens with a clear cover of 1.5-in. (38-mm). Bar sizes were varied (#4, #5 and #6) to achieve reinforcement ratios ranging from 0.23% to 0.96%. Glass FRP bars had a tensile strength of 100 ksi and modulus of elasticity of 6,000 ksi. Similarly, carbon FRP bars had tensile strength of 326 ksi and a modulus of elasticity of 21,300 ksi. Concrete strength varied between 8600 psi and 9600 psi at the time of testing. One glass FRP reinforced specimens, with 150-mm deep and 0.95% reinforcement ratio and one with 200-mm deep and 0.77% reinforcement ratio, failed due to shear failure. The glass bars, crossed by a crack extending vertically almost along the entire depth of the slab in the shear span, were ruptured at failure. It is interesting to note that the measured crack widths on this particular crack in both beams were 9/16 in. (15 mm) wide and the compression zone depth was measured as 9/16 in. (15 mm) prior to failure. It was concluded that the large crack widths eliminated shear transfer by aggregate interlock and the small concrete compression zone contributed little to the shear transfer. Therefore shear was transferred by dowel action beyond the dowel action capacity of the glass FRP bars, which eventually ruptured the bars. From an analytical study, it was found that the dowel action of the bars in these two beams varied from 7.5% to 13.8% of the tensile strength of glass FRP reinforcement. It was recommended that the calculated shear strength of FRP bar reinforced concrete members be multiplied by the ratio of modulus of elasticity of FRP bars to that of steel to determine conservative shear strength estimates. This recommendation was incorporated into Provisional Recommendations for Design of Concrete Members Reinforced with FRP Reinforcement (ACI 440, 2000), prepared by ACI Committee 440 (Committee on FRP Reinforced Concrete)

JSCE Recommendations for Design and Construction of Concrete Structures Using Continuous Fiber Reinforcing Materials (JSCE, 1997) discusses the shear strength of FRP bar reinforced concrete members without stirrups. This document reports that:

> *"Previous studies indicate that the shear capacity of beam members with CFRM (FRP reinforcement) used for tensile reinforcement but without shear reinforcement can generally be evaluated by taking into account the axial rigidity of the tensile reinforcement. V_{cd} is therefore calculated according to the equation used for steel, allowing for the ratio of the Young's modulus of CFRM to that of steel."*

The term V_{cd} is the equivalent of V_c in the ACI 318-99 Building Code. The JSCE document indicates that the reinforcement ratio term (ρ) used in calculations is multiplied by the ratio of modulus of elasticity of FRP bar to that of steel to consider the effect of the axial rigidity of tensile reinforcement.

FRP and steel reinforcement may differ from each other in their physical and mechanical characteristics. These differences are likely to change the behavior of concrete members reinforced with FRP bars from those reinforced with steel. As indicated, the modulus of elasticity of FRP bars has the potential to significantly affect the shear strength of beams without stirrups. This hypothesis is supported by the limited experimental work available in the literature. Experimental work conducted on the shear strength of FRP bar reinforced concrete members without stirrups, however, is extremely limited. Therefore, further research is necessary to develop safe but economical design methods for FRP reinforced concrete members under shear loads.

2. OBJECTIVES AND SCOPE

The objective of this study was to investigate bond and shear performance of concrete reinforced with FRP (non-metallic) reinforcement and develop design recommendations for the development of such reinforcement in bridge decks. To evaluate the bond strength of glass and aramid FRP bars, three series of beam splice tests were conduced. In addition, the cracking and deflection behavior of the test specimens were investigated. To evaluate the shear strength of beams longitudinally reinforced with FRP reinforcement, two series of shear beam tests were conducted. In particular, the effect of the axial stiffness of the tensile reinforcement and the longitudinal reinforcement percentage on the concrete contribution to shear strength for beams with a/d ratios greater than 2.5 was investigated. The following report presents a summary of the experimental studies and the resulting design recommendations. Additional information regarding these studies is available in Mosley, 2000 and Tureyen, 2001.

3. BOND INVESTIGATION

3.1 Introduction

Three FRP reinforcing bars were investigated in the experimental program. Two types of Glass FRP and Aramid FRP reinforcement were supplied by manufacturers for the study. Three series of beams were tested to compare the bond strength of FRP reinforcing bars of various fiber types with the bond strength of conventional Grade 60 steel reinforcement. Each series consisted of four beams, one specimen for each of the three types of FRP reinforcement and one specimen reinforced with steel. Cracking behavior and stiffness of each specimen was observed and recorded.

3.2 Design of Specimens

Each series was designed such that the same test setup could be used throughout the experimental program. The specimen design was similar to that of other tests of bond strength, commonly referred to as beam tests. The configuration of load points and support points were arranged to create a constant moment region in the central span of the specimen (Figure 3.1). This central span is the most critical location for a splice as the constant moment region is devoid of shear forces and the entire splice length is experiencing maximum tensile stress. To provide ease and safety while recording crack widths and taking photographs, the reinforcement was placed in the top of the specimens, which were loaded at the ends and supported on the reaction floor at the quarter-points.

The length of the specimens was dictated by the spacing of the threaded inserts located in the reaction floor of the Kettlehut Structural Laboratory (the inserts are located at 6 ft intervals). Therefore, it was decided that the threaded-rods used to support the loading beam would be located 12 ft apart. The placement of the supports on the floor was important in two respects. First, if the distance between the support and the load point is too short, very high load is needed to produce the required failure moment. Therefore, the threaded inserts could yield or pullout of the floor, or the steel-loading beam could fail. Second, a short distance between the supports will not allow a random distribution of cracks in the constant moment region, thus influencing the cracking behavior of the specimens. Based on calculations, it was concluded that placing the supports 3 ft from the load points would provide adequate moment generating capacity for the range of splice lengths and bar spacings that would be tested in the experimental program. In addition, the 6 ft constant moment region would allow for random crack generation. To accommodate the loading head, an additional 8 ¼ in. was added to each end making the beams a total of 13 ft- 4 ½ in. The specimen dimensions are shown in Figure 3.1.

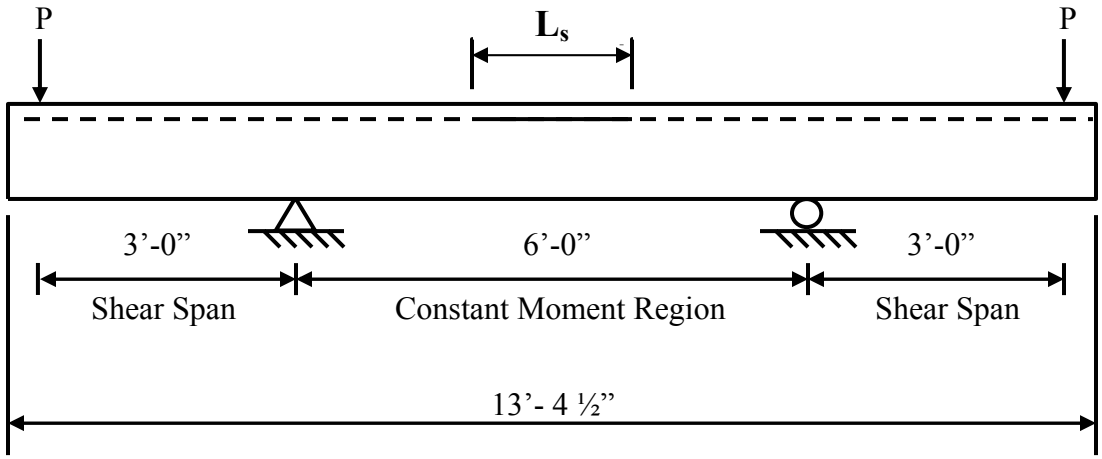

Figure 3.1: Test Setup

To allow bond strength comparisons between the individual tests, it is important that the reinforcement remains in its elastic deformation range. The specimens of each series were designed accordingly. The specimens were reinforced for negative moment by three longitudinal #5 bars in the top of the specimen and were lap spliced in the center of the constant moment region. Series I specimens had a 18 in. splice length, while Series II and III had a

12 in. splice length. There were two bar spacing configurations selected for the experimental program. Series I and II specimens were designed with clear spacing between the bars in the splice zone equal to 1 in. and the side cover equal to 1-½ in. This represents the minimum clear spacing of bars and the minimum cover for reinforced concrete exposed to weather as allowed by ACI 318-99 (ACI 318, 1999). Series III specimens had a center to center bar spacing of 6 in. and side cover of 2-11/16 in. This cover corresponds to half the clear bar spacing and was selected to represent a concrete deck with a constant bar spacing of 6 in. All three series had a top cover of 1-½ in., which represents the requirements of ACI 318-99 and AASHTO (AASHTO, 1996) for concrete containing primary reinforcement that is not exposed to weather. This condition was selected in light of the fact that the FRP reinforcement will not be subject to corrosion; therefore, the minimum cover for interior exposure should be appropriate. The spacing of the top longitudinal reinforcement for each series is shown in Figure 3.2.

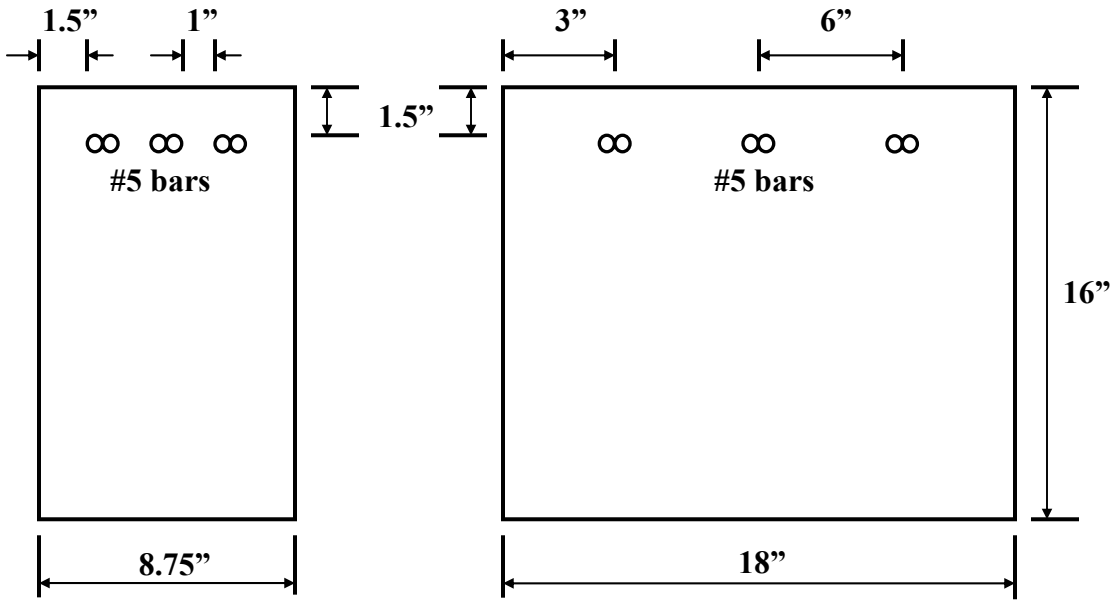

Figure 3.2: Specimen Details

In Series I and II, splitting of the side cover was considered as the likely failure mode since the average distance between bars and the side faces of the beam (1 ¼ in.) are less than the top cover (1 ½ in.). The failure mode of Series III switches from side cover splitting to top cover splitting since the top cover is the smaller dimension. The specimens of all three series had a depth of 16 in and more than 12 in. of concrete cast below the reinforcement. Therefore, the reinforcement was designed to be in the top cast position.

The shear spans of the beams were reinforced with closed stirrups, fabricated from #3 steel bars, at approximately 6 in. on center to prevent a shear failure in that region. The shear reinforcement provided enough shear capacity to insure yielding of the steel specimen in the event a splice failure did not occur. No shear reinforcement was provided in the constant moment region since it was desired to test the splice without the presence of transverse reinforcement as transverse reinforcement will increase the bond strength achieved by the splice (Orangun, 1977). Therefore, the tests were designed to produce a lower bound strength and are consistent with splices in a bridge deck where transverse reinforcement is not typical. Two steel #3 bars were provided in the bottom of the beam to secure the stirrups during cage construction and to provide tensile reinforcement for the beam for handling purposes after failure.

A summary of the details of each series is shown in Table 3.1. The specimens are identified first by the type of test performed (Bond Test), then by the type of reinforcing material used in the specimen, and finally by the series number. The reinforcing material abbreviations are as follows: S for conventional Grade 60 Steel rebar; G1 for Hughes Bros. Glass FRP rebar; G2 for Marshall Industries Glass FRP rebar; and A for Technora Aramid FRP rebar.

Table 3.1: Details of Bond Series						
Series	**Specimen Name**	**Bar Type**	**Splice Length (in.)**	**Top Cover (in.)**	**Side Cover (in.)**	**Clear Spacing (in.)**
I	B-S-1	Steel	18	1.5	1.5	1
	B-G1-1	Glass FRP				
	B-G2-1	Glass FRP				
	B-A-1	Aramid FRP				
II	B-S-2	Steel	12	1.5	1.5	1
	B-G1-2	Glass FRP				
	B-G2-2	Glass FRP				
	B-A-2	Aramid FRP				
III	B-S-3	Steel	12	1.5	2.69	4.75
	B-G1-3	Glass FRP				
	B-G2-3	Glass FRP				
	B-A-3	Aramid FRP				

3.3 Materials

3.3.1 Steel

All reinforcing steel used was Grade 60 conforming to ASTM A 615. The #5 bars were ordered from the same heat of steel to insure consistent yield strength for the bars. Three tension tests resulted in yield strengths of 74,500 psi, 74,500 psi, and 78,000 psi, indicating average yield strength of 76,000 psi.

The reinforcement used for the compression (bottom) reinforcement and stirrups was #3 Grade 60 rebar. The stirrups were prefabricated with standard bends and details required by ACI 318-99 (ACI 318, 1999).

3.3.2 Glass FRP

The glass FRP bars were received from their respective producers. In general, the reinforcement was in good condition with only minor surface defects. Hughes Brothers, Inc. provided #5 bars for the experimental program. Careful inspection of the reinforcement upon arrival led to the discovery of "resin puddles" that formed during production on the bottom side of the bars while being extruded through the resin bath and then hardened. The manufacturer indicated that it is a common phenomenon during production. The puddles were surface treated with a sand coating just as the rest of the bar, and therefore were not viewed as defects. Marshall Industries Composites provided #5 bars, commercially referred to as C-Bar, for the experimental program. Slight scaling of the thin protective coating of some of the bars was observed. While this may be a durability concern, it is highly unlikely that bond strengths were affected.

Tensile tests on the Hughes Brothers bar (Glass1) indicated failure at 88,000 psi with a modulus of elasticity of approximately 5,900 ksi, while the C-Bar specimens (Glass2) failed at 82,000 psi with a modulus of elasticity of approximately 5,400 ksi. The modulus of elasticity was of primary interest, but it should be noted that both bar types failed at a lower ultimate stress than specified by the manufacturer. Other researchers (Ehsani, 1996) have reported similar findings with respect to tensile tests on FRP bars. The range of stresses experienced by the specimens did not approach the ultimate strength of any of the FRP bars, therefore, this was not of concern in the experimental program. The stress-strain curves for each type of glass FRP bar are shown in Figure 3.3.

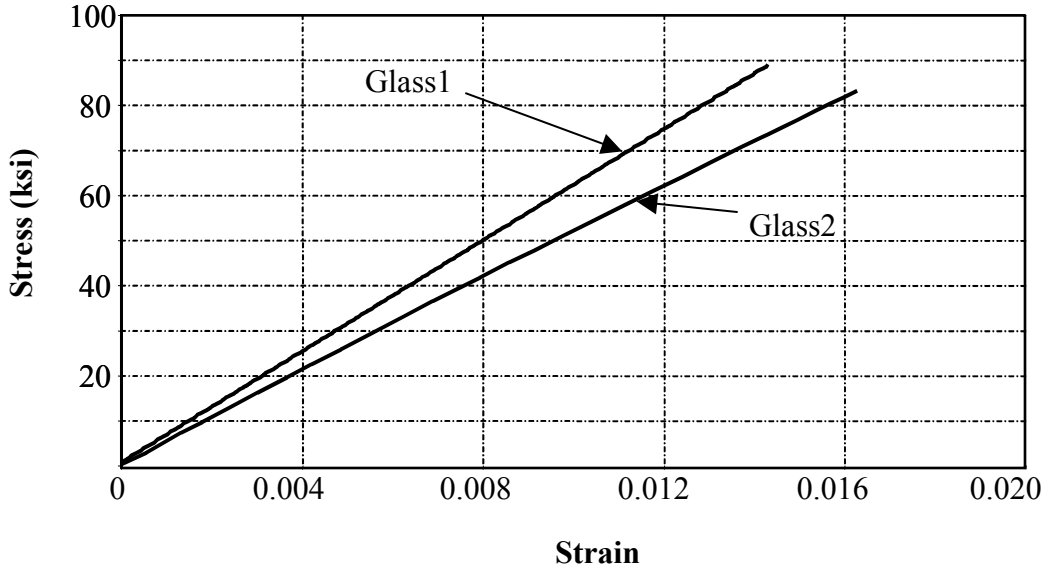

Figure 3.3: Stress-Strain Curve for GFRP

3.3.3 Aramid FRP

A Japanese producer, Technora, provided the aramid FRP reinforcement. The reinforcement was in good condition upon arrival to the laboratory. Tensile tests were performed up to 117,000 psi, which is significantly lower than the ultimate strength specified by the producer. Unlike the tensile tests on GFRP specimens, the ultimate load was governed by a grip failure. As stated earlier, the ultimate tensile strength of the reinforcement was not a concern for the experimental program. The tension tests indicated a modulus of elasticity of 6,800 ksi. The stress-strain curve for the aramid FRP bar is shown in Figure 3.4.

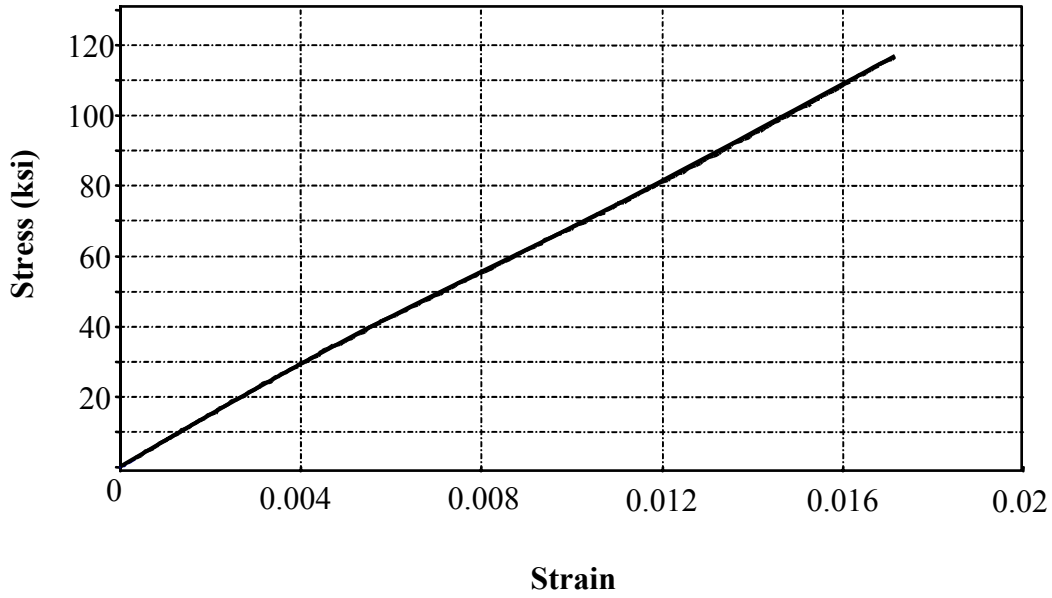

Figure 3.4: Stress-Strain Curve for AFRP

3.3.4 Concrete

A local ready-mix concrete supplier delivered all concrete used in the experimental program. The same batch of concrete was used for all specimens in a series. The batch weights for each series are shown below in Table

3.2. Adjustments based on the water content of the aggregates were made by the supplier. Water added to the mix before placement to adjust slump is included in the total. The coarse aggregate had a maximum size of ¾ in. in all series.

Table 3.2: Concrete Batch Weights Per Cubic Yard			
Material	**Series I**	**Series II**	**Series III**
Cement – Type 1 (lbs)	440	385	368
Fly Ash – Type C (lbs.)	100	0	97
Fine Aggregate (lbs.)	1375	1590	1451
Coarse Aggregate (lbs.)	1850	1850	1847
Water (lbs.)	234	234	152
Air (oz.)	5.5	1	1
Water Reducer/Retarder (oz.)	9	8	10

Series I, II, and III specimens had a slump of 5 to 6 in. The compressive strength of the specimens was monitored by testing 6" x 12" cylinders at 7, 14, 21, and 28 days. In addition to testing cylinders for compressive strength, split cylinder (6" x 12") tests and flexure beam (6' x 6" x 18") tests were performed on days in which specimens were tested. Flexure beams were not tested on the day of testing for Specimens B-G1-2 and B-G2-3 due to the proximity of previous or subsequent tests. Table 3.3 shows the average compressive strength (f_c) based on 6" x 12" compression cylinders, average tensile strength (f_t) based on split cylinders, and average rupture strength (f_r) based on flexure beams for each specimen.

Table 3.3: Average Concrete Strengths					
Series	Specimen	Age (days)	f_c (psi)	f_t (psi)	f_r (psi)
I	Steel (B-S-1)	104	5,520	442	641
	Glass1 (B-G1-1)	111	5,600	430	758
	Glass2 (B-G2-1)	120	5,490	462	790
	Aramid (B-A-1)	113	5,690	472	813
II	Steel (B-S-2)	45	4,200	458	633
	Glass1 (B-G1-2)	50	4,210	401	-
	Glass2 (B-G2-2)	108	3,920	410	784
	Aramid (B-A-2)	76	4,160	419	663
III	Steel (B-S-3)	38	5,880	552	686
	Glass1 (B-G1-3)	63	5,980	514	709
	Glass2 (B-G2-3)	59	5,930	548	-
	Aramid (B-A-3)	68	5,750	536	744

3.4 Test Setup and Procedure

The test setup was designed to load the ends of the specimens with hydraulic rams. The rams were secured to the loading beams using threaded rods and bolts. As shown in Figure 3.5, rams were located at either end of the beam. The rams reacted against steel load transfer beams that were secured to the reaction floor using threaded pipe. The reaction supports were attached to the floor using hydrostone. A plate was cast on the top of each support; one flat plate and one grooved plate. Steel rods were located between the plates on the support and the bearing plates that were attached to the underside of the beams (with hydrostone) at the support points. This configuration was selected to simulate a pin-roller support system. Bearing plates were also used at the loading points on the end of the specimens. Hydrostone was used for the attachment of all plates due to its high rate of strength gain and high ultimate compressive strength.

Load cells were used to monitor load application during the tests. The load cells used for the first two series were rated for 20 kips, while a 100 kip and 150 kip load cell were used for the third series. All load cells were calibrated before testing using a 120 kip universal testing machine. The calibration of the load cells was performed in the range in which they were used during testing.

Deflections were measured at several points along the specimen using linear voltage displacement transducers (LVDT's) that were mounted on the beam. All tests included deflection readings at each end of the specimen (load points), at the support points, and at the middle of the beam. The LVDT's located at the support points were used to detect support settlement, which were used to correct the values obtained at the ends and middle of the beam.

Load, deflection, and strain readings were recorded continuously throughout the tests. Load was applied at 1 kip intervals. After the first flexural cracks appeared, cracks were marked and crack widths were recorded at each load stage until it was deemed unsafe due to eminent failure of the beam. In some instances, loading was momentarily stopped and crack widths were recorded between load stages.

Figure 3.5: Loading Detail

3.5 Experimental Results

3.5.1 General Behavior

3.5.1.1 Flexural Cracking

For a given series, each specimen cracked at approximately the same load while exhibiting approximately the same stiffness up to the cracking load. The first cracks occurred in the constant moment region of the specimens, generally either over a support or at the end of the splice region. As the load increased, additional flexural cracks occurred in the constant moment region, and flexural cracks began to form in the shear span. Overall, the crack pattern closely resembled the bending moment diagram for the specimens.

It was observed that the cracks in the FRP reinforced specimens propagated deeper into the section than that of the companion steel specimen at a given load (stress level), as shown in Figure 3.6. With the reinforcement at a stress of approximately 36 ksi, the flexural cracks of the steel specimen (Figure 3.6a.) have propagated roughly two-thirds through the 16 in. deep section, while the cracks of a comparable aramid specimen have propagated much further. The crack widths observed in the FRP reinforced specimens were several times larger than those observed in the companion steel specimen.

The FRP reinforced specimens exhibited extensive branching of the principle flexural cracks near the level of reinforcement as compared to the steel specimens. Figure 3.7 shows the constant moment region of Specimen B-S-1 (Figure 3.7a) and Specimen B-G2-1 (Figure 3.7b). Although the steel specimen (B-S-1) is at a higher longitudinal stress, the cracking has not branched from the principle flexural cracks as it has for the glass specimen (B-G2-2).

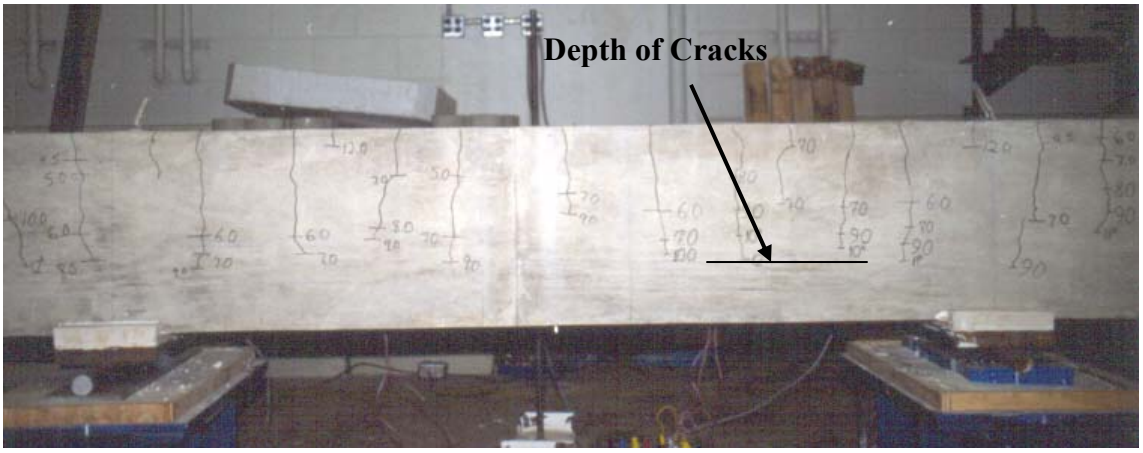

(a.) Steel Specimen at 36 ksi (B-S-2)

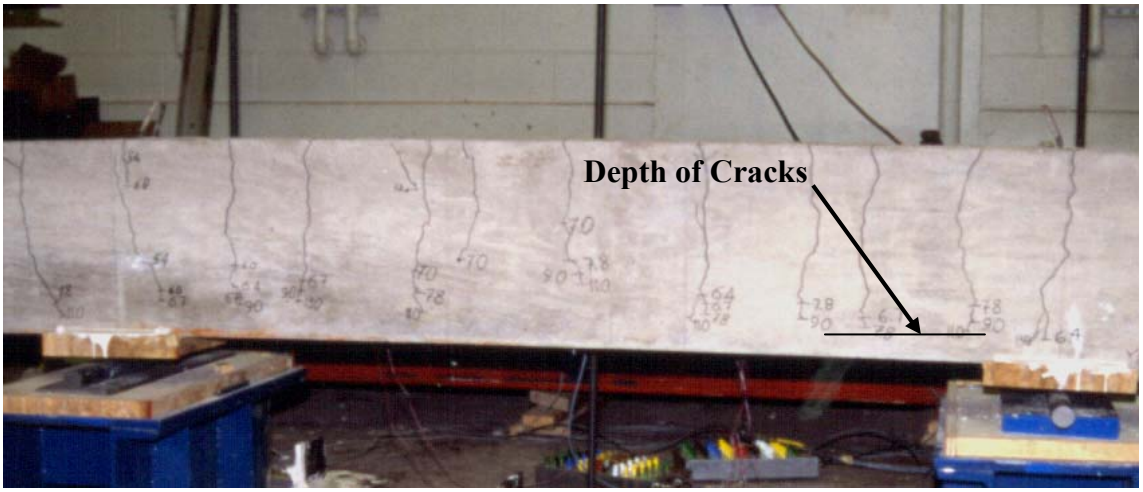

(b.) Aramid Specimen at 36 ksi (B-A-2)

Figure 3.6: Comparison of Crack Propagation

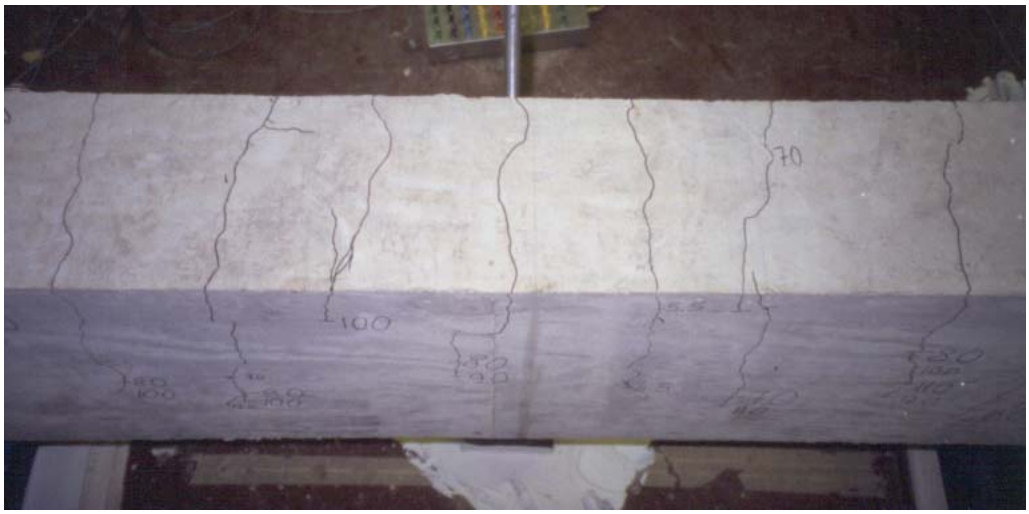

(a.) Top View of Specimen B-S-1 at 40 ksi

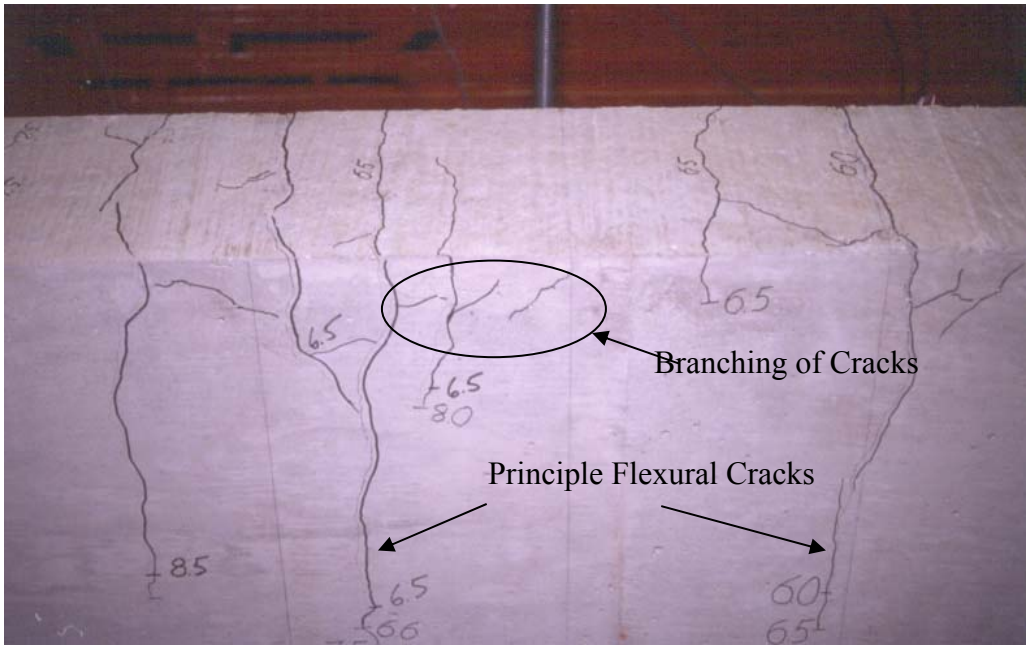

(b.) Splice Region of Specimen B-G2-1 at 25 ksi

Figure 3.7: Comparison of Cracking

3.5.1.2 Failure

All specimens in the experimental program failed by a splitting mode in the splice region. The specimens failed abruptly; the first and second series specimens failing by side cover splitting, while the third series with a wider bar spacing, failed due to top splitting. Because hydraulic rams were used for loading, the load was partially removed at the initiation of failure. Failure of the specimens commenced when the cover in the splice region "blew

apart" due to excessive radial stress imparted on the concrete by the reinforcement. The nature of the brittle splitting failure is captured in Figure 3.8.

(a.) Wide Angle View of Failure of B-S-2

(b.) Failure of B-S-2

Figure 3.8: Brittle Splitting Failure

3.5.1.3 Appearance After Failure

The splice regions of the specimens were investigated immediately after failure. The side splitting failure mode of the first and second series is shown in Figure 3.9(a.). Figure 3.9(b) shows the top splitting failure mode of the third series. The cover for each series was removed as much as possible by hand (if the force of the failure had not removed it), and the concrete fragments were reassembled as shown in Figure 3.10. The reassembled cover was used to determine the exact bar locations. Both the reassembled cover and the reinforcement in the splice zone were carefully examined to determine whether any localized crushing had occurred in the concrete around the reinforcement deformations, or in the case of the FRP reinforcement, whether there was damage to the deformations. A visual determination of bond quality was also made.

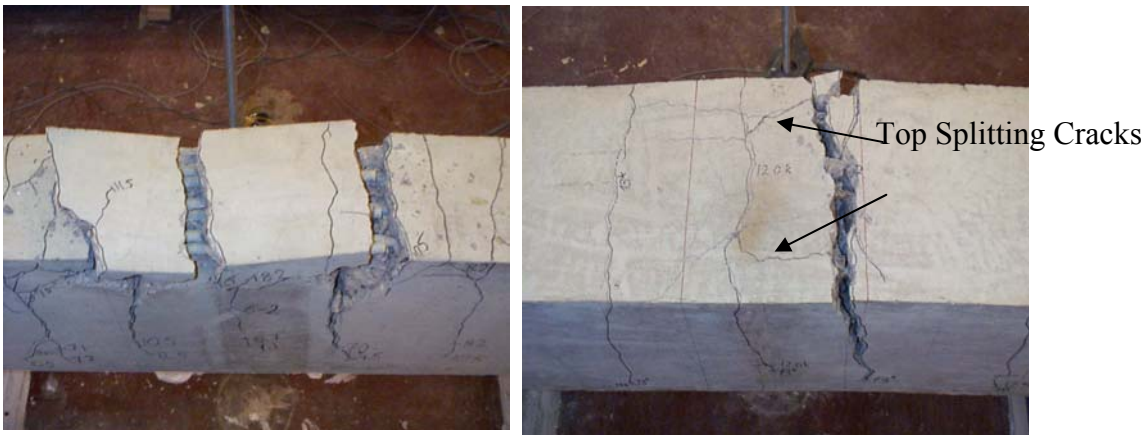

(a.) Side Cover Splitting **(b.) Top Cover Splitting**

Figure 3.9: Splitting Failure Modes

Figure 3.10: Reassembled Concrete Cover

3.5.2 Test Results

The maximum load and corresponding reinforcement stress achieved for each test specimen is provided in Table 3.4. Specimen characteristics such as concrete strength, splice length, top cover, and clear bar spacing, are also provided for ease of comparison. The reinforcement stress values in Table 3.4 were calculated based on the load achieved and a cracked section analysis. The Hognestad concrete stress block (MacGregor, 1997) was used in the calculation of reinforcement stress to account for the non-linear behavior of concrete at high stress levels. All calculations were based on the design cross-sectional dimensions.

In general, calculation of the depth of the neutral axis from the cracked section analysis agreed well with the observed depth of crack propagation. In addition, the stresses measured from the strain gages at the end of the splice zone were generally similar to the calculated values.

Table 3.4: Bond Test Results

Series	Specimen	f_c (psi)	l_s (in.)	Cover (in.)	Clear Spacing (in.)	P_u (k)	f_{bu} (ksi)
I	B-S-1	5,600	18	1.5	1	24.4	73.2
	B-G1-1	5,600				13.4	38.3
	B-G2-1	5,600				11.4	32.5
	B-A-1	5,600				14.1	40.4
II	B-S-2	4,100	12	1.5	1	18.4	55.6
	B-G1-2	4,100				10.1	28.9
	B-G2-2	4,100				10.3	29.5
	B-A-2	4,100				10.8	31.1
III	B-S-3	5,900	12	1.5	1	25.9	75.6
	B-G1-3	5,900				17.5	49.3
	B-G2-3	5,900				16.6	46.7
	B-A-3	5,900				18.3	51.7

It is significant to note that the reinforcing stress in Specimen B-S-1 and B-S-3 did not yield according to the calculations (average f_y = 76 ksi). These calculations were supported by the load-deflection curves (Figures 3.11-3.13).

3.5.3 Beam Stiffness

As stated earlier, all specimens within each series cracked at approximately the same load. Analysis of the load vs. deflection curves (Figures 3.11-3.13) of each series shows that the specimens within each series had approximately the same stiffness up to cracking. The average load applied to each end of the beam as determined by the calibrated load cells is presented on the vertical axis, while the average deflection of the specimens at the loading points as determined by LVDT's, including corrections for support settlement is presented on the horizontal. After cracking, the stiffness of the specimens change, evident by the change in slope of the load vs. deflection curve, as the reinforcement must now resist tensile stress that was resisted primarily by the concrete. The modulus of elasticity (stiffness) of the reinforcement becomes the governing parameter determining the stiffness of the beam specimens, as the cracked moment of inertia of the FRP reinforced specimens is approximately 20-30% that of the steel specimens.

The saw-tooth pattern of the load vs. deflection curves after initial cracking reflects the fact that the tests were essentially deflection controlled. In instances in which the curves seem discontinuous, new cracks formed in the specimens or old cracks were propagating deeper into the section.

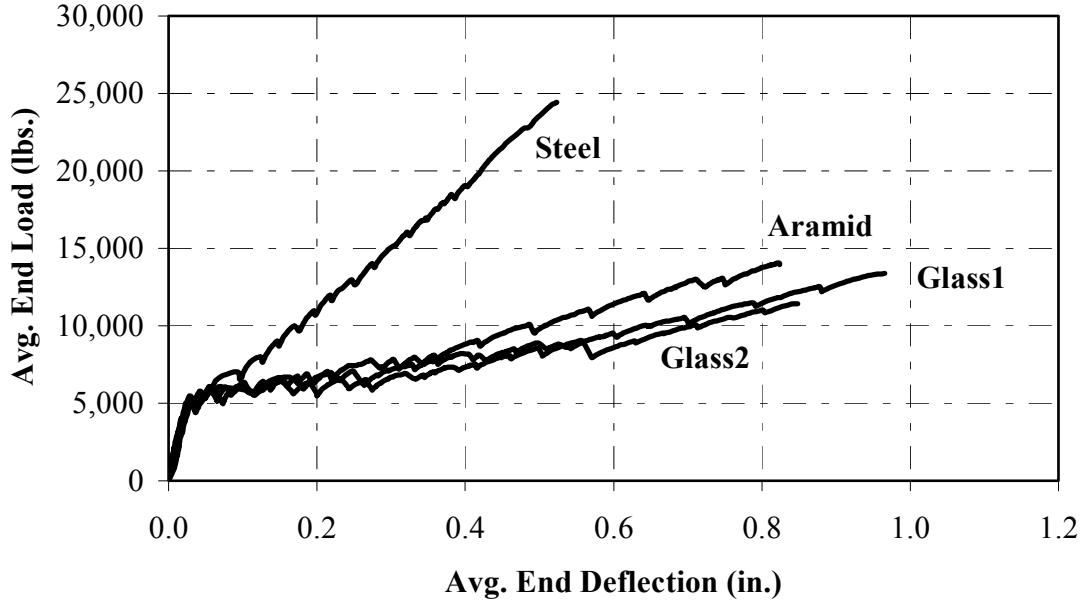

Figure 3.11: Series I Load vs. Deflection Plot

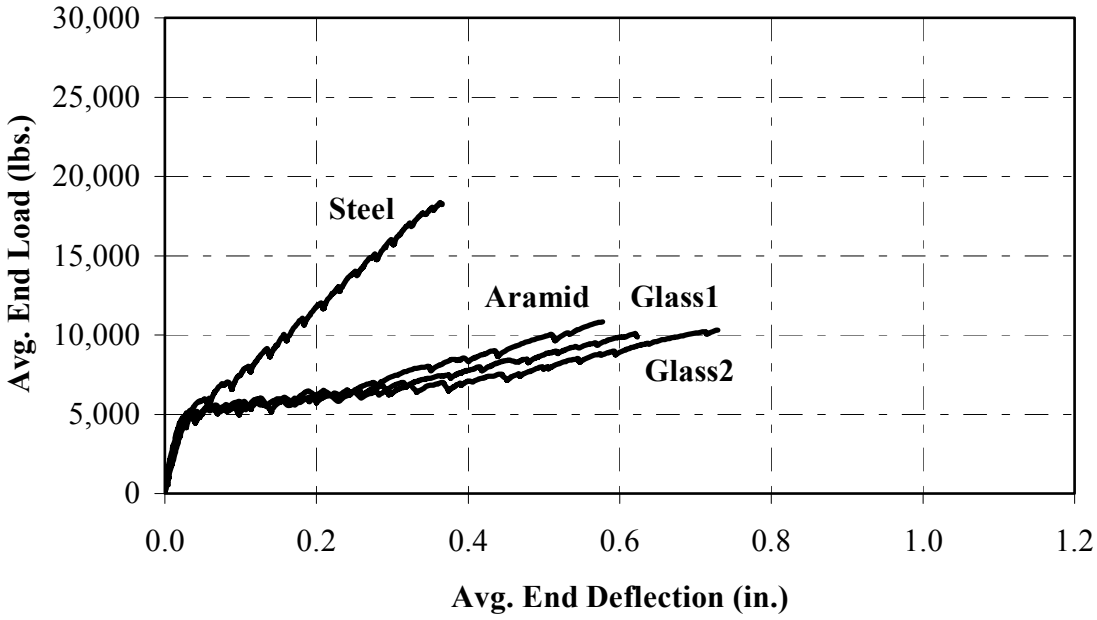

Figure 3.12: Series II Load vs. Deflection Plot

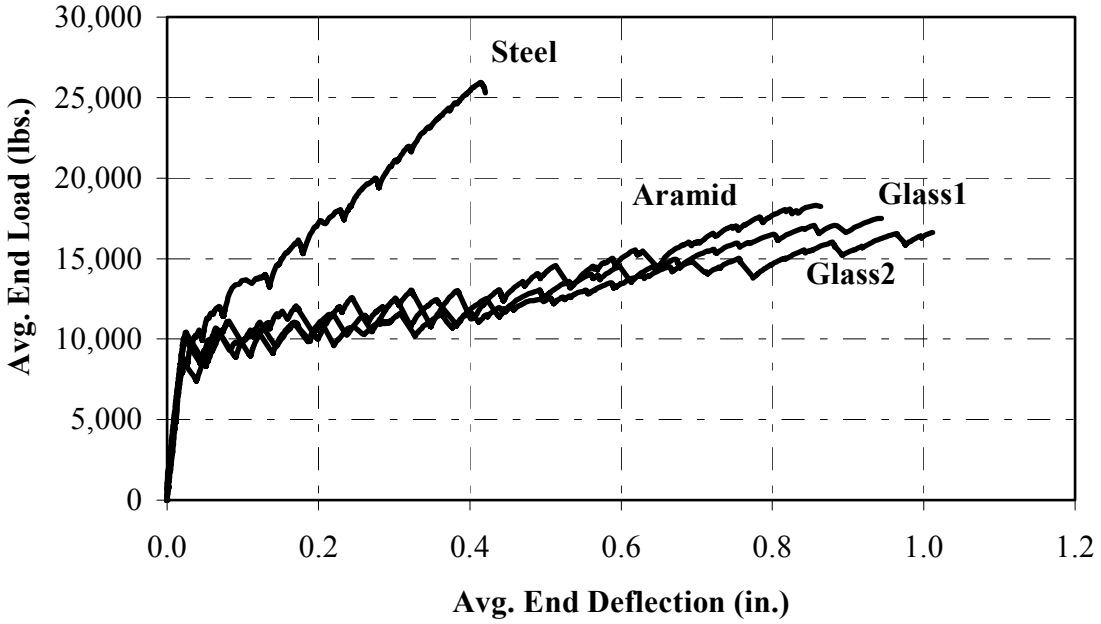

Figure 3.13: Series III Load vs. Deflection Plot

3.5.4 Crack Widths

Crack widths associated with each type of reinforcement were compared by analysis of the reinforcement stress vs. average crack width curves. These curves for each series are shown in Figures 3.14-3.16. The calculation of reinforcement stress was based on the load cell reading at the time the crack widths were measured using the Hognestad concrete stress block. Calculations were based on the design dimensions of the cross-section. Cracks that occurred over the support, in the splice region, and at the ends of the splice zone were not included in the average. Cracks over the support and at the end of the splice zone occurred as a result of the configuration of the test setup, and therefore do not represent a random distribution of cracking. The cracks that occurred in the splice zone were restrained by double the reinforcement as the other cracks in the beam, leading to significantly reduced crack widths. The crack width curves end before specimen failure, when it was deemed unsafe to take readings due to eminent failure of the specimens.

As shown in Figures 3.14-3.16, the curves for the steel specimens as compared to the FRP specimens are remarkably different. At a given stress level, the average crack width in the steel specimens were several times less than (as much as 10 times) that of FRP reinforced specimens within the same series. The rate at which the average crack widths increased as the reinforcement stress increased (slope of the curve) in the steel specimen is several times less than the FRP specimens as well. The FRP specimens in each series achieved average crack widths that exceeded 0.016 in. at relatively low stress levels (approximately 20 ksi).

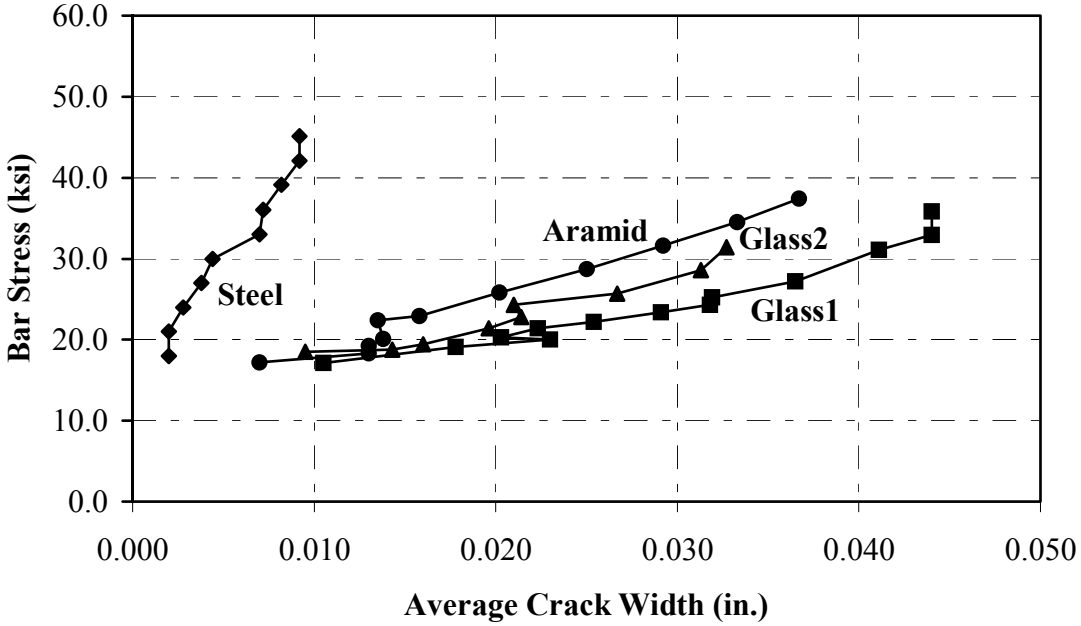

Figure 3.14: Series I Bar Stress vs. Avg. Crack Width

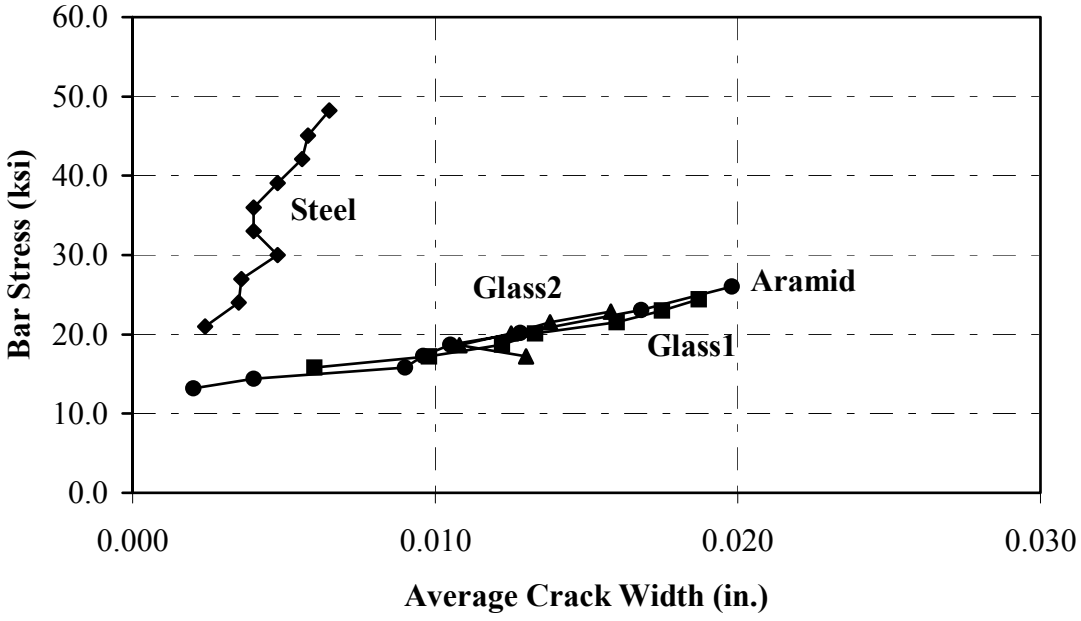

Figure 3.15: Series II Bar Stress vs. Avg. Crack Width

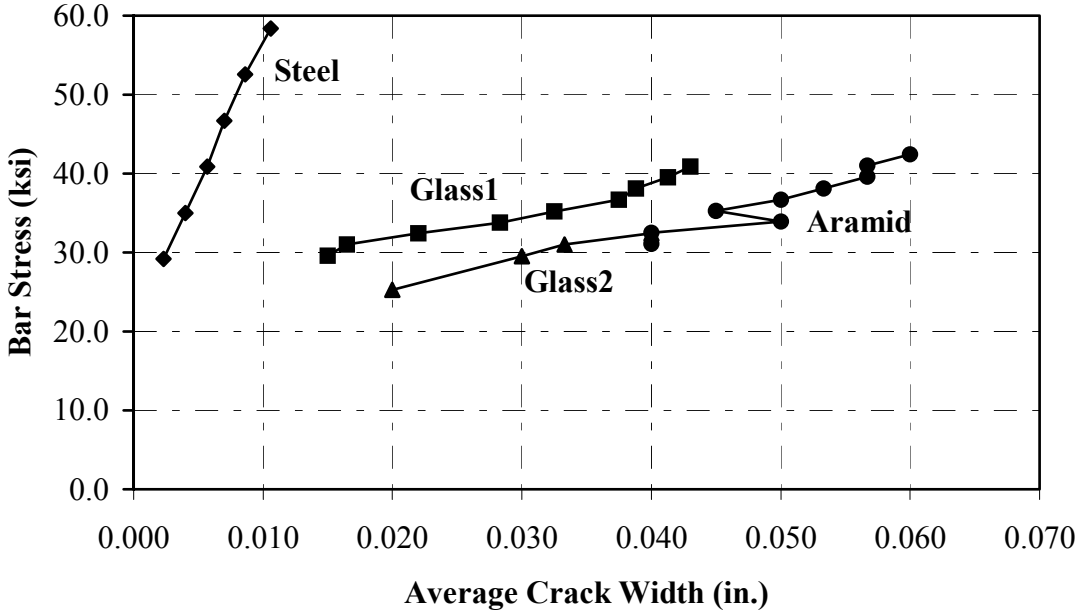

Figure 3.16: Series III Bar Stress vs. Avg. Crack Width

Based on this data, it is difficult to make any generalizations about the performance of one type of FRP reinforcement compared to another. In the first series, the aramid FRP specimen achieved a smaller average crack width at a given stress when compared to the two glass FRP specimens. However, in the third series, the Glass1 specimen achieved smaller crack widths than the Aramid specimen. One trend that is evident in the curves is the similarity of the slope of the FRP specimens. In each series, the FRP specimens average crack width increases with stress level at approximately the same rate. Although the deformation pattern on each type of FRP reinforcement is different, the cracking behavior is quite similar for all bar types.

3.5.5 Bond Strength

The bond strength for the specimens of each series of specimens is presented in Table 35. The strengths were determined by calculating the average bond stress acting along the splice length. The nominal bar diameter and design dimensions were used in all calculations. The bond ratio shown in the table represents the ratio of bond stress (or bar stress) for the specimen to the bond stress of the steel specimen within that series. The Series I and II FRP specimens attained a bond stress of approximately one half that of the steel specimens. With wider bar spacing (Series I), the FRP specimens achieved roughly two-thirds of the bond stress of the steel specimen. It is evident that the bond stress achieved appears to be related to the modulus of elasticity of the reinforcing materials, as the steel specimens had the highest bond strength and modulus of elasticity, followed by the aramid FRP specimens, and finally the glass FRP specimens.

Table 3.5: Lap-Splice Bond Strengths

Series	Specimen	P_u (k)	f_{bu} (ksi)	Bond Strength, u_{avg} (psi)	Bond Ratio (u_{avg} / u_{steel})
I	B-S-1	24.4	73.2	635	1.00
	B-G1-1	13.4	38.3	332	0.52
	B-G2-1	11.4	32.5	282	0.44
	B-A-1	14.1	40.4	351	0.55

II	B-S-2	18.4	55.6	483	1.00
	B-G1-2	10.1	28.9	251	0.52
	B-G2-2	10.3	29.5	256	0.53
	B-A-2	10.8	31.1	270	0.56
III	B-S-3	25.9	75.6	656	1.00
	B-G1-3	17.5	49.3	428	0.65
	B-G2-3	16.6	46.7	405	0.62
	B-A-3	18.3	51.7	449	0.68

3.6 Data Analysis

3.6.1 ACI 318-99 Design Provisions

The design provisions of ACI 318-99 (ACI 318, 1999) have their roots in the recommendations presented by Orangun et. al. (Orangun, 1977). It should be noted that these recommendations were based on available data of steel reinforced specimens; therefore, this equation is not meant to be used with other reinforcing materials. It is possible, however, that slight modifications could result in its applicability for different types of reinforcing materials.

The development length equation of ACI 318-99 (Equation 3-1) is shown for the purpose of this discussion:

$$\frac{l_d}{d_b} = \frac{3}{40}\frac{f_y}{\sqrt{f'_c}}\frac{\alpha\beta\gamma\lambda}{\left(\frac{c+K_{tr}}{d_b}\right)} \qquad \text{(Eq. 3-1)}$$

The 3/40 (0.075) coefficient on the right side of the equation is a value that provides conservative development lengths for the majority of available steel data. Ultimately, an equation of the same form could be utilized for other types of reinforcement, but a multiplier (X), based on test data for that type of reinforcement, would have to be used. By dividing Equation 1-3 by the 5/4 overstrength factor contained within the equation, the 3/40 coefficient becomes 3/50. The modified equation is shown below:

$$\frac{l_d}{d_b} = \frac{3}{50}\frac{f_b}{\sqrt{f'_c}}\frac{M_f}{\left(\frac{c+K_{tr}}{d_b}\right)}X \qquad \text{(Eq. 3-2)}$$

where:

l_d = *development length of reinforcement, (in.)*

d_b = *diameter of reinforcing bar, (in)*

f_b = *specified stress in reinforcement, (psi)*

f'_c = *specified compressive strength of concrete, (psi)*

M_f = *product of modification factors* $\alpha, \beta, \gamma,$ *and* λ

c = *lesser of clear cover or 1/2 clear spacing between bars, (in.)*

K_{tr} = *transverse reinforcement index*

X = *modification factor for reinforcement type*

Values for X for each of the specimens (including steel) tested in the experimental program are shown in Table 3.6. Values were determined for the steel specimens for the purpose of comparison with the values obtained for FRP specimens. The values calculated were based on solving Equation 4-1 for X. The values of l_d and c were based on design dimensions, while the values of f_b and f'_c were taken as the calculated bar stress at failure and the

average compressive strength at the time of testing. The modification factor for bar location was not considered since its inclusion would likely provide unconservative values for the *X* factor.

Table 3.6: X Factors Based on Experimental Results		
Series	**Specimen**	**X Factor**
I	Steel (B-S-1)	1.03
	Glass1 (B-G1-1)	1.95
	Glass2 (B-G2-1)	2.30
	Aramid (B-A-1)	1.85
II	Steel (B-S-2)	0.78
	Glass1 (B-G1-2)	1.50
	Glass2 (B-G2-2)	1.47
	Aramid (B-A-2)	1.39
III	Steel (B-S-3)	1.01
	Glass1 (B-G1-3)	1.56
	Glass2 (B-G2-3	1.64
	Aramid (B-A-3)	1.48

The values of *X* in the last column of Table 3.6 indicate that the current form of the ACI 318-99 development length equation is considerably unconservative (*X* is much greater than 1.0) for all of the FRP reinforced specimens. In the case of the steel reinforced specimens, the equation provides results in X factors very close to 1.0, even though the 5/4 overstrength factor and the bar location factor have been removed from Equation 4-1. Comparing results of all the specimens in Series I and II indicates that Equation 4-1 is more conservative for Series II, with a shorter splice length. While the ACI 318-99 development length equation may consistently calculate conservative results if appropriate multiplication factors are used, the inconsistent level of conservatism indicates that the equation does not reflect the actual bond behavior.

Clearly, if Equation 4-1 is to be used with FRP reinforcement, an appropriate *X* factor should be selected for each type of reinforcement. For the FRP reinforcement used in this experimental program, the *X* factor selected for each type of FRP reinforcement is 2. It should be noted that this recommendation is only for the types of FRP reinforcement used in this experimental program. No overstrength factor has been included since providing such a factor does not insure ductility in design with FRP reinforcement.

3.6.2 ACI Committee 440 Proposed Recommendations

ACI Committee 440 (ACI 440, 2000) has proposed recommendations for the design of members reinforced with FRP. The development length equation proposed by ACI Committee 440 for splitting failure is:

$$l_{bf} = K_2 \frac{d_b^{\,2} f_{fu}}{\sqrt{f'_c}} \qquad \text{(Eq. 3-3)}$$

where:

l_{bf} = development length required, (in.)

K_2 = constant determined experimentally

d_b = reinforcing bar diameter, (in.)

f_{fu} = design tensile strength of reinforcement considering environmental factors, (psi) $= C_E f_{fu}^*$

C_E = environmental reduction factor, dependent on fiber type and exposure conditions

f_{fu}^* = guaranteed tensile strength, (psi)

f'_c = specified concrete strength, (psi)

The value of f_{fu} is defined as the mean tensile strength of a sample of test coupons minus three standard deviations. The committee proposes values of C_E based on fiber type and exposure conditions, which are shown in Table 3.7.

Table 3.7: Proposed Values of C_E

Exposure Condition	Fiber Type	Environmental Reduction Factor, C_E
Concrete not exposed to earth and weather	Carbon	1.0
	Glass	0.8
	Aramid	0.9
Concrete exposed to earth and weather	Carbon	0.9
	Glass	0.7
	Aramid	0.8

The calculated development length is dependent on the bar diameter (bar area), longitudinal stress to be generated, and the concrete strength. ACI Committee 440 has proposed including in the K_2 factor the $\pi/4$ term from the area of the bar.

ACI Committee 440 has not specifically endorsed a proposed K_2 factor, but has reported the factors determined by many investigators. The average of all K_2 values reported was 1/18.2 with the largest being reported as 1/15.6 by Tighiouart (Ehsani, 1996). The K_2 factors determined for the all specimens tested in this experimental program are shown in Table 3.8.

In the determination of K_2, the calculated stress and the average concrete strength at the time of testing were used. An overstrength factor similar to that used in ACI 318-99 (ACI 318, 1999) was not used in the determination of the K_2 values presented in Table 3.8 since the Committee's recommendations do not include such a factor. This factor is not recommended since the ultimate bar stress is used in design. Providing an overstrength factor does not provide ductility. The modification factor of 1.3 for top bar location was not used in the calculations, which is a conservative assumption.

Table 3.8: K_2 Factors Based on Experimental Results

Series	Specimen	Required K_2	Percent of 1/18.2	Percent of 1/15.6
I	Steel (B-S-1)	1/16.2	112%	96%
	Glass1 (B-G1-1)	1/11.2	164%	140%
	Glass2 (B-G2-1)	1/9.4	194%	166%
	Aramid (B-A-1)	1/11.7	156%	134%
II	Steel (B-S-2)	1/21.5	85%	73%
	Glass1 (B-G1-2)	1/11.2	164%	140%
	Glass2 (B-G2-2)	1/11.4	160%	137%
	Aramid (B-A-2)	1/12.0	152%	130%
III	Steel (B-S-3)	1/24.7	74%	64%
	Glass1 (B-G1-3)	1/16.1	113%	98%
	Glass2 (B-G2-3)	1/15.2	120%	103%
	Aramid (B-A-3)	1/16.8	108%	92%

The percentages shown in the fouth column of Table 3.8 are the ratio of the required K_2 determined for each test to the average of the K_2 values presented by ACI Committee 440. The percentages in the last column are the ratio of the required K_2 to the largest value determined by the investigators (Tighiouart, 1998). The values obtained for Series III FRP specimens indicate that the average of the K_2 factors proposed by the investigators is slightly unconservative (percentages above 100%) for the particular cover and spacing. Series III had development length of 12 in., while the clear spacing between bars was 4 ¾ in. For the FRP specimens of Series I and II, which had minimum cover and clear spacing, the proposed K_2 factors become very unconservative. It appears that changing the development length, as is the case with Series I and II, does not affect the required K_2. However,

comparison of the value of K_2 in Series I and II with the value in Series III indicates that the value changes as the cover or clear spacing is changed

According to the proposed recommendations, pullout failures are more likely when concrete cover is greater than $2d_b$. All three series had a concrete cover greater than $2d_b$, thus the calculation of development length using Equation 3-4 should be applicable according to the recommendations.

$$l_{bf} = \frac{d_b \ f_{fu}}{2700} \qquad \text{(Eq. 3-4)}$$

The development length and bar diameter used in each series of tests was substituted into Equation 3-4, and the equation was subsequently solved for the bar stress. The results of this calculation are shown in Table 3.9 and compared to the actual bar stress achieved in each specimen.

Table 3.9: Calculated Stress by Equation 3-4

Series	Specimen	Stress Achieved (ksi)	Calculated Stress by Equation 3-4 (ksi)
I	Glass1 (B-G1-1)	38.3	77.8
	Glass2 (B-G2-1)	32.5	77.8
	Aramid (B-A-1)	40.4	77.8
II	Glass1 (B-G1-2)	28.9	51.8
	Glass2 (B-G2-2)	29.5	51.8
	Aramid (B-A-2)	31.1	51.8
III	Glass1 (B-G1-3)	49.3	51.8
	Glass2 (B-G2-3)	46.7	51.8
	Aramid (B-A-3)	51.7	51.8

Comparison of the actual and calculated stress in Table 3.9 indicate that Equation 3-4 is extremely unconservative in cases with minimum cover and spacing, which is the case with Series I and II. Although the equation is meant for use in instances where pullout failure governs, this comparison is valid since the proposed recommendations indicate that a pullout failure was likely for all specimens in the experimental program. Clearly, the recommendations should be modified to correct this problem.

Based on the tests in this experimental program, it is clear that the proposed recommendations of ACI Committee 440 should be modified. It has been found that the K_2 factor (Equation 3-3) proposed by other investigators is modestly unconservative for a top cover of 1.5 in. and a clear spacing of 4.75 in. (Series III), but becomes seriously unconservative for the minimum bar spacing of 1 in. (Series I and II). While a larger K_2 factor or other modification factors could be incorporated into Equation 3-3 to provide more conservatism, there is an inherent problem with the form of the equation; Equation 3-3 does not account for the influence of cover on the required development length. Therefore, the use development length provisions of the proposed ACI Committee 440 document are not recommended.

3.6.3 AASHTO Design Provisions

The development length equation set forth in *AASHTO Standard Specifications, Sixteenth Edition* (AAHSTO, 1996) is of the same form as Equation 3-3 of the proposed recommendations of ACI Committee 440 (ACI 440, 2000). Therefore, the results presented in Section 3.6.2 are equally applicable. Due to the problems indicated with the equations presented, it is not recommended to use a modified form of the AASHTO design equations.

3.7 Crack Widths

While it is unlikely that cracking in FRP reinforced concrete will cause serious durability concerns; it is, however, an aesthetic concern. Due to the lower modulus of elasticity of many types of FRP reinforcing bars, deflections and crack widths will be larger than with a comparable reinforced steel structure as evidenced by the experimental results.

Several expressions have been proposed for calculating crack widths of steel reinforced members. ACI 318-99 (ACI 318, 1999) has adopted a crack width calculation procedure based on an expression developed by Frosch (Frosch, 1999). This expression is based on a physical model, and therefore, should be applicable to other types of reinforcement. The equation is reviewed below:

$$w_c = \beta \, \varepsilon_s \, S_c \qquad \text{(Eq. 3-5)}$$

where:

$w_c = crack\ width$

$\beta = \dfrac{(h - c)}{(d - c)} = amplification\ factor$

$h = overall\ depth\ of\ the\ member$

$c = depth\ from\ compression\ face\ to\ the\ neutral\ axis$

$d = effective\ depth$

$\varepsilon_s = reinforcing\ steel\ strain = \dfrac{f_s}{E_s}$

$S_c = crack\ spacing = \Psi_s \ d$ *

$f_s = reinforcing\ steel\ stress$

$E_s = reinforcing\ bar\ modulus\ of\ elasticity$

$\Psi_s = crack\ spacing\ factor: 1.0\ for\ minimum\ spacing;\ 1.5\ for\ average;$
$and\ 2.0\ for\ maximum$

In the form shown, Equation 3-5 is only applicable to steel reinforced members, since it uses the modulus of elasticity of steel, E_s. However, this model can be expressed for any type of reinforcement by simply using the appropriate modulus for the reinforcement used.

The maximum crack widths calculated using Equation 3-5 for all specimens in this experimental program were compared with the actual maximum crack widths measured during testing. The results of this comparison are shown in Figure 3.17. The results were grouped into reinforcement types to determine the accuracy of the model in each case. The reinforcement stress used in the calculation for crack widths was the calculated stress based on the load determined by the load cells.

Figure 3.17 indicates that Equation 3-5 results in calculated crack widths for FRP reinforced specimens with the same order of precision as for steel specimens, but is slightly less conservative. The average ratio of calculated crack width to measured crack width was 1.2 for the steel reinforced specimens; 1.0 for the Aramid specimens; and 0.9 for the Glass1 and Glass2 specimens. Since the primary concern about crack widths in FRP reinforced concrete is aesthetics, modification of Equation 3-5 to make it more conservative is unnecessary.

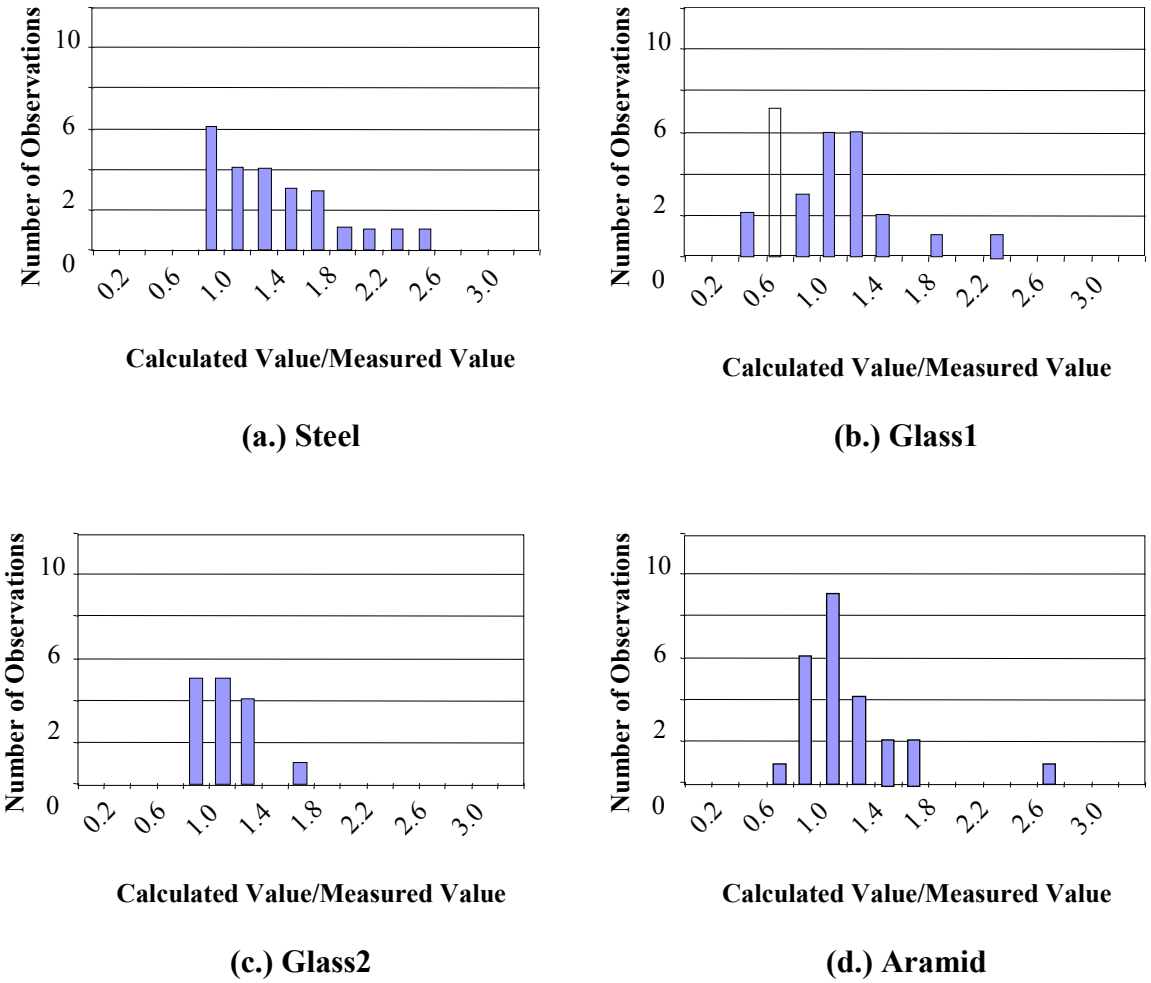

Figure 3.17: Maximum Crack Width Comparison

3.8 Deflections

The low modulus of elasticity of FRP reinforcement indicates that in many instances the design of concrete reinforced with FRP will be controlled by deflection. This requires that the calculation of deflections be as accurate as possible. As discussed in Section 3.5.3, the specimens of each series had approximately the same stiffness up to the cracking load (or cracking moment). After cracking the stiffness is highly dependent on the modulus of elasticity. These stiffnesses are commonly referred to as the uncracked stiffness (EI_g) and the cracked stiffness (EI_{cr}), respectively. The load vs. deflection plots for Series I were compared to the calculated cracked and uncracked stiffness in Figure 3.18. The uncracked *s*tiffness is approximately the same for each specimen, and therefore EI_g plotted in Figure 3.18 represents the average value for the entire series. The cracked stiffness for Specimen B-S-1 and the average cracked stiffness for the FRP specimens are shown in the figure as well.

The values of *EI* were calculated using the transformed section for both the uncracked and cracked case. The modulus of elasticity of the concrete was determined using the expression in ACI 318-99 (ACI 318, 1999):

$$E_c = 57{,}000\sqrt{f'_c} \qquad \text{(Eq. 3-6)}$$

where:

E_c = *calculated modulus of elasticity of concrete, (psi)*

f'_c = *compressive strength of concrete, (psi)*

In calculating the modular ratio, n (E_b/E_c), the modulus of elasticity of steel was taken as 29,000 ksi, while the modulus of the FRP bars was taken as 6,000 ksi, which is the average of the three types.

Figure 3.18 indicates that the use of the transformed section to determine the uncracked and cracked stiffness is an effective tool in determining the load-deflection relationship in a concrete member reinforced with FRP. In Series I, the average cracked stiffness calculated for the FRP specimens fell closer to the load-deflection curves than did the cracked stiffness calculated for the steel specimen.

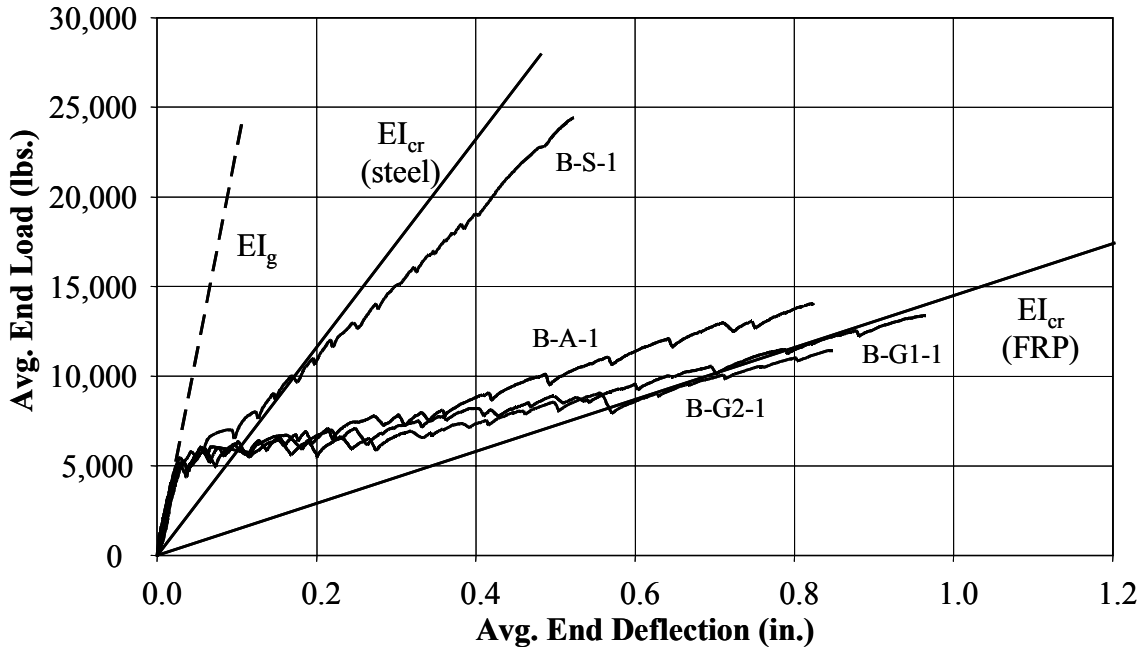

Figure 3.18: Series I Load vs. Deflection Plot

4. SHEAR INVESTIGATION

4.1 Introduction

The experimental program investigated the shear strength and behavior of beams reinforced only in the longitudinal direction with FRP bars. Two series of tests, Series 1 and Series 2, were conducted in which three different FRP bars (two types of Glass FRP and one type of Aramid FRP) were evaluated. For comparison, a steel reinforced specimen was included in each series in addition to three FRP reinforced specimens. The second series included a fifth specimen reinforced with a high-yield-strength steel bar to investigate the effect of axial rigidity of longitudinal bars on shear behavior.

4.2 Design of Specimens

Specimens were designed to be representative of a bridge deck. Therefore, only longitudinal reinforcement was provided to obtain the shear strength provided by the concrete. The specimen height was selected as 16-in. to be representative of typical slab span bridges used in Indiana. The nominal concrete strength was selected as 5000-psi, which is typical bridge deck design strength.

The shear strength of reinforced concrete beams is influenced significantly by the shear-span to effective depth ratio (a/d). The aim was to size and test the specimens so that beam behavior rather than arch behavior would be dominant. In addition, it was desirable to set the a/d ratio close to 2.5 where the shear strength due to concrete contribution is lowest. Considerations of the a/d ratio together with space and manageability constraints in the laboratory resulted in an 8-ft. span length, (a/d = 3.4).

The longitudinal reinforcement ratio is also known to affect the shear strength of reinforced concrete members. Minimum and maximum longitudinal reinforcement amounts for steel reinforcement are typically specified by design codes. These limits are a function of strength and ductility requirements and vary with concrete strength. According to the AASHTO Bridge Design Specifications (AASHTO, 1996) and the ACI 318-99 Building Code (ACI 318, 1999), the reinforcement ratio to satisfy these requirements ranges from 0.35 to 2.5% for 5000-psi concrete. In Shear Series 1, 1% longitudinal reinforcement was used, which is closer to the lower end of the limits and a typical amount used in practice. A lower percentage of reinforcement was not tested due to concerns regarding serviceability requirements. Since the modulus of elasticity of FRP bars is low, cracking and deflections may often control design and a minimum amount of longitudinal reinforcement is required for their control. The width of specimens was controlled by the percentage of longitudinal reinforcement and the allowable bar spacing and cover requirements, which were all satisfied by providing an 18-in width.

Shear Series 2 specimens were designed to investigate the practical upper limit of longitudinal reinforcement, which is allowed by the AASHTO Bridge Design Specifications and the ACI-318-99 Building Code. Twice the reinforcement was used to study the effect of varying longitudinal reinforcement ratio on shear behavior. By using two layers of reinforcement and the same beam width, the practical limit, which is controlled by minimum spacing requirements, is calculated as 2.15%. However, ease in laying out the bars was preferred to strictly complying with the calculated ratio, which resulted in a design reinforcement ratio of 2%. Series 2 specimens provide a direct comparison with those in Series 1. An additional specimen reinforced with high yield-strength steel bars was included in this series. The reinforcement ratio provided for this specimen was selected as 0.36% so that the axial stiffness of the steel reinforcement used in this specimen would be approximately equal to the axial stiffness of reinforcement in the beams reinforced with 2% glass FRP bars. Therefore, Shear Series 2 also allowed a comparison between the shear strengths of beams that were provided with the same axial stiffness of reinforcement but different reinforcing bars.

Anchorage length required beyond supports to prevent premature bond failures prior to shear failure was calculated as 16-in. However, 2.5-ft anchorage beyond supports was provided to eliminate pull out of bars due to splitting of concrete cover, a typical failure mode observed in shear tests when the longitudinal bars are not properly anchored. These anchorage requirements resulted in an overall beam length of 13-ft.

A summary of design properties for each specimen is provided in Table 4.1. The test setup is shown in Figure 4.1 while cross-section details used in each series are illustrated in Figures 4.2. The specimens are designated in the following manner. The first letter, V, stands for a shear series specimen. The second letter after the hyphen describes the type of reinforcement used in the specimen; S for steel, D for high strength steel, G for glass, and A for aramid bars. The number following the second letter in the glass FRP reinforced specimens designates the type of glass bar used; 1 for ribbed, 2 for indented and sand coated. The last number the test series, 1 for Series 1 and 2 for Series 2.

Table 4.1: Shear Specimen Nominal Design Values					
Series	**Specimen**	**f_c (psi)**	**E_r (ksi)**	**a/d**	**ρ (%)**
1	V-S-1	5000	29000	3.4	1
	V-G1-1	5000	5920	3.4	1
	V-G2-1	5000	5650	3.4	1
	V-A-1	5000	7700	3.4	1
2	V-S-2	5000	29000	3.4	2
	V-D-2	5000	29000	3.4	0.36
	V-G1-2	5000	5920	3.4	2
	V-G2-2	5000	5650	3.4	2
	V-A-2	5000	7700	3.4	2

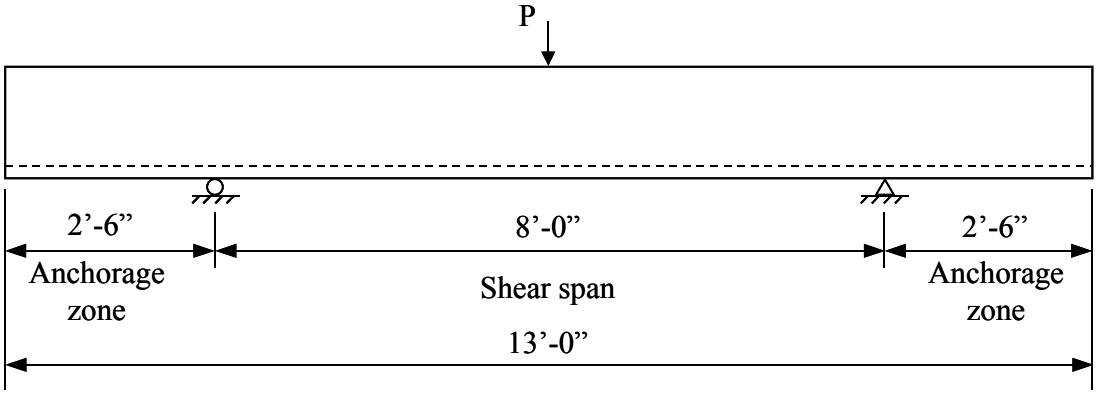

Figure 4.1: Test Setup

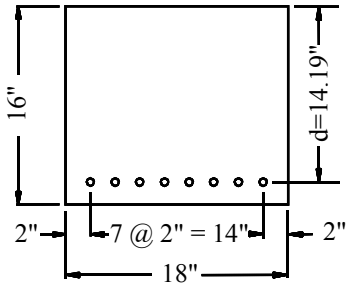

(a) Series 1 Specimens

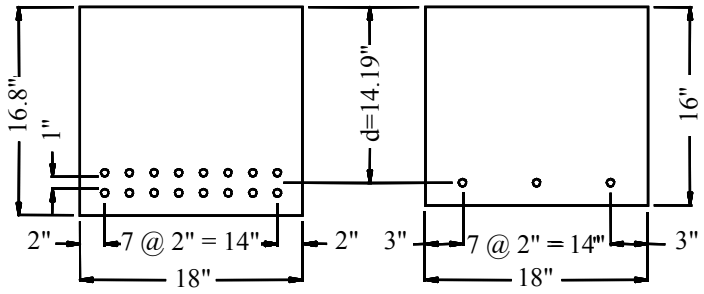

(b) Series 2 Specimens with two layers of reinforcement

(c) Series 2 Specimen with one layer of reinforcement

Figure 4.2: Cross Section Details

4.3 Materials

4.3.1 Reinforcement

Five types of reinforcement were used in this investigation, three types of FRP bars and two types of steel bars. FRP reinforcement included 2 types of glass FRP bars, Glass 1 and Glass 2, and one aramid FRP bar. Steel reinforcement consisted of a conventional steel bar, Steel, and high yield strength steel bar, Dywidag. Properties of the reinforcement are presented in Table 4.2. Details regarding each bar type except the Dywidag bars are as presented previously in Section 3.3.

Table 4.2: Mechanical properties of reinforcing materials

Bar Type	E (ksi)	σ_y (ksi)	σ_u (ksi)	ε_y	ε_u
Steel	29000	76	91	0.0026	-
Dywidag	29000	108	145	0.0038	-
Glass 1	5880	-	88	-	0.0150
Glass 2	5450	-	86	-	0.0158
Aramid	6830	-	206	-	0.0302

4.3.1.1 High Yield Strength Steel (Dywidag)

High yield #5 bars were obtained from Dywidag Co. These bars were used because of their high yield strength (156-ksi) so that a beam with very low percentages of longitudinal reinforcement (0.36%) could be tested without yielding the reinforcement. Three tension tests were conducted which resulted in average yield strength of 108-ksi and an ultimate strength of 145-ksi. The mechanical properties of the bar are listed in Table 4.2 and a representative stress strain curve in Figure 4.3.

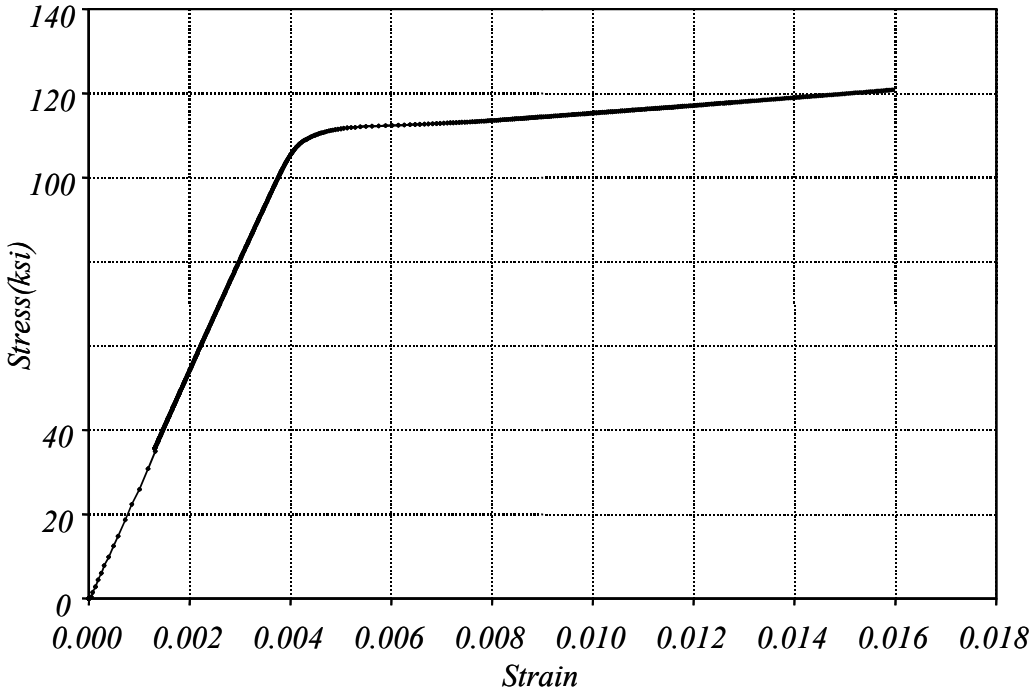

Figure 4.3: Stress-Strain Curve for Dywidag Steel Bars

4.3.2 Concrete

Concrete was obtained from a local ready-mix concrete supplier. The same mix design was used for all specimens and batch weights for each series are listed in Table 4.3. The concrete consisted of ¾" maximum aggregate (river gravel), minimal water reducer and air entrainment. Slump was adjusted after arrival of the truck through the addition of water. Concrete for Series 1 and 2 had 6-½" slumps. Compressive strength of the specimens was monitored by testing three standard 6"x12" cylinders at 7, 14, and 28 days.

Table 4.3: Concrete Batch Weights Per Cubic Yard

Material	Series 1*	Series 2
Cement (lbs)	517	515
Fine Aggregate (lbs)	1485	1531
Coarse Aggregate (lbs)	1850	1851
Water (lbs)	212	230
Air (oz)	1	1
Water Reducer/Retarder (oz)	10	10

*Design mix-proportion, not actual.

Specimen compressive strength and split cylinder strength on the day of testing were obtained by testing three 6X12 cylinders for both Series 1 and Series 2 specimens. Additionally, flexural strength of Series 2 specimens was obtained by testing two 6"x6"x30" modulus of rupture beams on the day of testing. The average cylinder compressive strength (f_c), split cylinder strength (f_t), and rupture strength (f_r) on the day of testing are tabulated in Table 4.4.

Table 4.4: Average Concrete Strengths

Series	Specimen	Age (days)	f_c (psi)	f_t (psi)	f_r (psi)
1	V-S-1	63	5780	495	-
	V-G1-1	67	5760	497	-
	V-G2-1	71	5930	533	-
	V-A-1	74	5850	530	-
2	V-S-2	117	6150	409	858
	V-D-2	133	6330	406	779
	V-G1-2	140	6190	407	817
	V-G2-2	150	6170	540	829
	V-A-2	167	6010	581	715

4.4 Test Setup and Procedure

Test setups were designed to apply a concentrated load at the mid-span of the simply supported beams (Figure 4.1). In Series 1 and Series 2, two different test setups, a 600-kip Universal Testing Machine and a 220-kip MTS hydraulic actuator respectively, were used. In Series 2 specimens, concrete surface strains were measured with a Wittemore gage, which required a displacement controlled loading system. Since the setup used in Series 1 was not capable of displacement controlled loading, a new test setup allowing for both load and displacement controlled loading was prepared for loading Series 2 specimens.

The supports, which were made from welded steel channels and plates, were secured on the strong floor with hydrostone in Series 1 and seated on top of two load cells at each end in Series 2. A roller support was obtained by placing a 1-½" diameter steel rod between two steel flat plates. The pin support was obtained by placing a steel plate on top of a beveled steel rod and placing a flat steel plate on top of the rod. The pin and roller

support assembly are shown in Figure 4.4. The beam was positioned, leveled, and cast on the top plates by hydrostone. To alleviate bearing conditions under the concentrated load a steel plate was hydrostoned to the top of the beam at midspan. Hydrostone was used for attaching the steel plates for its high rate of strength gain and high compressive strength.

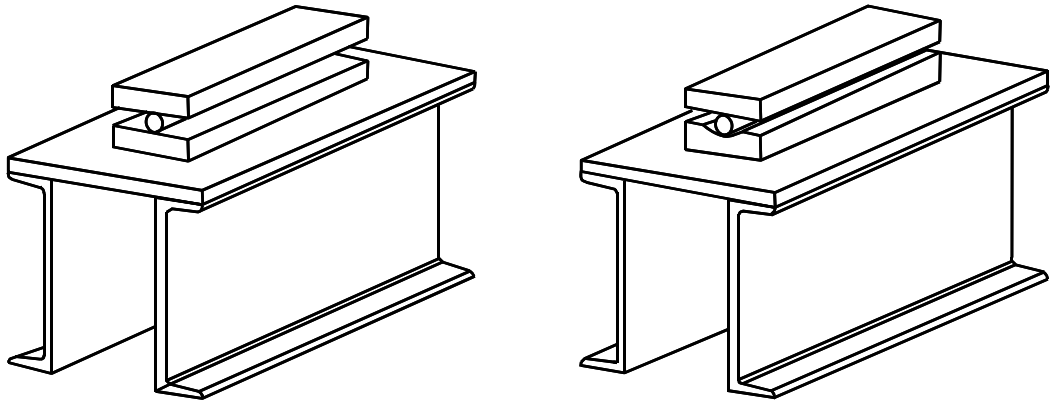

(a) Roller support **(b) Pin support**

Figure 4.4: Supports

As previously mentioned, Series 1 specimens were loaded with a 600-kip universal testing machine under load control (Figure 4.5). The load was increased continuously until first cracking was observed and increased in 5-kip increments afterwards. At the end of each interval, the load was held constant while cracks were marked and crack widths were measured while photographs were taken. A load cell placed under the concentrated load measured the load while deflections were measured at 2-ft intervals with linear voltage displacement transducers (LVDT).

Figure 4.5: Series 1 Test Setup

Shear Series 2 specimens were loaded with a 220-kip MTS hydraulic actuator (Figure 4.6). The load was increased continuously until first cracking. Following first cracking, the load was increased in 5-kip increments under load control. At each load stage, cracks were marked and their widths measured. At every other load stage (10-kip increments), the displacement of the actuator head was held constant. During this time, strains on the

concrete were measured with Wittemore gages and photographs of the beam were taken. The applied load was measured by the internal load cell on the actuator as well as by load cells placed under the supports. The load measurements reported in this document are the ones obtained from the load cells.

Figure 4.6: Series 2 Test Setup

To monitor the strain profile along the reinforcement Series 2 beams were instrumented with strain gages attached to the reinforcing bars at 1-ft intervals from support to support. In addition, two surface strain gages were attached on the concrete top surface 4.5-in from midspan. Displacements were measured at 1-ft intervals along the span and at the supports to obtain the deflected profile of the specimens. To determine the strain distribution in the concrete a Wittemore gage contact point grid was attached on the side surface of the beam. Figure 4.7(a) illustrates the instrumentation plan for LVDTs and strain gages while Wittemore gage contact point grid is given in Figure 4.7(b).

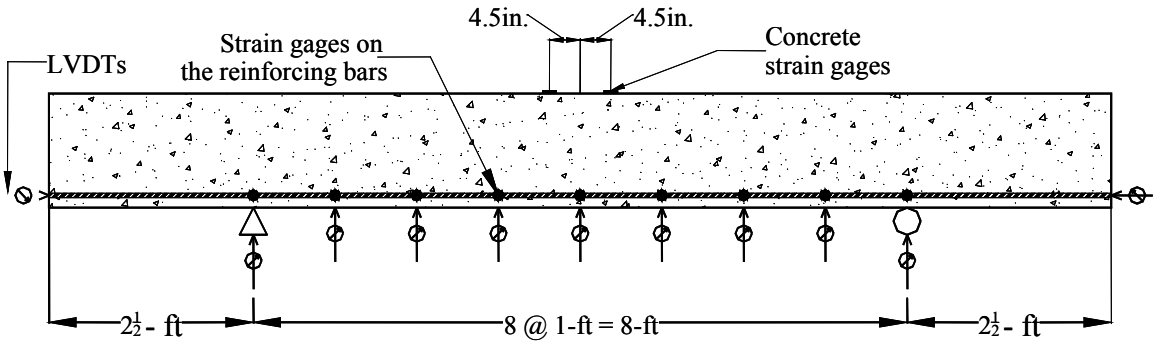

(a) LVDT and Strain Gages

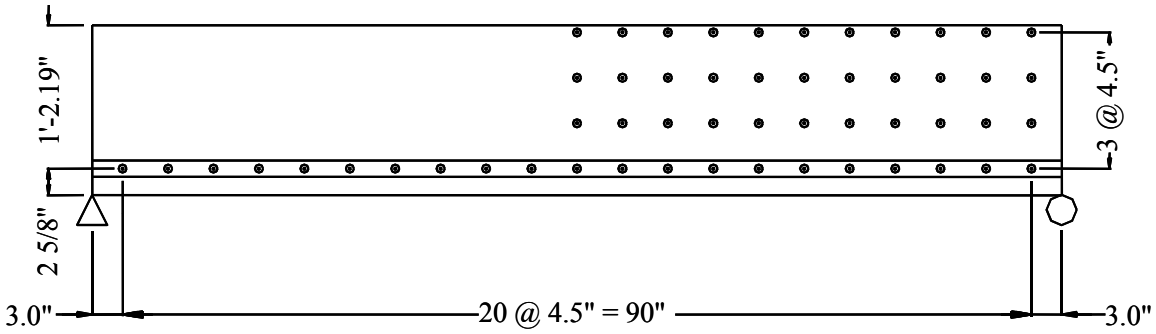

(b) Wittemore gage contact points

Figure 4.7: Instrumentation Plan for Series 2

4.5 Experimental Results

4.5.1 General Behavior

4.5.1.1 Loading

In all specimens the deflections increased linearly with increasing load prior to first cracking. First cracking during the test was observed in the load deflection curve by a marked reduction in the stiffness. The initial crack occurred under the concentrated load or within its close vicinity. New flexural cracks developed closer to the supports while the existing cracks grew with increasing load. The cracks were vertical during early stages of loading (when the total shear on the specimens was low) but propagated by inclining towards the concentrated load as the load was further increased (Figure 4.8). In general, the closer the crack to the support, the more inclined it became through the course of loading. At loads very close to the specimen's shear capacity, the heights of the outermost inclined crack and the cracks under or closer to the load were approximately the same (Figure 4.9). The inclination and height of the outermost crack usually indicated the imminence of shear failure. Crack patterns on each side between the supports and the concentrated load were generally symmetric prior to shear failure. However, in some cases the crack pattern and the inclined crack on one side of the concentrated load were more developed (severe) than the other side. In other words, the outer inclined crack on one side would penetrate high into the section, which indicated the side that the diagonal tension crack would form.

4.5.1.2 Failure

All specimens failed brittlely in "diagonal tension". The diagonal tension crack was usually a continuation of one of the outermost flexural cracks closest to the supports, also known as a flexural-shear crack. The flexural crack, which initiated the diagonal tension failure, propagated deeper into the beam and became more inclined with increasing shear load. In 7 beams out of the 9 the height of inclined cracks, which lead to failure, were equal to or more than the height of those under the load as illustrated in Figure 4.9. The crack might have penetrated into the compression zone. The inclined crack kicked back towards the level of reinforcing steel prior to failure. With further loading two different kinds of behavior were observed. In the first scenario, splitting along the reinforcement past the support took place simultaneously with the diagonal tension crack growing towards the concentrated load. Providing a very conservative anchorage length beyond the supports eliminated the possibility of bond failure due to insufficient anchorage. In the second scenario, the splitting crack along the reinforcement reached the bottom of the beam immediately before the support without causing splitting past the support. Examples of failed beams illustrating these differences in failure pattern are shown in Figures 4.10.

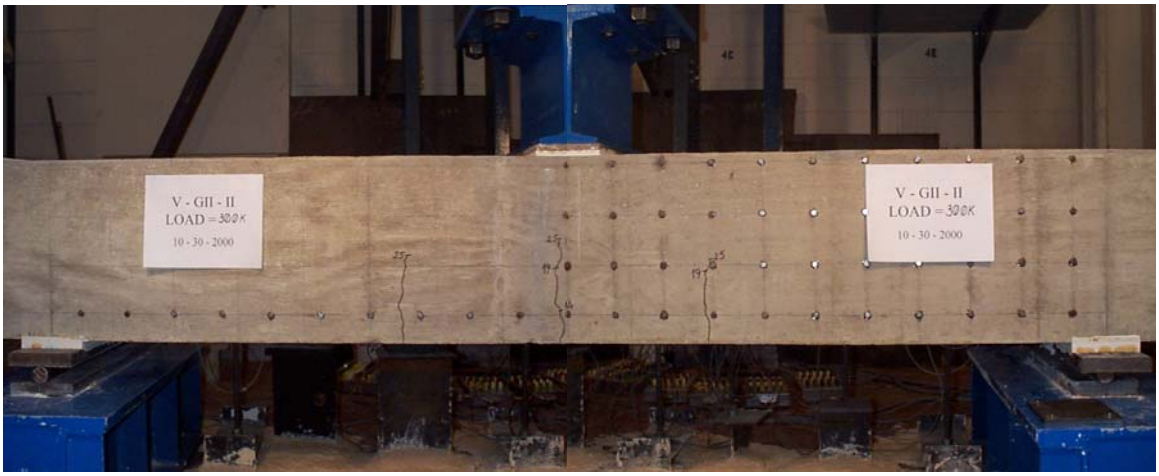

(a) Cracking Pattern at 30-kip

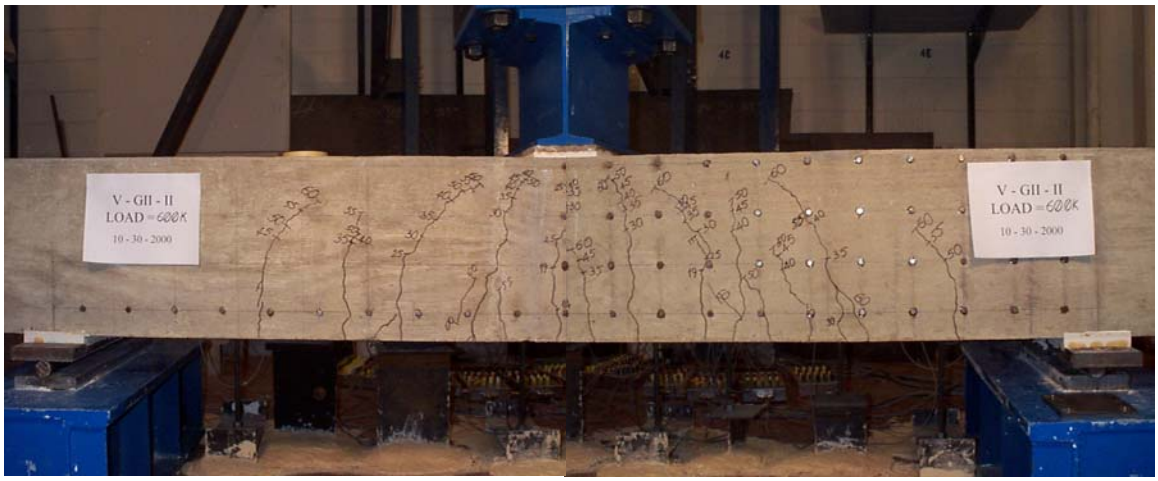

(b) Cracking Pattern at 60-kip
Figure 4.8: Specimen V-G2-2 During Two Different Load Stages

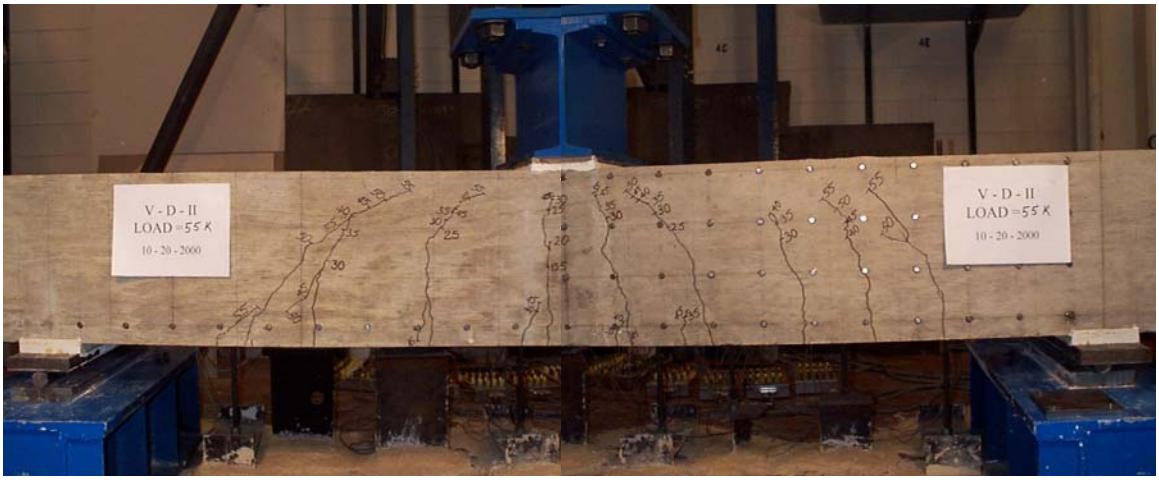

Figure 4.9: Specimen V-D-2 Prior to Failure

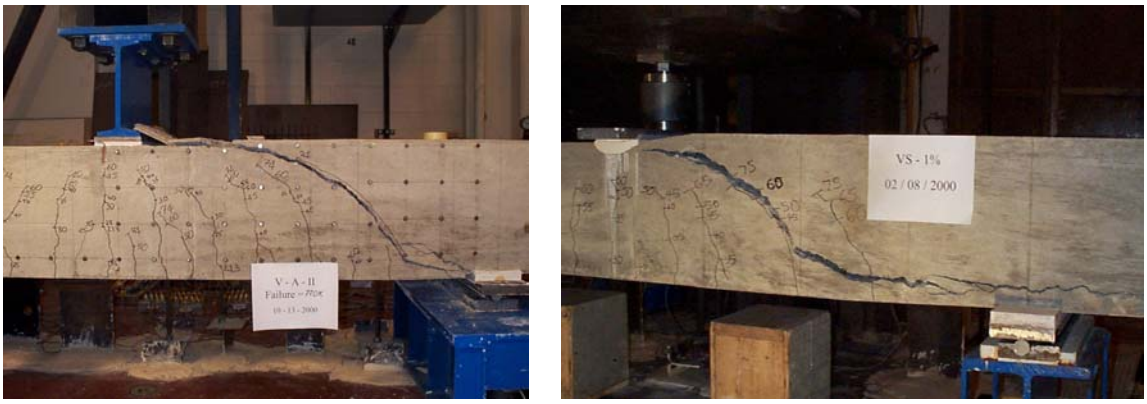

(a) Shear Crack Reaching Bottom Before Support **(b) Splitting along Reinforcement Past Support**

Figure 4.10: Specimens after Failure

A tension crack, an example of which is shown in Figure 4.11, formed on the concrete compression zone above the diagonal tension crack approximately 15-in. to 30-in. away from the concentrated load. These tension cracks extended across the width of the specimens on the top surface. The trace of the diagonal tension crack, which lead to failure, at the back surface of the specimens was not identical to its trace on the front surface in most tests.

(a) Side View **(b) Top View**

Figure 4.11: Tension Crack on the Top Surface After Failure (V-S-2)

4.5.2 Cracking Load

The specimens in each series cracked at approximately the same load with the exception of steel reinforced specimens, which cracked at a load significantly higher than the flexural cracking load of the FRP reinforced specimens. Although cracking loads may be expected to differ due to different modulus of elasticity of the bars used, the increase observed in the experiments could not be explained considering this effect. Even when the difference between concrete strengths were also considered, the difference between the flexural cracking loads of steel reinforced and FRP bar reinforced specimens in each series could not be explained. If shrinkage were to be the cause, it would have worked against what was observed. Shrinkage would have caused more severe cracking in the specimens with higher stiffness reinforcement. The difference in the flexural cracking loads cannot be explained by differences in storage and handling either since these were identical. The seemingly lower flexural cracking load of specimen V-D-2 within its own series was due to its smaller depth. The FRP reinforced specimens in Series 1, which had the same depth as this specimen, cracked at approximately the same load.

4.5.3 Shear Strength

The ultimate shear strength, V_u, and the shear at formation of the "critical inclined crack", V_c, and the mode of failure for each specimen are given in Table 4.5. Test variables such as concrete compressive strength and longitudinal reinforcement ratio are also provided for ease of comparison. In this investigation, the "critical inclined crack" is defined as the crack whose inclination has become more than 45^o to the vertical and pointing towards the concentrated load or one which has kicked back towards the level of reinforcement. In testing Shear Series 1 specimens, no special effort was made in order to determine when the "critical inclined crack" formed. Therefore, the values reported in Table 4.5 are found from crack patterns observed in photographs and sketches of Series 1 specimens. The "critical inclined cracking" loads found in this way were then compared with the load deflection curves, where it was observed that the stiffness changed slightly in the vicinity of these loads.

In general, it can be seen that the difference between the "critical inclined cracking" load and the ultimate load is small. In most cases these values were within 15% of each other. When a/d ratios greater than 2.5 are used (3.4 in this study) and the longitudinal reinforcement ratio is not high, redistribution of internal stresses is limited or cannot take place. Therefore, the inclined cracking shears are typically around the same value as the ultimate shear.

Only diagonal tension failures were observed in the tests. In the failure mode column of Table 4.5, DT indicates that the specimen failed in diagonal tension. The high yield strength steel bars in the specimen marked as Y-DT experienced yielding under the concentrated load prior to failing in diagonal tension.

Table 4.5: Shear Test Results

Series	Specimen	f_c (psi)	ρ(%)	V_c (kip)	V_u (kip)	Failure Mode
1	V-S-1	5930	1	75	79	DT
	V-G1-1	5760	1	40	47	DT
	V-G2-1	5780	1	40	41	DT
	V-A-1	5850	1	45	50	DT
2	V-S-2	6000	2	90	90	DT
	V-D-2	6330	0.36	55	59	Y-DT
	V-G1-2	6130	2	55	60	DT
	V-G2-2	6170	2	64	67	DT
	V-A-2	6180	2	74	77	DT

It can be seen that an increase in the shear strength was observed as the longitudinal reinforcement percentage increased. However, the rate of increase changed from specimen to specimen. For example, the increase in strength of Series 1 and Series 2 specimens reinforced with Glass 1 was 24% whereas it was 58% for specimens reinforced with Glass 2 bars. These percentages were adjusted by considering the change in concrete strengths and that the shear strength is proportional to the $\sqrt{f_c}$. To provide a clearer view of the different shear strengths obtained in each series, a bar chart is shown in Figure 4.12. It is noted that the percentage increase in the shear strength of FRP bar reinforced specimens were more than that in the steel reinforced specimens when the longitudinal reinforcement ratio was increased from 1% to 2%. From Series 1 to Series 2, the FRP bar reinforced specimens experienced an average increase in shear strength of 44% whereas this increase was limited to only 13% for steel reinforced specimens. If we compare V-D-2 and V-S-2, the increase in shear strength is 56% for an approximately 5-fold increase in the longitudinal reinforcement ratio. However, recall that the specimen V-D-2 yielded prior to failure. Yielding of the reinforcement could only have decreased the shear strength of this specimen and it would have carried slightly more shear had yielding not taken place, thereby, decreasing the percentage increase in shear strength. This figure also illustrates that the shear strength of the specimen reinforced with high

yield strength steel bars was approximately the same as that from specimens reinforced with the glass FRP bars in Series 2.

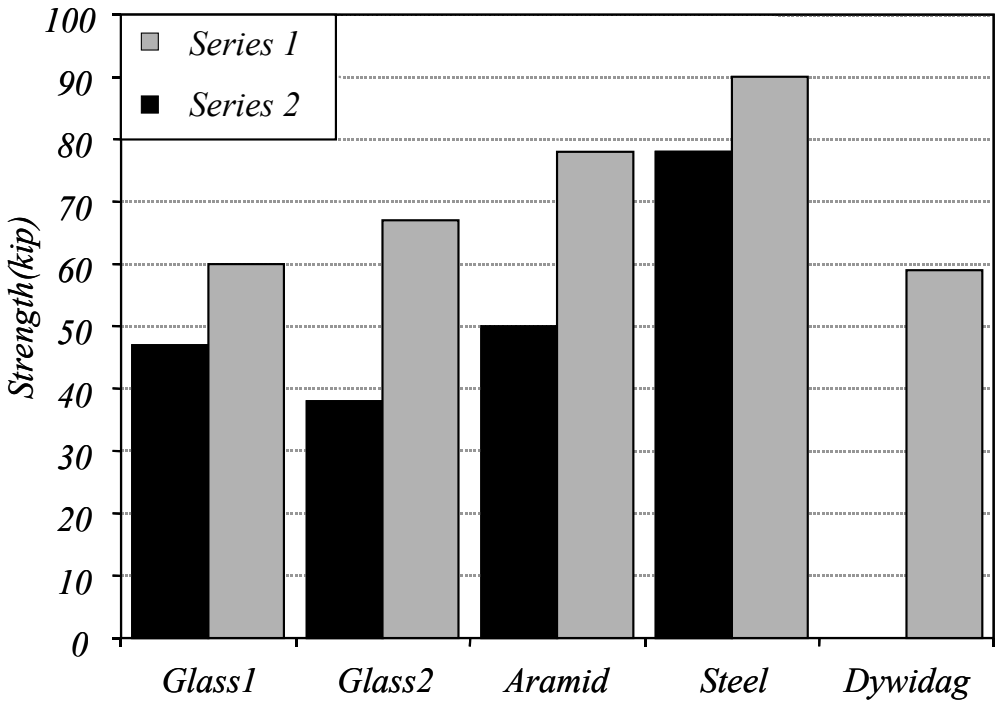

Figure 4.12: Shear strength of specimens

4.5.4 Load-Deflection Curves

Deflections of all the specimens were measured using linear voltage displacement transducers (LVDT) and recorded using a data acquisition system. Load vs. midspan deflections for each test series were plotted on the same figure to allow for easy comparisons. Figure 4.13 shows load-deflection plots of Series 1 specimens while Figure 4.14 illustrates the same plot for Series 2 specimens.

All load-deflection plots exhibit the same characteristics. Specimen behavior can be defined by noting four distinct stages in the load deflection plots. Prior to inclined cracking the curves are approximately linear. In this range, the stiffness of all specimens in a given series was the same. Since the deflections prior to cracking were unaffected by the type of reinforcing bar used, deflection calculations can be made by using either the gross-section or transformed section moment of inertia. Both result in approximately the same value for the reinforcement ranges tested in this investigation. The second stage was a transition stage, during which the beam transformed into a fully cracked state as new cracks formed. In this stage, the stiffness gradually decreased. As the third stage is reached, the stiffness was a function of the bar type and the amount of reinforcement and remained relatively constant. The beam stiffness dropped slightly in the fourth stage, which occurred at a load slightly below the failure load. This final stage ended by failure due to diagonal tension.

The transition stage (Stage 2) was longer in Series 1 FRP bar reinforced specimens as compared to the rest of the specimens tested. In Series 1 specimens, it was observed that the lower the modulus of elasticity of the reinforcing material, the lower the stiffness in the third stage. In Shear Series 2, the stiffness of glass FRP reinforced specimens (V-G1-2 and V-G2-2) and Specimen V-D-2, all of which had similar axial stiffness of longitudinal reinforcement, were almost the same. A straight line best fit to the data of each specimen in their third stage gives approximately the same slope for Specimens V-G1-2, V-G2-2, and V-D-2. The ratio of the stiffness of steel reinforced specimens to that of FRP reinforced specimens calculated from the straight line best fit was approximately 4.0 in both Series 1 and Series 2. It is noteworthy that the beam stiffness ratio was roughly the same as the ratio of the modulus of elasticity of steel bar to that of the average of the modulus of elasticity of FRP bars, which was measured as 4.8.

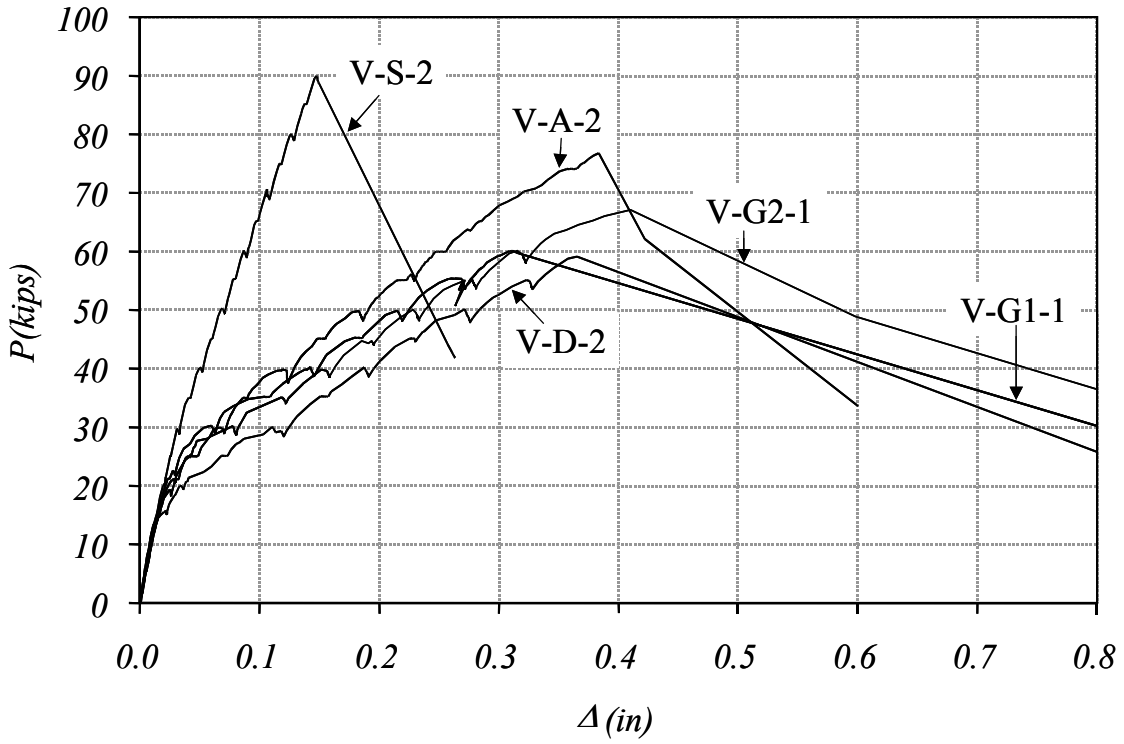

Figure 4.13: Load deflection curves for Series 1 specimens

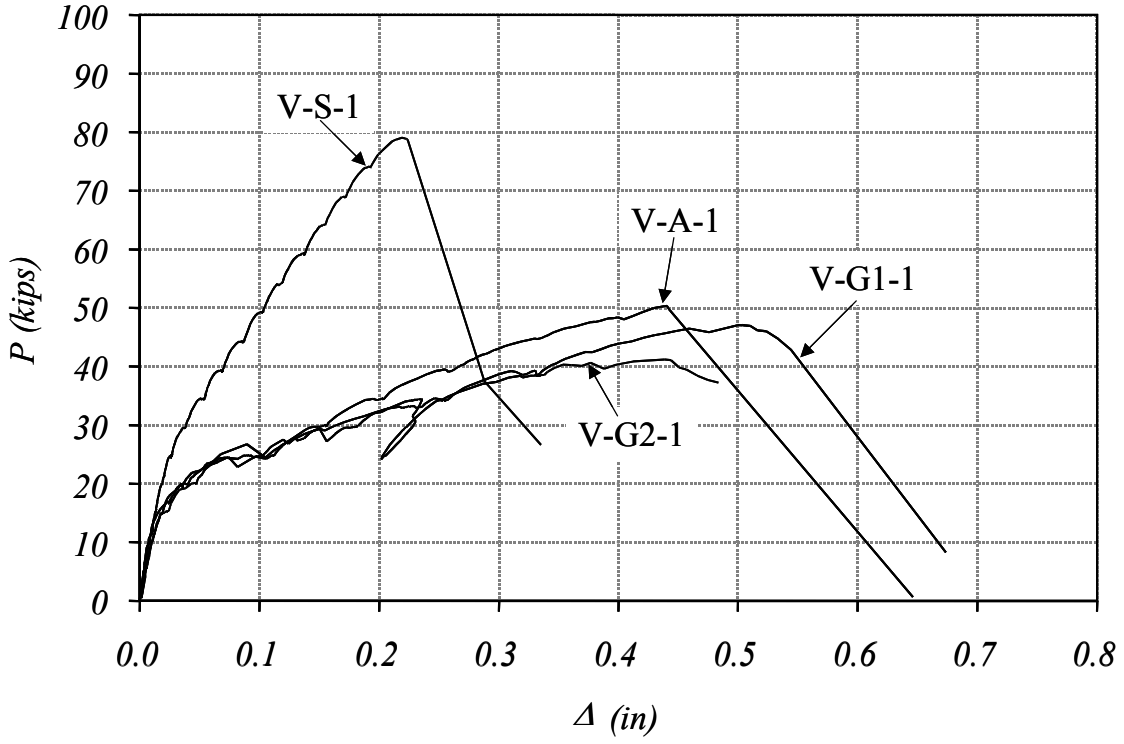

Figure 4.14: Load deflection curves for Series 2 specimens

In both test series, the steel reinforced specimen attained the highest load followed by the Aramid FRP reinforced specimen followed by either of the Glass FRP reinforced specimens. However, in both series, the deflection levels obtained at failure by the FRP reinforced specimens were always larger than those of steel reinforced specimens. It was also noticed that the deflections obtained by FRP reinforced specimens at ultimate within each series were approximately the same. Furthermore, the average ultimate displacement at failure of FRP reinforced specimens was approximately 2.5 times the ultimate displacement reached by steel reinforced specimens in both test series.

4.6 Data Analysis

4.6.1 ACI 318-99 Building Code

The concrete contribution to shear strength of the specimens in this investigation can be calculated by two methods in ACI 318-99 Building Code. One of these equations is the well-known shear strength equation $2\sqrt{f_c'}b_w d$, (Eqn. 4.1). Since the amount of longitudinal reinforcement was varied in this investigation, the strengths of the specimens were calculated also using an alternate equation, (Eqn. 4.2), which includes ρ as one of the variables. These two formulas are also used by the AASHTO Standard Specifications, 16th Edition. In addition the 1999 AASHTO LRFD Bridge Design Specifications allows for the use of formula, $2\sqrt{f_c'}b_w d$, when certain restrictions such as when the member depth is less than 16-in. or a minimum amount of transverse reinforcement specified in the code is provided.

$$2\sqrt{f_c'}b_w d \qquad \text{(Eq. 4.1)}$$

$$V_c = \left(1.9\sqrt{f_c'} + 2500\rho_w \frac{V_u d}{M_u}\right) b_w d \le 3.5\sqrt{f_c'}b_w d \qquad \text{(Eq. 4.2)}$$

where:

$$\frac{V_u d}{M_u} \le 1.0$$

V_c : Nominal shear strength provided by concrete, lbs
f'_c : Specified compressive strength of concrete, psi
ρ_w: Area of longitudinal tension steel divided by $b_w d$
V_u : Factored shear force at section, lbs
M_u: Factored moment at section, (in.-lbs)
d : Distance from extreme compression fiber to centroid of longitudinal tension reinforcement, in.
b_w : web width, in.

The strength of specimens computed according to the ACI-318-99 procedures, (Eqn. 4.1 and 4.2) are tabulated in Table 4.6 along with the experimental results. A column chart presenting the ratio of experimental to calculated values by both methods is also shown in Figure 4.15. The following observations were made from the comparison of the ACI calculated and experimental results. Equation 4.1 is only a function of the tensile strength of concrete ($\sqrt{f_c'}$) and, therefore, results in approximately the same shear strength regardless of reinforcing material. Although Equation 4.2 includes ρ as one of its variables, it does not take the effect of varying modulus elasticity of reinforcing bars; thereby, resulting in unconservative calculations for FRP bar reinforced specimens. Furthermore, Eqn. 4.2 is relatively insensitive to the variations in the amount of longitudinal reinforcement. The shear strengths of all FRP bar reinforced specimens were over-estimated by both procedures. Shear strength calculations for Series 1 and Series 2 specimens differ only slightly according to the ACI procedures. However, the measured shear strengths of specimens reinforced with the same material but varying ρ were noticeably different for both the steel and FRP bar reinforced beams tested.

Table 4.6 Analysis Results						
Specimen	**P_u (kip)**	**Eqn. 4.1 (kip)**	**Eqn. 4.2 (kip)**	**Eqn. 4.3 (kip)**	**Eqn.4.4 (kip)**	**Eqn. 4.5 (kip)**
V-S-1	79	79	78	78	55	56
V-G1-1	47	78	77	16	11	56
V-G2-1	41	78	77	15	10	56
V-A-1	50	78	78	18	13	56
V-S-2	90	79	82	82	109	66
V-D-2	59	81	79	79	20	58
V-G1-2	60	80	83	17	22	57
V-G2-2	67	80	83	16	20	57
V-A-2	78	80	84	20	26	57

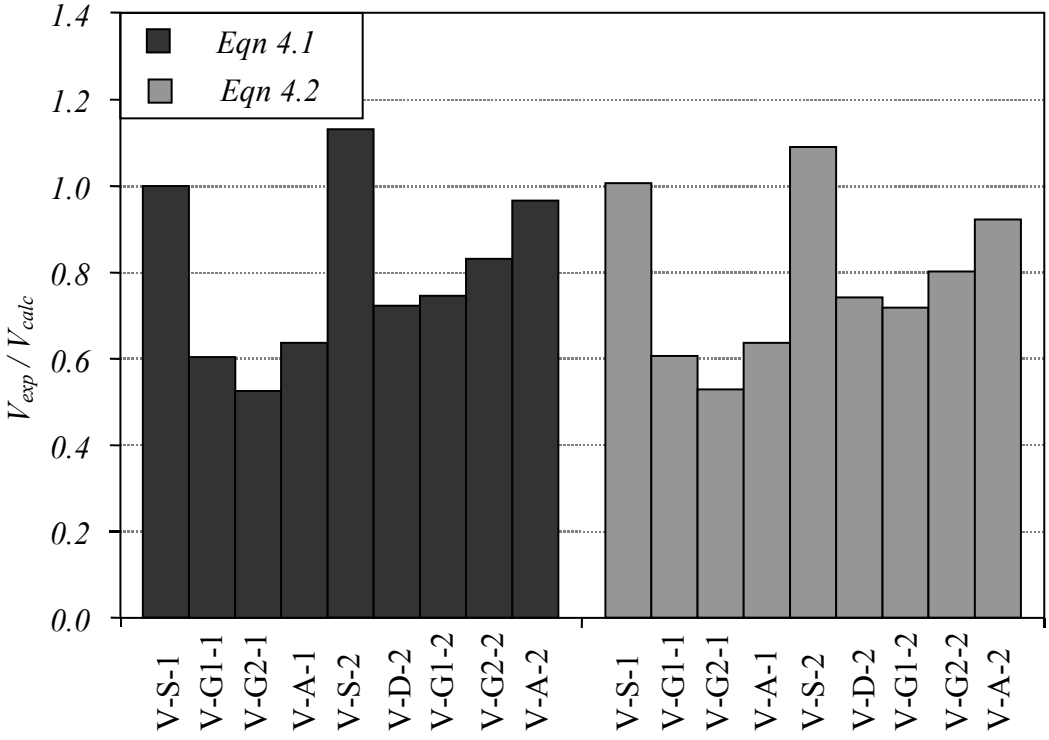

Figure 4.15: Comparison of Strength Calculations by ACI 318-99 Code

ACI-ASCE Committee 326 (ACI 326, 1962), which was a sub-committee on shear and diagonal tension under the ACI Building Code main committee (Committee 318) first proposed Eqn. 4.2 for the concrete contribution to shear strength (V_c) in 1960. Committee 326 proposal was adopted by ACI 318 Committee without any changes and first implemented in the ACI 318-61 Building Code. Eqn 4.2 still serves as the backbone of shear strength equations used in ACI 318-99 Building Code. The data used in the development is plotted in Figure 4.16 together with Eqns 4.1 and 4.2. Note that Eqn. 4.1 is a lower bound to the data points from steel reinforced specimens. In addition the data obtained from the tests of FRP bar reinforced specimens conducted here are plotted for comparison. The data points for FRP bar reinforced concrete beams are noticeably separate from the rest of the data

points. The ACI shear strength equation is an empirical equation, which was developed as a reasonable fit to the available experimental data from steel reinforced concrete specimens. Therefore, satisfactory shear strength calculations of FRP bar reinforced concrete beams should not be expected from this equation.

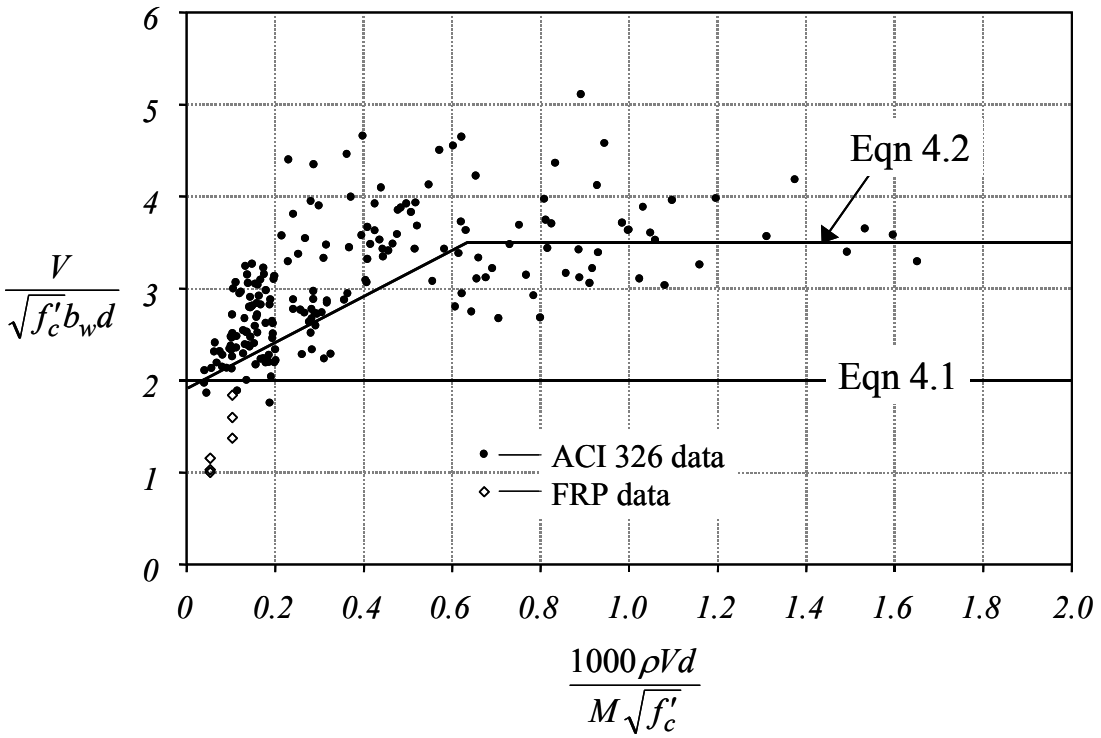

Figure 4.16: ACI Committee 326 design curve development

The ACI equation calculates the shear strength of FRP beams in this investigation poorly. Furthermore, the ACI 318 calculation procedure results in an inconsistent level of safety against shear failure for varying a/d ratios and longitudinal reinforcement ratios even for steel reinforced concrete members. Therefore, the ACI equation is not suitable to determine the concrete contribution to shear strength of FRP reinforced concrete members in this investigation.

4.6.2 ACI Committee 440 Proposed Design Recommendations

ACI Committee 440 has proposed design recommendations for the determination of the shear strength FRP bar reinforced beams. There are two alternative equations proposed by the ACI Committee 440 (Proposals 1 and 2), both of which are modified forms of ACI 318-99 Building Code equation. Both will be used to analyze the beams in this investigation. The first method is presented in Eqn. 4.3 while the second method is given in Eqn. 4.4.

Proposal 1:

$$V_c = 2\sqrt{f_c'}b_w d\frac{E_{FRP}}{E_{steel}} \qquad \text{(Eqn 4.3)}$$

Proposal 2:

$$V_c = 2\cdot\sqrt{f_c'}\cdot b_w\cdot d\cdot\frac{\rho_{FRP}\cdot E_{FRP}}{90\cdot\beta_1\cdot f_c'} \qquad \text{(Eqn. 4.4)}$$

where:

b_w: *web width, in.*

d: *effective depth, which is the distance between the extreme compression fiber and the centroid of the tensile reinforcement, in.*

E_{FRP}: *modulus of elasticity of FRP reinforcement in tension, psi*

E_{steel}: *modulus of elasticity of reinforcing steel, 29,000,000-psi*

f'_c: *concrete compressive strength, psi*

β_1: *factor for calculating the depth of Whitney stress block as defined in ACI 318-99 (Sect. 10.2.7.3)*

ρ_{FRP}: *reinforcement percentage of FRP bars*

The calculated shear strengths according to Eqns. 4.3 and 4.4 are shown in Table 4.6. Also, the ratio of experimental to calculated strengths by both Eqn 4.3 and Eqn 4.4 are given in Figure 4.17.

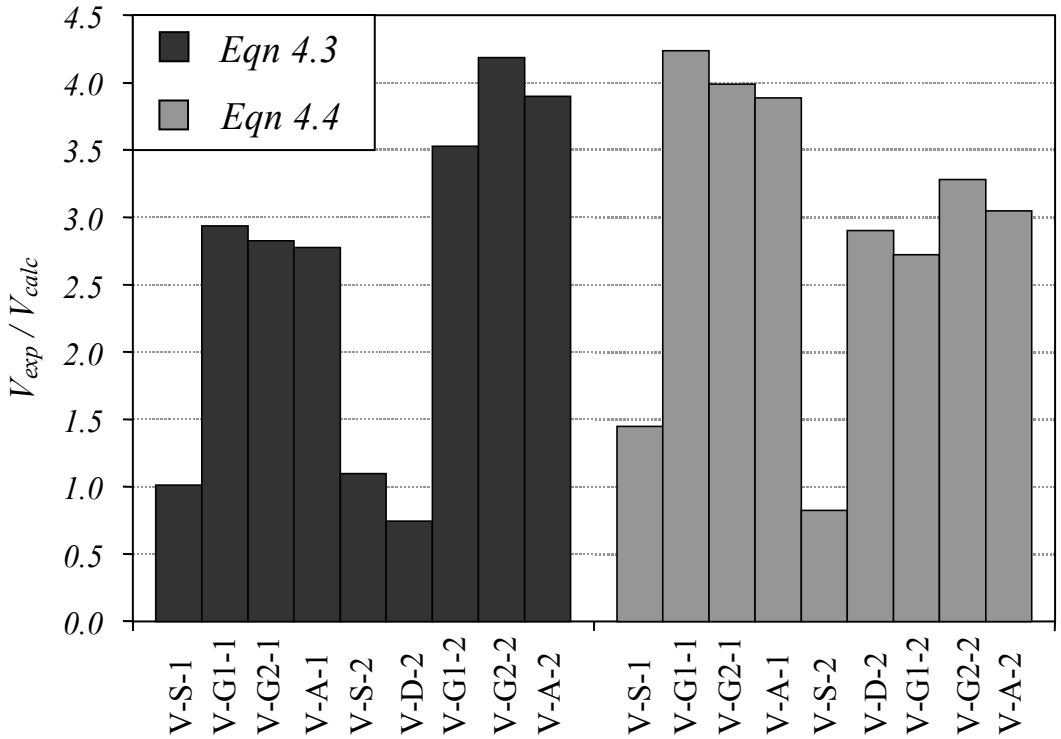

Figure 4.17: Comparison of Strength Calculations by ACI 440 Proposed Recommendations

The aim of the modification of the ACI 318-99 Code calculation method recommended by ACI Committee 440 was to address the effect of the difference in the Young's modulus of FRP bars on the concrete contribution to shear strength. The modification introduced (Eqn 4.3) results in the concrete contribution to shear strength calculated for the FRP bar reinforced specimens very conservative compared to the experimental values. The conservatism increases as the reinforcement ratio increases from 1% to 2% in Series 1 and Series 2 respectively. The experimental results indicate that the shear strength is not a linear function of the modulus of elasticity or the axial stiffness of tensile reinforcement. Therefore, Eqn 4.3 is not adequately calculating the concrete contribution to shear strength of FRP reinforced concrete specimens in this investigation.

To improve the accuracy of concrete contribution to shear strength calculations, ACI Committee 440 proposed an adjustment to Eqn 4.3, which resulted in Eqn. 4.4. However, shear strength calculations using Eqn. 4.4 results in results that are not more reasonable than those provided by Eqn. 4.3. The second proposal by ACI

Committee 440 calculated the shear strengths of the specimens in Series 2 more accurately than those of Series 1 (Figure 4.17). Eqn. 4.3, however, should not be used for steel reinforced concrete beams since the strength calculations for 1% and 2% steel reinforced beams are not reasonable. Proposal 1 resulted in decreasing calculation accuracy as the longitudinal reinforcement ratio was increased from 1% to 2% in Series 1 and Series 2 respectively (Figure 4.17). Proposal 2, however, resulted in increasing calculation accuracy as the longitudinal reinforcement ratio was increased from 1% to 2% in Series 1 and Series 2 respectively (Figure 4.17).

Both equations proposed by ACI Committee 440 for calculating the concrete contribution to shear strength of FRP beams resulted in very conservative and uneconomical strength calculations. Furthermore, since the formulas are based on ACI 318-99 Code calculation method, they inherit the same shortcomings of Eqn. 4.1 discussed previously. Therefore, the ACI Committee 440 proposed equations were not able to reasonably calculate the shear strength of the specimens in this investigation.

4.6.3 1998 AASHTO LRFD Bridge Design Specifications

The shear strengths of specimens were also calculated using the 1999 AASHTO-LRFD Bridge Design Specifications (AASHTO, 1996). The nominal shear resistance V_n is calculated from the lesser value obtained from the two following equations:

$$V_n = V_c + V_s + V_p$$
$$V_n = 0.25 f'_c b_v d_v + V_p \qquad \text{(Eqn. 4.5)}$$

where:

$$V_c = 0.0316 \beta \sqrt{f'_c} b_v d_v$$

b_v *: effective web width, in.*

d_v *: effective shear depth in inches taken as the distance, measured perpendicular to the neutral axis, between the resultants of the tensile and compressive forces due to flexure; it need not be taken less than the greater of* $0.9d_e$ *or* $0.72h$

d_e *: effective depth from the extreme compression fiber to the centroid of the tensile force in the tensile reinforcement, in.*

h *: overall thickness or depth of a member, in.*

f'_c *:specified compressive strength of concrete at 28 days, unless another age is specified, ksi*

V_p *: component in the direction of the applied shear of the effective prestressing force; positive if resisting the applied shear, kip*

β *: factor relating effect of longitudinal strain on the the shear capacity of concrete, as indicated by the ability of diagonally cracked concrete to transmit tension*

In this method, a sectional design approach is followed in which the shear strength of several sections along the length of a member is calculated and compared to the demand at those sections. The β factor in the V_c term is calculated using design aids provided in the form of figures and tables. An iterative solution technique is necessary to obtain the correct value of β, which is a function of the assumed crack inclination angle, crack spacing, provided reinforcing material, amount of reinforcement, and ultimate load that the member will experience at the section considered. The strength of specimens calculated according to 1999 AASHTO LRFD Bridge Design Specifications are provided in Table 4.6. The results of the calculation method are graphically presented in Figure 4.18.

Shear strength calculation by this method is relatively insensitive to the type of reinforcement as well as to the reinforcement ratios (0.36%, 1% and 2%) used in this investigation. For example, the calculated shear strengths for Series 1 and Series 2 specimens with the exception of specimen V-S-2 are practically the same regardless of the reinforcing material or the reinforcement ratio (Table 4.6). Figure 4.18 indicates that for Series 1 specimens, the shear strength calculations of FRP reinforced specimens were unconservative whereas that of steel reinforced specimen was conservative. Calculated shear strengths in Series 2 on the other hand were conservative for all specimens. Note that the factor of safety of the calculated shear strength increased as the axial stiffness of the reinforcing material ($\rho \times E$) increased. It is also noted that the calculated shear strength of FRP bar reinforced specimens by this method was not sensitive to changes in the longitudinal reinforcement ratio. The calculated shear

strengths for companion FRP bar reinforced specimens in Series 1 and Series 2 (1% and 2%) were very close although the reinforcement ratio varied considerably. The method, however, was more sensitive to a change in the steel reinforcement ratio as the strength calculated for Series 2 steel reinforced specimen was higher than that of the Series 1 specimen.

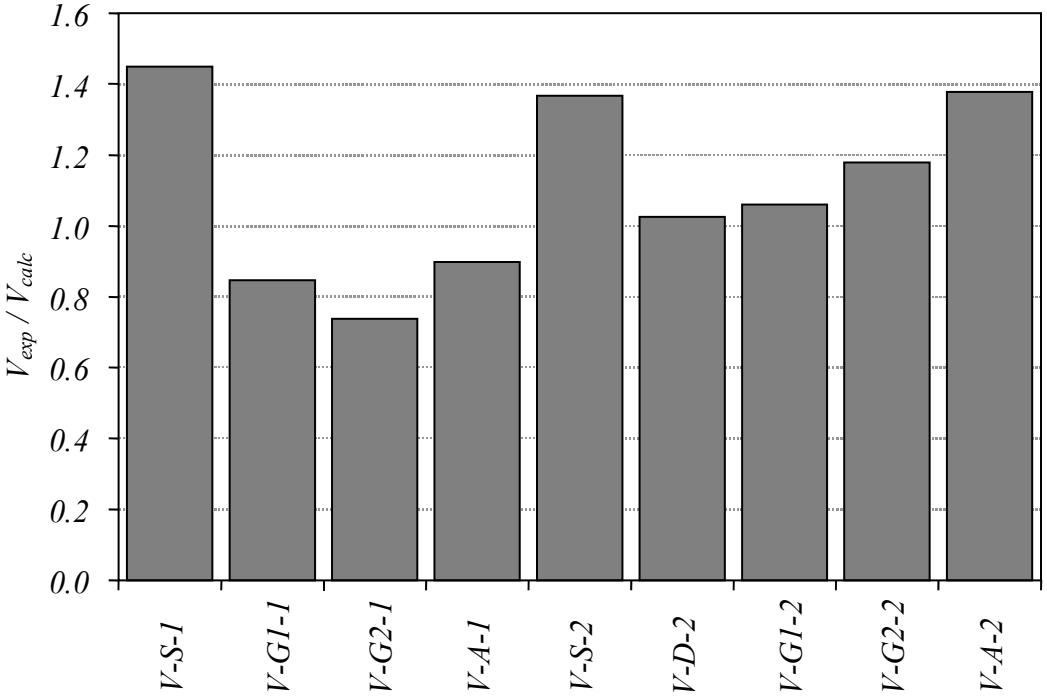

Figure 4.18: Comparison of Strength Calculations by 1999 AASHTO LRFD Code

The 1999 AASHTO LRFD Bridge Design Specifications equation (Eqn 4.5) is based on Modified Compression Field Theory developed by Collins and Mitchell (Collins, 1997). The method used in the specifications, however, is simplified by the introduction of tables and monograms as design aids. Although the development of the method is rational it was calibrated by using data from steel reinforced concrete members as previously discussed. In addition lower and upper bounds for the calculation of shear strength were added to these tables in the code version. The lower and upper bounds in the code regulates the values of β for given values of strain in the tensile reinforcement and the crack spacing. Since the axial stiffness of FRP reinforced specimens in this investigation were very low, the calculated reinforcement strain for all FRP bar reinforced specimens fell below the lower bound specified in the code. Therefore the 1999 AASHTO LRFD Bridge Design Specifications equation was not capable of handling the effect of the changes in the longitudinal reinforcement ratio on the shear strength of FRP bar reinforced specimens in this investigation. Furthermore, the iterative nature of the method is not very practical for design applications.

4.7 Alternative Analysis

To illustrate the effect of the lower modulus of elasticity of FRP bars on shear strength clearly, the nominal shear strength data from the FRP reinforced beams obtained in this investigation as well as data obtained from the literature for steel reinforced beams was plotted vs. ρ as shown in Figure 4.19. The shear strength was normalized by $\sqrt{f'_c}$. For the steel data plotted, the a/d ratio was less than 2.75 and the concrete strength, f'_c, was less than 8500 psi. The longitudinal reinforcement ratio for FRP data in Figure 4.19(a) indicates that the shear strength of FRP reinforced concrete specimens is lower than those of steel specimens with similar ρ. The FRP data points plot just below the lower limit of the steel data (Figure 4.19(a)). It is also noted from Figure 4.19(a) that the increase in the nominal shear strength of FRP bar reinforced specimens normalized with respect to $\sqrt{f'_c}$ (ρ is used instead of ρ_{eff}) is approximately the same as that for steel reinforced specimens with increasing ρ.

In Figure 4.19(b) the same data used in Figure 4.19(a) is plotted vs. the effective longitudinal reinforcement ratio ($\rho_{eff} = \rho \frac{E_{FRP}}{E_{Steel}}$). Therefore, in Figure 4.19(b), the reinforcement ratio of the FRP specimens was normalized by the ratio of the modulus of elasticity of FRP to steel (modular ratio). It is observed that the shear strength of the FRP reinforced concrete specimens follows the same trend as that of steel reinforced concrete beams. Therefore, the effect of the modulus of elasticity of the reinforcement on shear strength can be taken into consideration by the concept of "effective longitudinal reinforcement ratio." There is considerable scatter in the data which occurs due to differences in the concrete strength, a/d ratio, and testing conditions (support conditions, loading equipment, loading schedule, etc.). However, the data plotted in Figure 4.19(b) shows a trend the lower extremes of which may safely be used as the limiting shear strength of reinforced concrete beams without transverse reinforcement. One possible lower bound curve is illustrated. Based on the lower bound curve in Figure 4.19(b), the following equation is recommended to design FRP bar reinforced concrete beams without transverse reinforcement and with a/d > 2.75:

$$\begin{cases} \left(0.75 + 0.625\rho_{eff}\right) \cdot bd\sqrt{f'_c} & \text{for } \rho_{eff} \le 2.0 \\ \left(1.25 + 0.375\rho_{eff}\right) \cdot bd\sqrt{f'_c} & \text{for } \rho_{eff} > 2.0 \end{cases} \qquad \text{(Eqn. 4.6)}$$

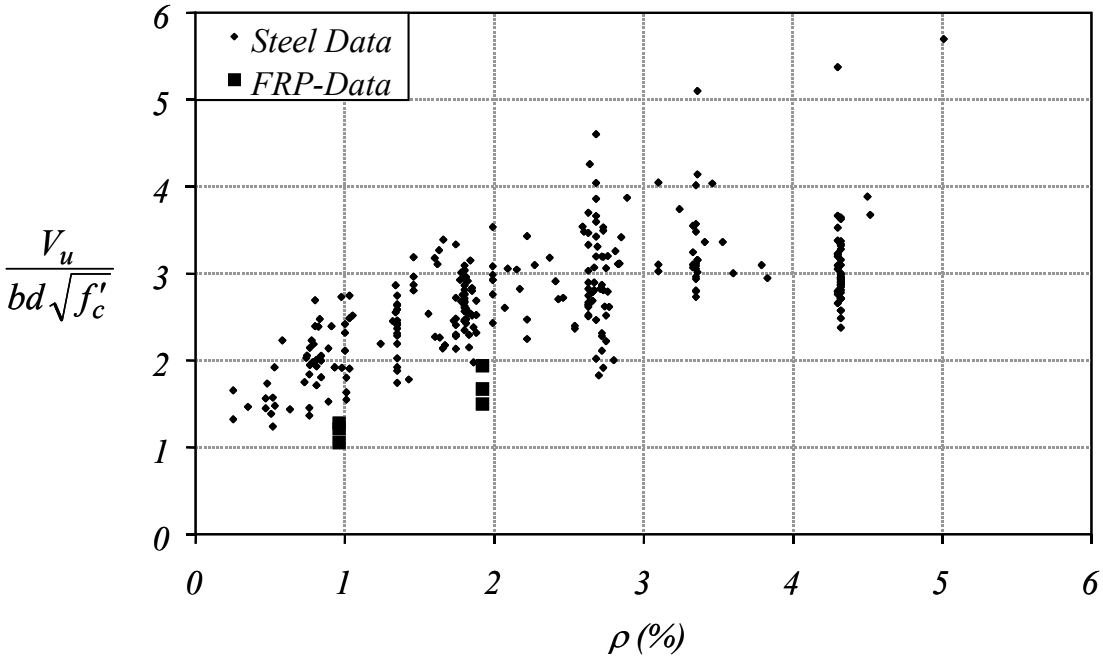

(a) FRP Reinforcement Ratio Not Normalized

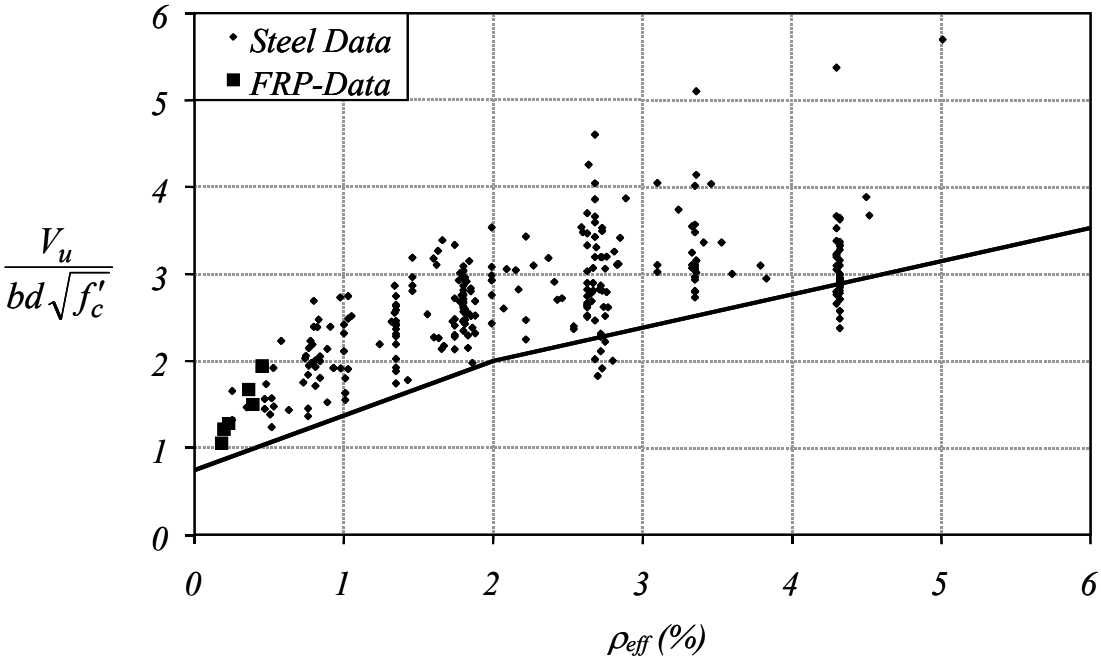

(b) FRP Reinforcement Ratio Normalized with Modulus of Elasticity

Figure 4.19: Influence of ρ on v_u

A bar chart illustrating the results of the proposed method is presented in Figure 4.20 for comparison.

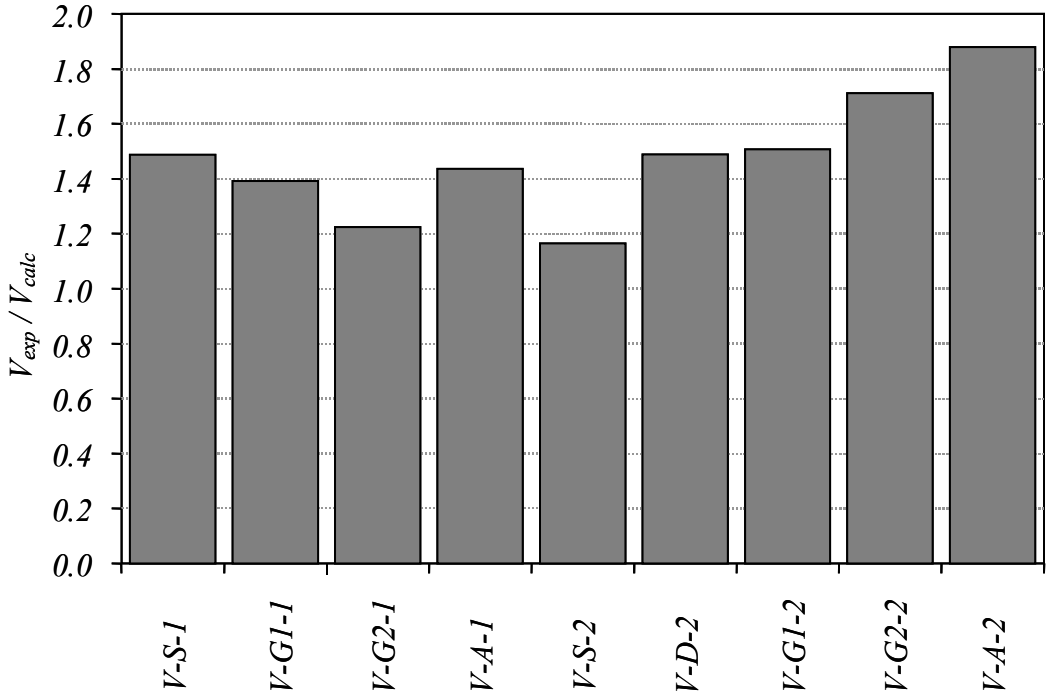

Figure 4.20: Comparison of Strength Calculations by The Proposed Method

Figure 4.20 indicates that the proposed method for the computation of shear strength is conservative for the FRP reinforced specimens tested in this investigation. The method can safely be applied for calculating the shear

strength of both FRP and steel reinforced concrete beams and is simple in application. Therefore, the proposed method (Eqn. 4.6) is a simple and reliable way to calculate the concrete contribution to shear strength of FRP reinforced and steel reinforced concrete without transverse reinforcement.

5. CONSTRUCTION RECOMMENDATIONS

5.1 Introduction

FRP reinforcement is gradually becoming a viable solution for highway concrete structures in corrosive environments. There are several demonstration and research (D&R) projects utilizing FRP bars as concrete reinforcement in Japan, Canada and Europe. In the U.S., there is growing interest in the transportation industry and a number of concrete highway bridge structures have been built as D&R projects. These projects include:

- Rogers Creek Bridge
  Bourbon County, Kentucky, 1997
- Rouge River Bridge
  Southfield, Michigan, 1997
- Buffalo Creek Bridge
  McKinleyville, West Virginia, 1997
- Sierrita de la Cruz Creek Bridge
  Amarillo, Texas, 2000

The construction recommendations herein are intended to provide general guidance for the construction of FRP bar reinforced concrete structures. The recommendations are based on field investigations before and during the casting of the Sierrita de la Cruz Creek Bridge as well as a literature survey (JSCE, 1997, ACI 440, 2000).

5.2 Handling And Storage

The fibers in FRP bars are covered with a plastic resin matrix, which protects them against physical damage and damage from environmental factors such as moisture, ultraviolet light, certain chemicals, and the alkalinity of concrete. Durability of FRP bars is, therefore, strongly affected by damage to the resin matrix. For example, glass FRP bars are very susceptible to degradation due to exposure of glass fibers to alkalis and aramid fibers in aramid FRP bars are susceptible to damage due to UV light exposure of the aramid fibers. Therefore, FRP bars, like epoxy coated steel bars, should be handled, stored, and placed carefully to avoid damage. The following handling and storage guidelines are recommended to avoid damage to the bars and bar handlers:

- FRP bars should be handled with work gloves to avoid injuries to the bar handlers from exposed fibers or sharp edges. If cutting is necessary, a dust mask is recommended
- FRP bars should be handled in such a manner as to prevent damage to the surface. If necessary, handling equipment should have padded contact areas. Since FRP bars are very flexible, bundles of FRP bars should be lifted with a strong back, spreader bar, multiple supports, or a platform bridge. FRP bars should not be dropped or dragged. When necessary, cutting should be accomplished with a high-speed grinding cutter, a hacksaw, or a fine blade saw. FRP bars should never be sheared or bent unless allowed by the manufacturer.
- FRP bars should be stored free from direct contact with the ground. Proper supports to avoid excessive deformations should be provided for storage. Necessary measures should be taken to avoid exposure to excessive heat, direct sunlight, and chemicals that are harmful to FRP bars.

5.3 Placing & Assembling of Reinforcement And Pouring of Concrete

FRP bars should be accurately placed to conform to the requirements as provided in the design drawings, details, and notes. Construction practices such as reinforcement placing and pouring of concrete is similar to that of steel reinforcement and common practices should apply with the following exceptions:

- All FRP bars should be visually inspected prior placement. The bars should be free from defects such as deep scores and cuts and such bars should be replaced immediately. If the FRP bar surface is contaminated with dirt, grease, oil, or other foreign materials, it should be cleaned using appropriate methods and materials recommended by the bar manufacturer. The FRP bars should be transported to their place in the forms in a manner to prevent excessive deformation and damage. All minor surface damage and the cut ends of the bars should be coated with repair material as specified by the manufacturer or equivalent prior to concrete placement.

- FRP reinforcement should be adequately supported using concrete chairs (preferably epoxy or plastic coated Figure 5.1). FRP bars are very flexible and may significantly sag during concreting if they are not supported at close intervals. Therefore, the number of chairs supporting the FRP bars may have to be increased to maintain the bars at the correct depth. The reinforcement should be adequately secured in place to prevent displacement due to concrete placement operations. Since the specific gravity of FRP bars is very low, they should be securely tied down to avoid floating of the bars in fresh concrete (Figure 5.2). Coated tie wire, plastic or nylon ties, and plastic snap ties may be used in tying the reinforcement (Figure 5.3).
- Concrete can be placed according to common practices (Figures 5.4 and 5.5). Compaction can be performed using internal or external vibrators (Figure 5.6). Since FRP bars may be damaged by direct contact with an internal vibrator, use of internal vibrators protected with polyurethane is recommended (JSCE, 1997). The location of bars should be carefully inspected during concreting and if necessary concreting should be stopped until adequate measures to keep the bars in the correct location are taken. The effects of curing temperature should be discussed with the manufacturer, and if necessary curing temperatures should be kept within certain limits according to the manufacturer's recommendations.
- Construction should be planned to finish any potentially harmful operations to FRP bars prior to placement of reinforcement. Two examples of bar damage is illustrated in Figures 5.7(a) and (b) due to poor construction scheduling. Figure 5.7(a) illustrates a damaged bar due to rubbing of FRP bars to steel lifting hooks on the pre-cast concrete panels. Figure 5.7(b) shows a burned bar due to a flame cutting operation very close to the FRP bars.

Figure 5.1: Epoxy Coated Steel Chairs (Sierrita de la Cruz Creek Bridge, Amarillo, Texas, 2000)

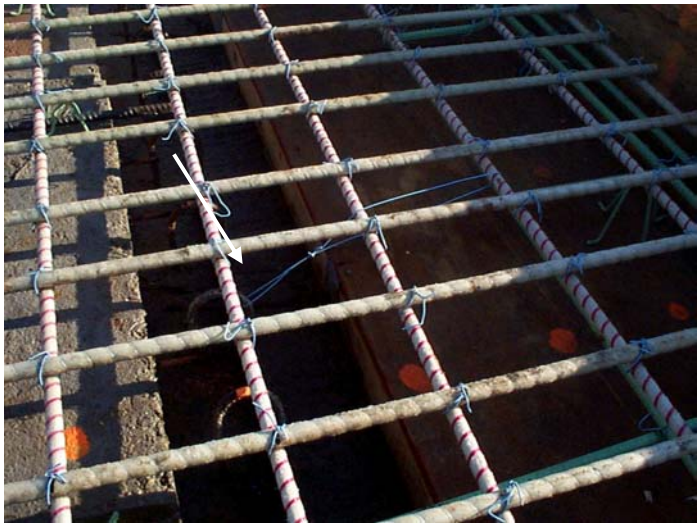

Figure 5.2: FRP Bars Securely Tied Down to Prevent Floating (Sierrita de la Cruz Creek Bridge, Amarillo, Texas, 2000)

Figure 5.3: Plastic Coated Steel Tie-Wires (Sierrita de la Cruz Creek Bridge, Amarillo, Texas, 2000)

Figure 5.4: Casting Operations
(Sierrita de la Cruz Creek Bridge, Amarillo, Texas, 2000)

Figure 5.5: Deck Finishing
(Sierrita de la Cruz Creek Bridge, Amarillo, Texas, 2000)

Figure 5.6: Internal Vibrator Compaction (Sierrita de la Cruz Creek Bridge, Amarillo, Texas, 2000)

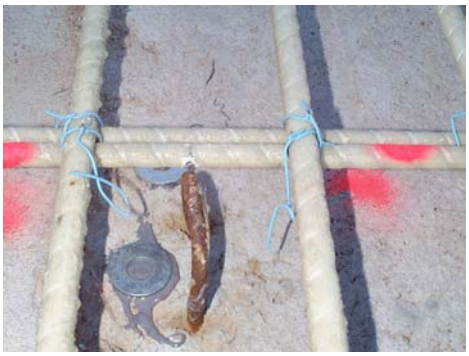

(a) Damaged FRP bar due to repeated rubbing

(b) Burned FRP bar due to the use of a flame cutter

Figure 5.7: Damage to glass FRP bars due to poor construction planning (Sierrita de la Cruz Creek Bridge, Amarillo, Texas, 2000)

5.4 Quality Control

In general, each FRP bar manufacturer has their own resin formulation and manufacturing process. As a consequence, bars of the same fiber type (glass, carbon, aramid) but from different manufacturers, are likely to exhibit different mechanical properties, structural performance, and durability. Since, there are not well-established quality standards for FRP bars in the U.S., each type of FRP bar should be tested prior to use to ensure that they meet the required performance criteria. It is recommended that the quality characteristics of the bars for use in concrete highway bridge structures be determined using the following tests performed on at least 3 specimens.

- Tensile strength and tensile modulus of elasticity
- Fatigue
- Creep
- Coefficient of thermal expansion
- Alkaline immersion

These tests should be performed on representative samples provided by the manufacturer at least 3 months prior to the start of construction. In addition, the manufacturer should provide ample information on the chemical composition and the guaranteed physical and mechanical properties of the type of FRP bars to be furnished. Each lot of FRP bars supplied by the manufacturer should be produced by the same formulation and production method as the tested samples. If a change in production method occurs, the same tests should be performed on the new FRP bars to ensure that they meet the same standards as the previous lot.

Currently, there are no guidelines or standards for the recommended tests listed above in the U.S. However, the ACI Committee 440 is in the process of preparing a report on testing methods for FRP reinforcement (ACI 440, 2000). In Japan, the Japan Society of Civil Engineers (JSCE) has published guidelines for design and construction of FRP reinforced concrete structures (JSCE, 1997), which contains a complete description of the procedures for the recommended tests.

6. DESIGN RECOMMENDATIONS

The following design recommendations are based upon the experimental studies and the analysis of the data as provided in detail in this report.

6.1 Development Length

Equation 6-1 should be used in design to determine the required development length of FRP reinforcement in concrete. This equation is a modification of ACI 318-99 Equation 12-1 (Section 1.3.4, Equation 1-3). The modification factor for FRP reinforcement, *X*, should be determined experimentally for the type of bar to be used. The experimental determination of *X* should be based on test configurations that generate a splitting failure of the concrete. For the FRP bar types used in this experimental program, it is appropriate to use *X* equal to 2.0.

$$\frac{l_d}{d_b} = \frac{3}{40}\frac{f_b}{\sqrt{f'_c}}\frac{M_f}{\left(\frac{c + K_{tr}}{d_b}\right)}X \qquad \text{(Eq. 6-1)}$$

where:

l_d = *development length of reinforcement, (in.)*
d_b = *diameter of reinforcing bar, (in)*
f_b = *specified stress in reinforcement, (psi)*
f'_c = *specified compressive strength of concrete, (psi)*
M_f = *product of modification factors* $\alpha, \beta, \gamma,$ *and* λ
c = *lesser of clear cover or 1/2 clear spacing between bars, (in.)*
K_{tr} = *transverse reinforcement index*
X = *modification factor for reinforcement type*

Concrete cover offers no additional durability benefits for concrete reinforced with FRP. The designer should be cautioned, however, that there is a higher tendency toward splitting with the FRP bars tested in this experimental program. Therefore, concrete cover less than the 1.5 in. provided in this experimental program is not recommended.

6.2 Crack Width

The crack width equation developed by Frosch (Frosch, 1999) performed satisfactorily for the FRP reinforced specimens. For design purposes, Equation 6-2 is recommended for calculating crack widths. It should be noted that the equation was not as conservative for the FRP reinforced specimens as the steel specimens, but the calculation method need not be modified since cracking in FRP reinforced concrete is primarily an aesthetic concern.

$$w_c = \beta\, \varepsilon_s\, S_c \qquad \text{(Eq. 6-2)}$$

where:

w_c = *crack width*

$\beta = \frac{(h - c)}{(d - c)}$ = *amplification factor*

h = *overall depth of the member*

c = *depth from compression face to the neutral axis*

d = *effective depth*

ε_s = *reinforcing steel strain* = $\frac{f_s}{E_s}$

S_c = *crack spacing* = Ψ_s d *

f_s = *reinforcing steel stress*

E_s = *reinforcing bar modulus of elasticity*

Ψ_s = *crack spacing factor : 1.0 for minimum spacing; 1.5 for average; and 2.0 for maximum*

6.3 Deflections

Due to the reduced modulus of elasticity of FRP reinforcement, design of members may be governed by deflection requirements. Therefore, accurate calculation of deflections becomes very important in design of FRP reinforced structures. The results of this experimental program indicate that basic principles of mechanics can be used to accurately calculate deflections of a member reinforced with FRP provided the modulus of elasticity is known.

6.4 Shear

Equation 6-3 should be used in design to determine the concrete contribution to shear strength of FRP reinforced concrete without transverse reinforcement.

$$V_c = (0.75 + 0.625\rho_{eff})b_w d\sqrt{f_c'} \qquad \text{for } \rho_{eff} \le 2.0$$

$$V_c = (1.25 + 0.375\rho_{eff})b_w d\sqrt{f_c'} \qquad \text{for } \rho_{eff} > 2.0 \qquad \text{(Eqn. 6-3)}$$

where:

b_w = *web width, in.*

d = *effective depth, which is the distance between the extreme compression fiber and the centroid of the tensile reinforcement, in.*

E_{FRP} = *modulus of elasticity of FRP reinforcement in tension, psi*

E_{Steel} = *modulus of elasticity of reinforcing steel, 29,000,000-psi*

f_c' = concrete compressive strength, psi

$$\rho_{eff} = \rho\frac{E_{FRP}}{E_{Steel}}$$

7. REFERENCES

AASHTO, AASHTO LRFD Bridge Design Specifications, 2nd Edition, 1998.

AASHTO, Standard Specifications For Highway Bridges, 16th Edition, 1996.

ACI ASCE Committee 326, "Shear and Diagonal Tension," ACI Journal, Proceedings Vol. 59, No. 1, Jan. 1962, pp. 1-30; No. 2 Feb. 1962, pp. 277-334; and No. 3, Mar 1962, pp 352-396.

ACI ASCE Committee 426, "The shear strength of Reinforced Concrete Members," Journal of the Structural Division, Vol. 99, No. ST6, American Society of Civil Engineers, Jun. 1973, pp. 1091-1187.

ACI Committee 318, 1971. "Building Code Requirements for Structural Concrete (318-77) and Commentary (318R-77)," American Concrete Institute, Farmington Hills, MI, 391 pp.

ACI Committee 318, 1999. "Building Code Requirements for Structural Concrete (318-99) and Commentary (318R-99)," American Concrete Institute, Farmington Hills, MI, 391 pp.

ACI Committee 440 FRP Reinforcement, "Provisional Design Recommendations For Concrete Reinforced With FRP Bars," Reported By ACI Committee 440 FRP Reinforcement, 2000, 89 p.

ACI Committee 440, Guide for the Design and Construction of Concrete Reinforced with FRP Bars, October 2000, American Concrete Institute, Farmington Hills, MI, 97 pp.

ACI-ASCE Committee 445, "Recent Approaches to Shear Design of Structural Concrete," Journal of Structural Engineering, Vol. 124, No. 12, American Society of Civil Engineers, Dec. 1998, pp. 1375-1417.

Al-Dulaijan, S. U., Nanni, A., Al-Zaharani, M. M., Bakis, C. E., and Boothby, T. E., "Bond Evaluation of Environmental Conditioned GFRP/Concrete Systems," Proceedings, 2nd International Conference on Advanced Composite Materials in Bridge Structures, M. El-Badry, editor, 1996.

Boothby, T. E., Nanni, A., Bakis, C. E., and Huang, H., "Bond of FRP Rods Embedded in Concrete," Engineering Mechanics, pp. 114-117.

Clark, J., L., 1993, "The Need for Durable Reinforcement," Alternative Materials for the Reinforcement and Prestressing of Concrete, Blackie, pp. 1-33.

Collins, M.P. and Mitchell, D., Prestressed Concrete Structures, Response Publications, Canada, 1997.

Cosenza, E., Manfredi, G., Pecce, M., and Realfonzo, R., "Bond between Glass Fiber Reinforced Plastic Reinforcing Bars and Concrete—Experimental Analysis," Fourth International Symposium: Fiber Reinforced Polymer Reinforcement for Reinforced Concrete Structures, ACI Proceedings, SP-188, pp. 347-358.

Deitz, D., H., "GFRP Reinforced Concrete Bridge Decks," PhD Dissertation Submitted to The School of Civil Engineering, University of Kentucky, Lexington, Dec. 1998, 201 p.

Ehsani, M.R.; Saadatmanesh, H.; and Tao, S.; "Bond of GFRP Rebars to Ordinary-Strength Concrete," International Symposium: Fiber Reinforced Plastic Reinforcement for Concrete Structures, ACI Proceedings, SP-138, 1992, pp. 333-345.

Ehsani, M.R.; Saadatmanesh, H.; and Tao, S.; 1996a, "Design Recommendation for Bond of GFRP Rebars to Concrete," Journal of Structural Engineering, V. 122, No. 3, pp. 247-257.

Ersoy, U., "Reinforced Concrete," Middle East Technical University Publications, Ankara, 1994, pp. 268-343.

Ersoy, U., "Reinforced Concrete," Middle East Technical University Publications, Ankara, 1994.

Fenwick, R., C., Paulay, T., "Mechanisms of Shear Resistance of Concrete Beams," Journal of the Structural Division, ASCE, Vol. 94, No. ST10, Proc. Paper 2325, Oct. 1968, pp. 2325-2350.

Fickelhorn, M., 1990, "Editorial," Materials and Structures Journal RILEM, Vol. 23, No. 137, p. 317.

Frosch, Robert J., "Another Look at Cracking and Crack Control in Reinforced Concrete," ACI Structural Journal, V. 96, No. 3, May-June 1999, pp.437-442.

Gao, D.; Benmokrane, B.; and Masmoudi, R.; 1998b, "Bond Properties of FRP Rebars to Concrete," Technical Report, Department of Civil Engineering, University of Sherbrooke, Sherbrooke (Quebec), Canada, pp. 27.

Gopalaratnam, V., S., Shah, S., P., "Softening Response of Plain Concrete in Direct Tension," ACI Journal, Proc., Vol. 82, No. 3, 1985, pp. 310-323.

Jerrett, C. V., and Ahmad, S. H., "Bond Tests of Carbon Fiber Reinforced Plastics (CFRP) Rods," Non-metallic (FRP) Reinforcement in Concrete Structures, 1995, pp. 180-191.

JSCE Research Committee on Continuous Fiber Reinforcing Materials, "Recommendation for Design And Construction of Concrete Structures Using Continuous Fiber Reinforcing Materials," Japan Society of Civil Engineers, Tokyo, Oct. 1997, 325 p.

Kanakubo, T., Yonemaru, K., Fukuyama, H., Fujisawa, M., and Sonobe, Y., "Bond Performance of Concrete Members Reinforced with FRP Bars," International Symposium: Fiber Reinforced Plastic Reinforcement for Concrete Structures, ACI Proceedings, SP-138, 1992, pp. 767-788.

Kanakubo, T., Yonemaru, K., Fukuyama, H., Fujisawa, M., and Sonobe, Y., "Bond Splitting Strength of Concrete Members Reinforced with FRP Bars," Transactions of the Japan Concrete Institute, Vol. 15, 1993, pp. 305-318.

Kani, M., W., Huggins, M., W., Wittkopp, R., R., "Kani on Shear in Reinforced Concrete," University of Toronto Press, Toronto, 1979, 225 p.

Karlsson, M., "Graduation Thesis: Bond Between C-Bar Reinforcement and Concrete," Chalmers University of Technology, Goteberg, March 1997, 71 pg.

Larralde J., Mueller-Rochholz, J., Schneider, T., and Willmann, J., "Bond Strength of Steel, AFRP and GFRP Bars in Concrete," Proceedings of the Second International Conference on Composites in Infrastructure ICCI '98, H. Saadatmanesh and M. R. Ehsani, Editors, Tucson, Arizona, USA, Jan. 1998, Vol. 2, pp. 92-101.

Larralde, J., and Silva-Rodriguez, R., "Bond and Slip of FRP Bars in Concrete," Journal of Materials in Civil Engineering, Vol. 5, No. 1, Feb. 1993, pp. 30-40.

Larralde, J., Silva-Rodriguez, R., Burdette, J., and Harris, B., "Bond Tests of Fiberglass-Reinforced Plastic Bars in Concrete," Journal of Testing and Evaluation, JTEVA, Vol. 22, No. 4, July 1994, pp. 351-359.

MacGregor, J. G., Reinforced Concrete: Mechanics and Design, Prentice Hall, New Jersey, 1997.

Makitani, E., Irisawa, I., and Nishiura, N., "Investigation of Bond in Concrete Members with Fiber Reinforced Plastic Bars," International Symposium: Fiber Reinforced Plastic Reinforcement for Concrete Structures, ACI Proceedings, SP-138, 1992, pp. 315-331.

Malvar, J. L., "Technical Report: Bond Stress Slip Characteristics of FRP Bars," Naval Facilities Engineering Service Center, Port Hueneme, CA, Feb. 1994, 45 pg.

Malvar, J. L., "Tensile and Bond Properties of GFRP Reinforcing Bars," ACI Materials Journal, Vol. 92, No. 3, May-June 1995, pp. 276-285.

Mashima, M., and Iwamoto, K., "Bond Characteristics of FRP Rod and Concrete After Freezing and Thawing Deterioration," International Symposium: Fiber Reinforced Plastic Reinforcement for Concrete Structures, ACI Proceedings, SP-138, 1992, pp. 51-69.

Mattock, A., H., "Diagonal Tension Cracking in Concrete Beams with Axial Forces," Journal of the Structural Division, ASCE, Vol. 95, No. ST9, Proc. Paper 6776, Sept. 1969, pp. 1887-1900.

Mattock, A., H., Hawkins, N., M., "Research on Shear Transfer in Reinforced Concrete," Journal of the Prestressed Concrete Institute, Vol. 17, No. 2, Mar-Apr., 1972.

Michaluck, C., R., Rizkalla, S., H., Tadros, G., Benmokrane, B., "Flexural Behavior of One-Way Slabs Reinforced by Fiber Reinforced Plastic Reinforcements," ACI Structural Journal, Vol. 95, No. 3, May-June 1998, pp. 353-365.

Mosley, C.P., "Bond Performance of Fiber Reinforced Plastic (FRP) Reinforcement in Concrete," Masters Thesis, School Civil Engineering, Purdue University, West Lafayette, Dec. 2000, 85 pp.

Nanni, A., Al-Zahrani, M. M., Al-Duajani, S. U., Bakis, C. E., and Boothby, T. E., "Bond of FRP Reinforcement to Concrete—Experimental Results," Non-Metallic Reinforcement for Concrete Structures, Proceedings of the Second International Symposium 1995, L. Taerwe, Editor, pp. 135-145.

Nanni, A., Bakis, C. E., and Boothy, T. E., "Test Methods for FRP—Concrete Systems Subjected to Mechanical Loads: State of the Art Review," Journal of Reinforced Plastics and Composites, Vol. 14, June 1995, pp. 524-557.

Nanni, A., Boothby, T. E., Bakis, C. E., and Huang, H., "Bond of FRP Rods Embedded in Concrete," Proceedings of Engineering Mechanics, Vol. 1, 1995, ASCE, New York, NY, USA, pp. 114-117.

Nanni, A., Dolan, C., W., "International Symposium on Fiber Reinforced Plastic Reinforcement for Concrete Structures," American Concrete Institute, SP-138, 1992, 977 p.

Nanni, A., Freimanis, A. J., Bakis, C. E., and Gremel, D., "A Comparison of Pull-Out and Tensile Behaviors of FRP Reinforcement for Concrete," Proceedings of the Second International Conference on Composites in Infrastructure ICCI '98, H. Saadatmanesh and M. R. Ehsani, Editors, Tucson, Arizona, USA, Jan. 1998, Vol. 2, pp. 52-65.

Nawy, E., G., Neuwerth, G., E., Philips, C., J., "Behavior of Fiber Reinforced Concrete Beams," Journal of the Structural Engineering, ASCE Proceedings, Vol. 97, No. ST9, Sept. 1971, pp 2203-2215.

Orangun, C. O., Jirsa, J. O., and Breen, J. E., "A Reevaluation of Test Data on Development Length and Splices," ACI Journal, March 1977, pp. 114-122.

Peters, S., T., "Handbook of Composites-Second Edition," Chapman & Hall, Editor S. T. Peters, 1998, 1118 p.

Pleimann, L.G., "Strength, Modulus of Elasticity, and Bond of Deformed FRP Rods," Proceedings of the Specialty Conference on Advanced Composite Materials in Civil Engineering Structures, Material Engineering Division, American Society of Civil Engineers, pp. 99-110.

Pleimann, L.G., “Tension and Bond Pull-Out Tests of Deformed Fiberglass Rods,” Final report for Marshall-Vega Corporation, Marshall, Arkansas, Civil Engineering Department, University of Arkansas, Fayetteville, Arkansas, pp. 5-11.

Reineck, K., H., "Ultimate Shear Force of Structural Concrete Members Derived from a Mechanical Model," ACI Structural Journal, Vol. 88, No. 5, 1991, pp. 592-602.

Reinhardt, H., W., Cornelissen, H., A., W., Hordijk, D., A., "Tensile Tests and Failure Analysis of Concrete," Journal of Structural Engineering , ASCE, Vol. 112, No. 11, 1986, pp. 2462-2477.

Samples, Lisa, “Durability of Concrete Bridge Decks with Emphasis on Epoxy-Coated Bars“ Ph.D. Dissertation, Purdue University, August 1998.

Schlaigh, J., Schaefer, K., Jennewein, M., "Towards a Consistent Design of Reinforced Concrete Structures," Journal of the Prestressed Concrete Institute, Vol. 32, No. 3, May-June 1987.

Shield, C. K., French, C. W., and Hanus, J. P., “Bond of Glass Fiber Reinforced Plastic Reinforcing Bar for Consideration in Bridge Decks,” Fourth International Symposium: Fiber Reinforced Polymer Reinforcement for Reinforced Concrete Structures, ACI Proceedings, SP-188, pp. 393-406.

Taylor, H., P., J., "Investigations of the Forces Carried Across Cracks in Reinforced Concrete Beams in Shear by Interlock of Aggregate." Technical Report 42.477, Cement and Concrete Association, London, England, 1970, 22 pp.

Taylor, H., P., J., "Shear Strength of Large Beams," Journal of the Structural Division, ASCE, Vol. 98, No. ST11, Nov. 1972, pp. 2473-2490.

Tepfers, R., Hedlund, G., and Rosinski, B., “Pull-out and Tensile Reinforcement Splice Tests with GFRP Bars,” Proceedings of the Second International Conference on Composites in Infrastructure ICCI ’98, H. Saadatmanesh and M. R. Ehsani, Editors, Tucson, AR, USA, Jan. 1998, Vol. 2, pp. 37-51.

Tighiouart, B., Benmokrane, B., and Gao, D., “Investigation of Bond in Concrete Member with Fiber Reinforced Polymer (FRP) Bars,” Construction and Building Materials Journal, December 1998, pp. 10.

Tighuart, B., Benmokrane, B., and Gao, D., “Investigation on the Bond of FRP Bars in Concrete,” Proceedings of the Second International Conference on Composites in Infrastructure ICCI ’98, H. Saadatmanesh and M. R. Ehsani, Editors, Tucson, AR, USA, Jan. 1998, Vol. 2, pp. 102-112.

Tompos, E, J, "Influence of Beam Size And Stirrup Effectiveness on The Shear Strength of Reinforced Concrete Beams," Masters Thesis, School Civil Engineering, Purdue University, West Lafayette, Dec. 2000, 89 pp.

Tureyen, A.K., “Influence of Longitudinal Reinforcement Type on the Shear Strength of Reinforced Concrete Beams without Transverse Reinforcement,” Doctoral Dissertation, School of Civil Engineering, Purdue University, December 2001, 232 pp.

Vintzeleou, E., N., Tassios, T., P., "Mathematical Models for Dowel Action under Monotonic Conditions," Magazine of Concrete Research, 1986, Vol. 38, pp. 13-22.

Zenon, A., Kypros, P., and Peter, W., “Bond of FRP Anchorage and Splices in Concrete Beams,” ECCM-8 European Conference on Composite Materials, Naples, Italy, June 1998, Vol. 2, pp. 277-284.

APPENDIX A. CONVERSION FACTORS

1 in. = 25.4 mm

1 kip = 4.448 kN

1 ksi = 6.895 MPa